Università degli Studi di Ferrara

DOTTORATO DI RICERCA IN "FISICA"

CICLO XXXII

COORDINATRICE/COORDINATORE Prof.
Eleonora Luppi

Multipurpose silicon detector for (polarized) internal target experiments at the COSY Storage Ring in Jülich.

Settore Scientifico Disciplinare FIS/01

Dottoranda/o
Dott. Kononov Anton

_____
(firma)

Tutore
Prof. Lenisa Paolo

_____
(firma)

Anni 2017/2020

Abstract

Experiments with polarized internal gas targets and polarized proton beams give a great opportunity to access a number of fundamental physics observables. In the frame of this thesis I consider experiments performed at the Cooler Synchrotron COSY storage ring at Forschungszentrum Jülich (FZJ).

The PAX (Polarized Antiproton eXperiment) collaboration plans to carry out Drell-Yan production experiments in proton-antiproton collisions, both polarized, in the Facility for Antiproton and Ion Research (FAIR) facility in Darmstadt. This type of process allows direct access to the transverse spin structure of the nucleon. Until now it has not been possible to produce antiproton beams with an acceptable polarization. The objective of the PAX collaboration is to develop an efficient method to polarize antiprotons in a storage ring. The collaboration successfully performed a spin-filtering test with COSY protons, using a transversely polarized hydrogen target. This led to the determination of the spin-dependent cross-section of "build-up" of the transverse polarization, proving that "spin filtering" is a valid method to polarize a beam in a storage ring.

PAX intends to use the unique experimental setup offered by COSY to apply this method to longitudinal polarization. In preparation for this test, a new detector (PAX detector) has been built through a collaboration between the University of Ferrara, the INFN of Ferrara and the Forschungszentrum Jülich. The new detector will be used both for the longitudinal spin-filtering experiment at COSY and for future experiments with antiprotons.

There is also a plan to use the new PAX detector for performing a Time Invariance Violation Interactions (TIVOLI). Now it is well understood that time reversal violation (T-V), like the equivalent violation of the combined symmetries of charge (C) and parity (P) (CP-V), is a necessary ingredient for addressing the mystery of the matter-antimatter asymmetry of our Universe - one of the biggest unsolved problems in contemporary physics and cosmology. It is widely accepted that a solution of this puzzle will involve new physics beyond the Standard Model (SM) of elementary particle physics (BSM).

TIVOLI experiment should constrain or even discover BSM physics by

investigating T-symmetry violations complementary to searches for Electric Dipole Moments (EDM). The objectives are (i) a search for direct T-V through a precise measurement of double polarized proton-deuteron elastic scattering, exploiting the particle spin as a "time reversal knob", and (ii) the development of a solid theoretical basis for the interpretation of T-V interactions, in particular the experimental findings of TIVOLI. The unique experimental environment offered by the cooler synchrotron (COSY) storage ring at Forschungszentrum Jülich promises to improve the present upper limit on T-V by one to two orders of magnitude, using COSY as a zero degree spectrometer and PAX detector.

This thesis focuses on the work done for the construction and commissioning of the new PAX detector, which consists of four identical quadrants arranged in a diamond configuration. Each of these quadrants consists of three layers of double-sided silicon striped sensors, which form a telescope structure. The sensors of the first two layers are $300\mu m$ thick and the third layer is $1000\mu m$ thick.

A first detector test, with two of the four quadrants installed opposite to each other, was successfully conducted at COSY using a beam of unpolarized protons and a target of vector-polarized deuterons. By operating the detector in the described configuration, an energy resolution 60 keV, was achieved for the first two layers of detectors. The spatial resolution is in the order of $\sigma \approx 200\mu m$.

The results of the test are illustrated in this thesis.

Riassunto

Gli esperimenti con bersagli polarizzati e fasci di protoni polarizzati offrono una grande opportunità per lo studio di un numero importante di osservabili fisiche fondamentali. Nell'ambito di questa tesi sono presi in considerazione esperimenti in programma presso l'anello di accumulazione COoler SYnchrotron (COSY) del Forschungszentrum Jülich (FZJ).

La collaborazione PAX (Polarized Antiproton eXperiment) pianifica di realizzare esperimenti di produzione Drell-Yan in collisioni protone-antiprotone, entrambi polarizzati, nella struttura Facility for Antiproton and Ion Research (FAIR) di Darmstadt. Questo tipo di processo permette un accesso diretto alla struttura di spin trasverso del nucleone. Finora non è stato possibile produrre fasci di antiprotoni con una polarizzazione accettabile. È obiettivo della collaborazione PAX sviluppare un metodo efficiente per polarizzare antiprotoni in un anello di accumulazione. La collaborazione ha svolto con successo un test di "spin-filtering" con protoni a COSY, usando un bersaglio di idrogeno polarizzato trasversalmente. Questo ha portato a determinare la sezione d'urto spin-dipendente di "build-up" ella polarizzazione trasversa, provando che lo "spin filtering" è un metodo valido per polarizzare un fascio in un anello di accumulazione.

PAX intende utilizzare il setup sperimentale unico offerto da COSY per applicare questo metodo alla polarizzazione longitudinale. In preparazione a tale test, è stato costruito un nuovo rivelatore mediante una collaborazione tra l'Università di Ferrara, l'INFN di Ferrara ed il Forschungszentrum Juelich. Il nuovo rivelatore sarà utilizzato sia per l'esperimeto di "spin-filtering" longitudinale a COSY, sia per i futuri esperimenti con antiprotoni.

È inoltre previsto l'utilizzo del nuovo rivelatore PAX per l'esecuzione di un'interazione di violazione dell'invarianza temporale (TIVOLI). Ora è ben chiaro che la violazione dell'inversione del tempo (T-V), come l'equivalente violazione delle simmetrie combinate di carica (C) e parità (P) (CP-V), è un ingrediente necessario per affrontare il mistero della l'asimmetria materia-antimateria del nostro Universo - uno dei più grandi problemi irrisolti nella fisica e nella cosmologia contemporanea. È ampiamente accettato che una

soluzione di questo rompicapo comporterà nuova fisica oltre il Modello Standard (SM) della fisica delle particelle elementari (BSM).

L'esperimento TIVOLI dovrebbe limitare o addirittura scoprire la fisica BSM indagando Le violazioni della simmetria a T sono complementari alle ricerche di Momenti di Dipolo Elettrico (EDM). Gli obiettivi sono (i) una ricerca di T-V diretta attraverso una precisa misurazione di diffusione elastica protone-deutone a doppia polarizzazione, sfruttando lo spin delle particelle come "manopola per l'inversione del tempo", e (ii) lo sviluppo di una solida base teorica per l'interpretazione delle interazioni T-V, in particolare i risultati sperimentali di TIVOLI. L'ambiente sperimentale unico offerto dal sincrotrone più freddo (COSY) anello di stoccaggio presso il Forschungszentrum Jülich promette

Questa tesi si concentra sul lavoro svolto per la costruzione e la messa in funzione di questo nuovo rivelatore, che consiste in quattro quadranti identici disposti in una configurazione a diamante. Ognuno di questi quadranti è formato da tre strati di sensori a strisce di silicio fronte-retro, che costituiscono una struttura a telescopio. I sensori dei primi due strati sono spessi $300\mu m$, quello del terzo $1000\mu m$.

Un primo test sul rivelatore, con due dei quattro quadranti installati l'uno opposto all'altro, si è svolto con successo a COSY utilizzando un fascio di protoni non polarizzati ed un bersaglio di deutoni polarizzati vettorialmente. Operando il rivelatore nella configurazione descritta, si è raggiunta una risoluzione in energia di 60 keV per i primi due strati di rivelatori. La risoluzione spaziale è nell'ordine di $\sigma \approx 200\mu m$.

I risultati del test sono illustrati in questa tesi.

Contents

Introduction

This thesis is devoted to the implementation of detector system for studies of low-energy spin-physics experiments employing polarized beam and targets, performed at the COoler SYnchrotron COSY storage ring of Forschungszentrum Jülich.

One objective of the investigations is the completion of the studies devoted to the identification of the viable method to produce an intense beam of polarized antiprotons undertaken some years ago by the PAX Collaboration [1]. In 2012, the Collaboration successfully performed a spin-filtering test with protons using a transversely polarized hydrogen gas target [2], and now plans to complete these studies with a test of the longitudinal polarization buildup at COSY. The results of the studies will be of great importance for the possible application in the polarization of antiprotons at the Facility for Antiproton and Ion Research (FAIR).

Another physics objective is a null test of Time Invariance Violation Interactions (TIVOLI) to an accuracy of 10^{-6}. The parity conserving time-reversal violating observable is the total cross-section asymmetry $A_{y,xz}$ accessible by scattering a vector polarized stored proton beam with energy of 135 MeV off a tensor polarized deuterium gas target [3]. The experiment proposed at the COSY storage ring promises to improve the present upper limit on Time Reversal Violation by at least one order of magnitude. The reaction will be measured using the integrated beam current transformer [4]. As a polarimeter will be used the PAX vertex silicon detector.

To develop the experimental activity, a dedicated interaction point including a polarized internal target and a vertex silicon detector, acting as a beam and target polarimeter, have been designed and realized. In addition, a dedicated solenoid (Siberian snake) and a sensitive beam-current monitor have already been installed in the ring.

In this frame the thesis discusses the development, technical design and realization as well the read-out electronics and detection system of the Detector for experiments on COSY.

An introduction to the physics case for longitudinal spin filtering and a time reversal invariance test are introduced in Chapter 1. A brief description of the COSY ring as well as experimental setup to be employed in these experiments are given in Chapter 2. Chapter 3 gives detailed explanation of the detector setup and developed tools, which are installed around the interaction point, and serves as a polarimeter. Chapter 4 describes the test benches directly related to the detector, as well as how to operate with the test benches, and intermediate results. Results of the commissioning effort are present in Chapter 5.

Chapter 1

Theory and physics motivation

An intense beam of polarized particles like protons or antiprotons will open new experimental opportunities to investigate the structure of the nucleon [1].

One main issue for studies at the COSY is spin-filtering experiments, involving vertical and horizontal orientation of spin. For this moment PAX collaboration has successfully performed spin-filtering test with protons of transversely polarized hydrogen gas target [2].

For the polarization of initially unpolarized beam in storage ring exists two possibilities. For the case of a beam of spin $-\frac{1}{2}$ particles (with two spin states) it could be achieved by either selectively reversing the spin of particles in one spin state ("flipping") or by selectively deduction of one spin state ("filtering").

Spin-flipping technology is more preferable than spin-filtering because the polarized beam intensity would be conserved. Unfortunately for today no viable method exploiting spin-flipping technology was found, and that why collaboration is focused on the spin-filtering technology.

Another object of the studies at the Cooler Synchrotron is test of time-reversal invariance. Thus will be possible to an accuracy of 10^{-6} accessing the null-test observable $A_{y,zz}$ by scattering a vector polarized stored proton beam with the energy of 135 MeV and internal tensor polarized deuteron gas target from the PAX atomic beam source [3]. The experiment probes the time-reversal invariance with parity being conserved (P-even, T-odd) in contrast to experiments of EDM search, which test parity and time reversal invariance simultaneously violate.

Both experiments are united with common instrumentation, available at COSY. Only longitudinal spin filtering requires additional device *"Siberian Snake"* to turn vertical polarisation of the stored beam to horizontal.

1.1 Spin-filtering of a stored proton beam

1.1.1 A physics case for polarized antiprotons

To achieve a full understanding of the nucleon quark structure three of eight leading quantities, so called parton distribution functions (PDFs) are necessary: the unpolarized quark distribution $q(x, Q^2)$, the helicity distribution $\Delta q(x, Q^2)$ and the transversity distribution $h_1^q(x, Q^2)$ (or $\Delta_T q(x, Q^2)$). The transversity distribution is the last leading-twist missing piece of the quantum chromodynamics (QCD). Δq describes the quark longitudinal polarization inside a longitudinally polarized proton, the transversity describes the quark transverse polarization inside a transversely polarized proton at infinite momentum. h_1^q and Δq are two independent quantities, which might be equal only in non-relativistic, small Q^2 limit. Moreover, the quark transverse polarization does not mix with the gluon polarization (since gluons carry only longitudinal spin), and thus the QCD evolutions of h_1^q and Δq are quite different. All the leading-twist structure functions have been measured it is not possible to understand the spin structure of the nucleon. Because of the fact that h_1^q is a chiral-odd function and consequently it decouples from inclusive deep–inelastic scattering h_1^q. h_1^q cannot uccour alone, but has to be coupled to a second chiral-odd quantity since electroweak and strong interactions conserve chirality.

This is possible in polarized Drell-Yan processes, where one measures the product of two transversity distributions, and in Semi-Inclusive Deep Inelastic Scattering (SIDIS), where one couples h_1^q to a new unknown fragmentation function, the Collins function [5]. Similarly, one could couple h_1^q and the Collins function in transverse single–spin asymmetries (SSA) in inclusive processes like $p^{\uparrow}p \to \pi X$ [6].

Currently the knowledge on transversity comes from Semi Inclusive Deep Inelastic Scattering (SIDIS) experimentally observed at the HERMES [7], COMPASS [8] and JLab 6 [9], bringing informations on the convolution of the transversity and the Collins function.

The first extraction of the transversity distribution was provided in [10]. It is based on the spin asymmetries in the SIDIS processes and on the data from Belle [11] which provided the first direct measurement of the Collins function by the Belle collaboration from $e + e- \to h_1 h_2 X$ processes [12].

The most direct way to obtain information on transversity is the measurement of the double transverse spin asymmetry A_{TT} in Drell-Yan processes 1.1 with both transversely polarized protons and antiprotons:

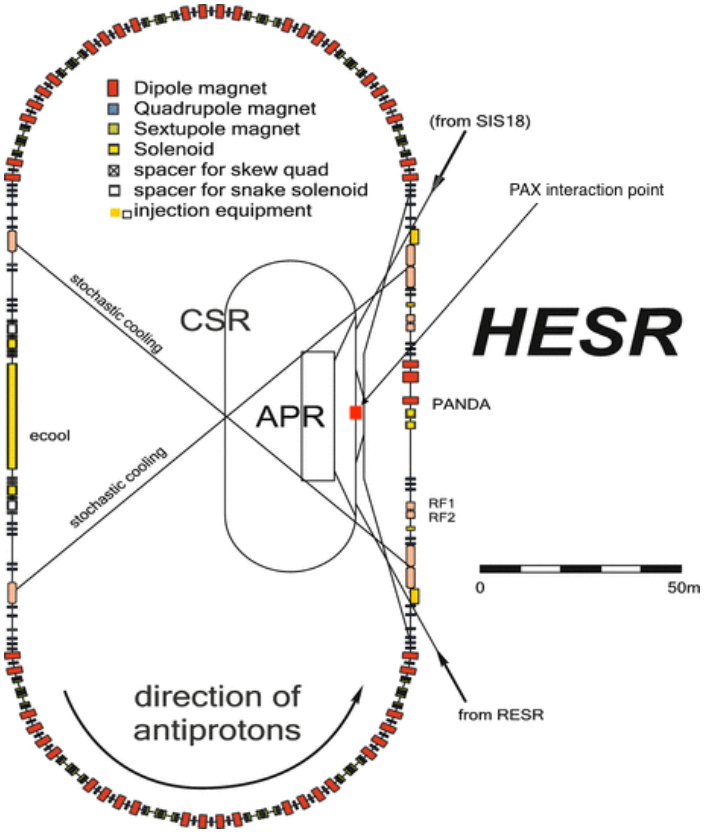

Figure 1.1: Floor plan for the HESR upgrade for FAIR. APR allows to spin-filter antiprotons. PAX interaction point serves for to collide antiprotons from CSR and protons from HESR [13].

$$A_{TT} \equiv \frac{d\sigma^{\uparrow\uparrow} - d\sigma^{\uparrow\downarrow}}{d\sigma^{\uparrow\uparrow} + d\sigma^{\uparrow\downarrow}} = \hat{a}_{TT} \frac{\sum_q e_q^2 h_1^q(x_1, M^2) h_1^{\bar{q}}(x_2, M^2)}{\sum_q e_q^2 1(x_1, M^2) \bar{q}(x_2, M^2)} \tag{1.1}$$

where $q = u, d \ldots$, and $\bar{q} = \bar{u}, \bar{d}, \ldots$, M is the lepton pair invariant mass and $\hat{a}_{TT}$ is the double spin asymmetry of the QED elementary process, $q\hat{q} \to l^+l^-$,

$$\hat{a}_{TT} = \frac{sin^2\theta}{1 + cos^2\theta} cos2\phi \tag{1.2}$$

where θ the polar angle of the lepton in the l^+l^- rest frame and ϕ the azimuthal angle with respect to the proton polarization.

The most valuable channel to perform a self sufficient measurement of A_{TT} is a process of $p\bar{p}$ interaction, where both the quark and antiquark from the proton and antiproton respectively contributions are large. The PAX collaboration has proposed a physics program with polarized antiporotons for the FAIR facility at Darmstadt [6].

PAX proposes to build a dedicated Antiproton Polarizer Ring (APR) in the High Energy Storage Ring (HESR) for the FAIR project at GSI (see

1.1). An asymmetric proton-antiproton collider, in which polarized protons with momenta of about 3.5 GeV/c collide with polarized antiprotons with momenta up to 15 GeV/c.

The machine has following features:

- An Antiproton Polarizer Ring build inside the HESR with the main point of polarizing antiprotons at kinetic energies around 50 MeV, to be accelerated and injected into the other rings.

- Cooler Synchrotron ring, where protons or antiprotons can be stored with a momentum up to 3.5 GeV/c. As COSY, the ring plans to have straight section, where PAX detector would be installed.

- The machine supports both of the collider of the fixed-target modes by deflection of the HESR beam into the straight section of the CSR.

Figure 1.2 shows the kinematical region covered by PAX experiment. For typical PAX kinematics in the fixed target mode ($s = 30GeV^2$) only quarks and antiquarks with large x contribute ($\tau = x_1 x_2 = M^2/s \simeq 0.2 - 0.3$), that means valence quarks for which h_1^q is expected to be large and not suppressed by the QCD evolution. The ratio A_{TT}/a_{TT} is expected to be as large as 30%. The (x_1, x_2) kinematical region covered by the PAX measurements, both in the fixed target and collider mode, are described in fig. 1.2 Left. The expected values of the asymmetry ATT as a function of Feynman $x_f = x_1 - x_2$, for $Q^2 = 16GeV^2$ and different values of s are shown in fig.1.2 Right. For the transversity distribution h_1^q this experiment plays the same role as polarized inclusive DIS played for the helicity distribution $\Delta q(x, Q^2)$, with a kinematical (x, Q^2) coverage similar to that of the HERMES experiment.

1.1.2 Production of polarized antiprotons

At workshops in Bodega Bay in 1985 [14], Daresbury in 2007 [15], different suggestions for polarization build-up techniques, like spin splitting in Stern-Gerlach separation [16] or production of polarized antiprotons form decay in flight of $\bar{\Lambda}$ hyperons [17] were proposed. Till now no polarized antiproton beams have been produced with only the exception of a low-intensity and low-quality, secondary beam from the decay of anti-hyperons that has been realized at Fermilab.

PAX collaboration is investigating possible mechanisms of production of polarized high intensity antiproton beams, making use of the COSY storage ring.

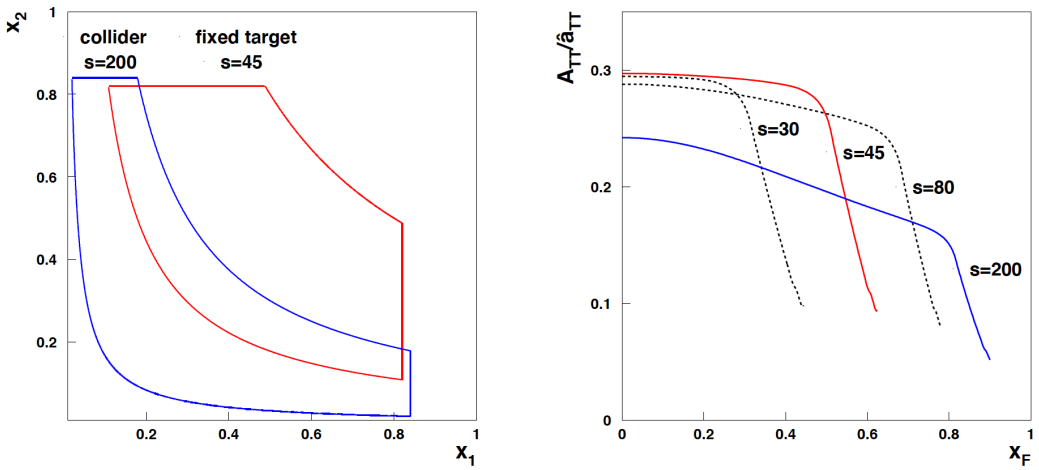

Figure 1.2: **Left:** Kinematic region covered by the $h_1^q(x)$ measurement at PAX. In the asymmetric collider scenario (blue) antiprotons of 15 GeV/c impinge on protons of 3.5 GeV/c at c.m. energies of $\sqrt{s} = \sqrt{200}$ GeV and $Q^2 > 4GeV^2$. The fixed target case (red) represents antiprotons of 22 GeV/c colliding with a fixed polarized target ($\sqrt{s} = \sqrt{45}$). **Right:**The expected asymmetry as a function of Feynman x_F for different values of s and $Q^2 = 16GeV^2$.

The COSY accelerator is utilized to test and commission experimental equipment and repeat spin-filtering experiment with protons in order to confirm understanding of spin filtering in terms of the machine parameters.

1.1.3 Spin filtering at COSY

After having shown the non-applicability of spin-flip to polarize a stored beam in situ [18], the PAX collaboration has successfully performed a spin-filtering test on protons with a transversely polarized hydrogen gas target [2]. The idea of spin filtering first was proposed by Csonka [19] and can be described as a spin-selective attenuation of the particles circulating in a storage ring. The total cross-section is different for parallel and antiparallel orientations of the spins of the beam and target protons, one spin orientation of the beam particles is depleted at a higher rate than the other. An initially unpolarized beam becomes increasingly polarized by repeated interaction with a nuclear polarized internal gas target (see Fig. 1.3) while intensity decreases with time.

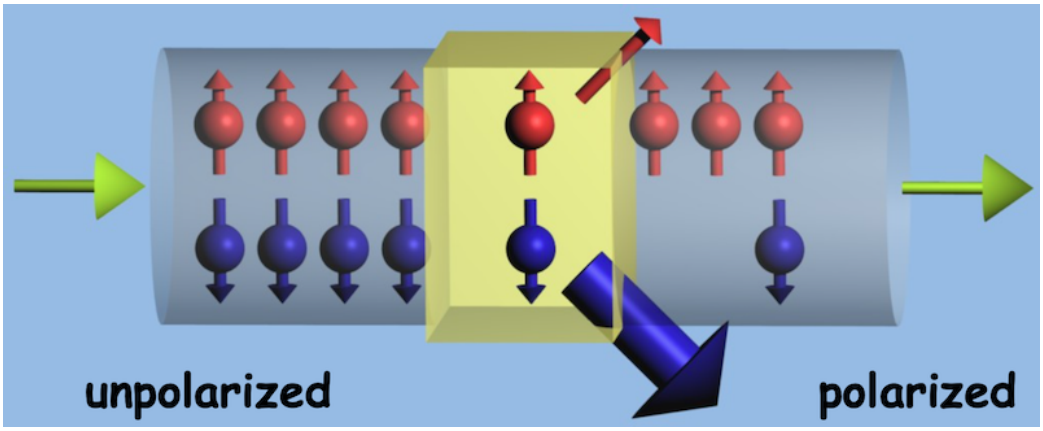

Figure 1.3: Spin-filtering concept. The spin-dependence of the hadronic interaction cause a selective discard of one spin state of the stored particles.

1.1.4 Transverse spin-filtering test

The purpose of the transverse spin-filtering at COSY was to measure of the spin dependence of the (pp) transverse cross section. The measurement can be determine the polarization induced in the stored beam as a result of interaction with a polarized hydrogen target.

The total interaction cross-section for the beam with the target could be expressed as [20]:

$$\sigma_{\pm} = \sigma_0 \pm Q\sigma_1 \tag{1.3}$$

where Q is the target polarization, σ_0 is the spin-independent part, σ_1 is the spin-dependent part of the total cross section. Parallel $(\uparrow\uparrow)$ or antiparallel $(\uparrow\downarrow)$ fractions of spin of the beam particles apply the positive or the negative signs respectively.

As a consequence of the interaction, the intensity of the spin-up and spin-down protons in the ring decreases exponentially with different time constants leading to a polarization buildup as function of time:

$$P(t) = \frac{N^{\uparrow}(t) - N^{\downarrow}(t)}{N^{\uparrow}(t) + N^{\downarrow}(t)} = \tanh\left(\frac{t}{\tau_1}\right). \tag{1.4}$$

The spin-dependent effective polarization buildup cross section $\tilde{\sigma}_1$ can be extracted from the observed time constant τ_1 of the buildup rate via

$$\frac{dP}{dt} \approx \frac{1}{\tau_1} = \tilde{\sigma}_1 Q d_t f \tag{1.5}$$

where Q is the target polarization, d_t it the target density in $atoms/cm^2$, f the particle revolution frequency and $\tilde{\sigma}_1$ indicates the effective polarizing

cross-section which accounts for the fact that only protons scattered at angles larger than the acceptance angle of the storage ring θ_{acc} contribute to the spin-filtering process $\tilde{\sigma}_1 = \sigma_1(\theta > \theta_{acc})$.

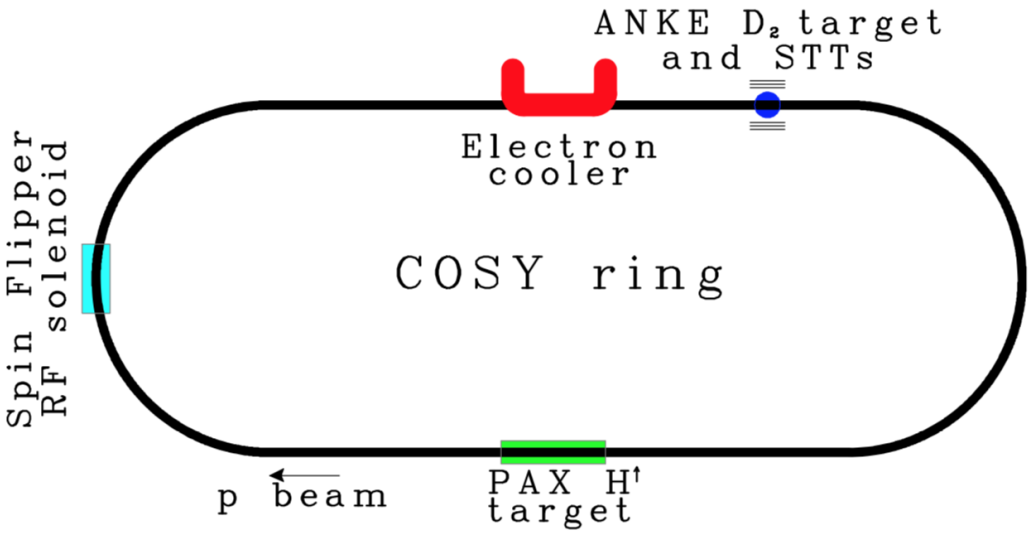

Figure 1.4: Schematic view of the COSY storage ring. The polarized hydrogen target is in- stalled in one of the straight sections of the ring; the RF solenoid of the Spin Flipper is located in one of the arcs, its use is explained in more detail in the text; the Electron Cooler, followed by the detector setup with Silicon Tracking Telescopes (STTs) to determine the beam polarization, is installed in the second straight section.

1.1.5 Spin filtering cycle

An overview of the COSY ring with the installations utilized in the test is presented in fig.1.4 The sequence of operation in a spin filtering cycle is as follows (see fig: 1.5)

- the unpolarized proton beam is injected in the COSY ring at 48 MeV. The beam is cooled and accelerated to an energy of 49.3 MeV for the measurement. This energy has been chosen because of the pd analyzing power, as already mentioned. The typical number of particles injected in the ring and accelerated for every cycle was $5 \cdot 10^9$.

- After the injection the spinfiltering cycle starts. At the PAX Interaction Point the polarized gas is injected into the storage cell and the holding

field coils are powered. The typical duration of a spin filtering cycle is 16000s, corresponding to two beam lifetimes.

- The PAX polarized target is switched off after the spinfiltering period, then the ANKE [21] deuterium cluster target and the data acquisition of the beam polarimeter are start. The beam polarization is reversed twice by means of the spin flipper during the spin polarization measurements, which allows the determination of the induced beam polarization for every cycle in order to reduce the systematic errors. The total duration of the polarization measurements is 2500 s.

- Spin filtering cycles are repeated for different directions of the target holding fields. A total of 48 spin filtering cycles with different orientations of the target holding field have been performed and more than $5 \cdot 10^{-7}$ deuterons and $2 \cdot 10^{-7}$ elastically scattered protons events have been recorded. A comparable contribution to the statistical error of the final result is expected from the two samples since the analyzing power of the protons is higher than the deuterons analyzing power.

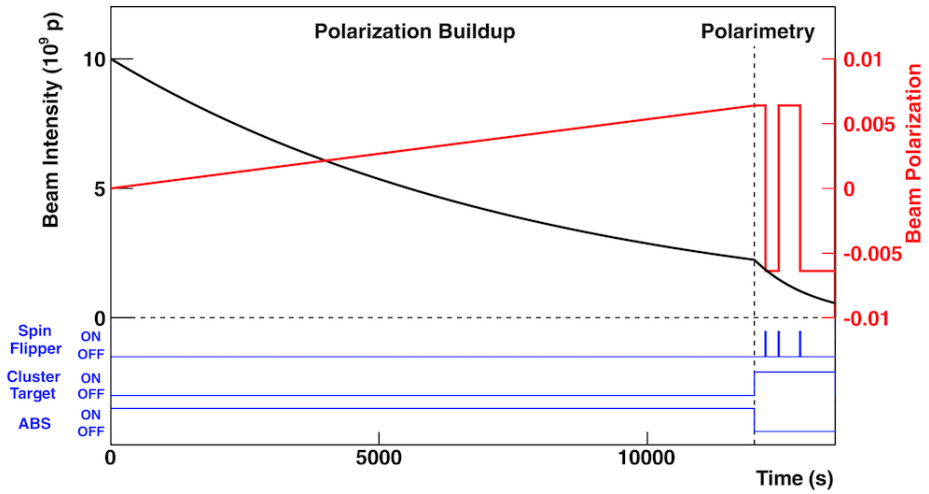

Figure 1.5: Schematic representation of a spin-filtering cycle. The black curve represents the beam current (left scale), the red one shows the polarization, induced in the beam (right scale). With the PAX polarized target on, while the beam current decreases, the polarization in the beam builds up. At the end of the spin-filtering cycle, the ANKE cluster target is used and the spin-flipper is switched on three-times to allow for the measurement of the beam polarization. Cycles with different orientations of the target holding field (HF) have been performed.

1.2 Longitudinal spin-filtering at COSY

Physical motivation for the longitudinal filtering measurement is the fact that different theoretical models for spin-filtering with antiprotons predict a significantly higher degree of polarization for the longitudinal case than for the transverse one.

PAX intends to transfer this method to longitudinal polarization to measure the complete spin-dependent cross section as described by the equation

$$\sigma_{tot} = \sigma_0 + \sigma_1(P \cdot Q) + \sigma_2(P \cdot k)(Q \cdot k), \tag{1.6}$$

where σ_0 denotes the total spin-independent hadronic cross section, σ_1 the spin-dependent cross section for transverse orientation of beam (P) and target polarisations (Q), σ_2 denotes the spin-dependent cross section for longitudinal orientation of beam and target polarisations, and k the beam direction (notation according to [22]). Once stored antiproton beams become available at FAIR, the collaboration would like to carry out the corresponding spin-filtering experiments to determine the unknown spin-dependent total cross sections σ_1 and σ_2 in double-polarized $p\bar{p}$ scattering.

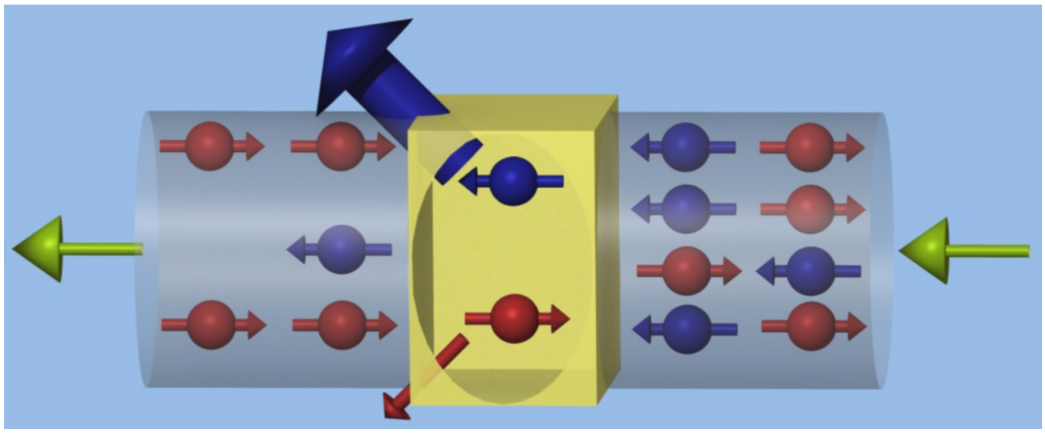

Figure 1.6: Spin-filtering concept. The spin-dependence of the hadronic interaction cause a selective discard of one spin state of the stored particles.

1.2.1 Experimental approach

The preferred direction of the polarization in a magnetic storage ring is vertical with respect to the beam momentum; longitudinal polarization requires the introduction in the ring of a dedicated solenoid, a so-called Siberian snake, by means of which the spin-closed orbit at the target is oriented along

the longitudinal direction. Such a snake has been installed at COSY in 2017 in the opposite straight section with respect to the PAX target installation and is ready for operation [23].

A conceptual scheme of a typical polarization buildup measurement cycle is shown in Fig.1.6. Spin-filtering and polarization measurement interval will be alternated to monitor the polarization buildup. The beam polarization will be determined by making use of the beam correlation parameter $C_{z,z}$ of the longitudinal spin-dependent p-p cross section:

$$\frac{d\sigma}{d\Omega} = \frac{d\sigma}{d\Omega_0} \cdot (1 + C_{z,z} P_z Q_z), \tag{1.7}$$

According to Eq. 1.7, the beam polarization can be measured by detecting the difference in the detector rates induced by reversing the direction of the target or beam polarization. As the polarization measurement requires the reversal of target or beam polarization, therefore stopping the polarization buildup process itself, the time intervals have to be properly optimized. The energy dependence of the longitudinal cross section favours the performance of the test at the maximal possible energy in the ring, where electron cooling is still possible. The experiment will therefore be performed at a proton beam energy of $T_p = 135 MeV$. A conceptual scheme of a typical polarization buildup measurement cycle is shown in Fig. 1.7. Spin-filtering and polarization measurement interval will be alternated to monitor the polarization buildup.

1.3 Test of time reversal invariance

1.3.1 Baryon Asymmetry of the Universe

The Big Bang theory predicts that in the initial stage of the Universe matter and antimatter were produced in equal amounts. Our everyday experience shows, however, that today the world around us consists almost entirely of matter. The so called "Baryon Asymmetry of the Universe" (BAU) represents one of the most fundamental challenges for the Standard Model (SM) of elementary particle physics, since it predicts a BAU of many orders of magnitude below observations.

The Standard Model is founded on the concept of symmetries, which is why precision experiments that test fundamental symmetries, offer the highest potential for the discovery of physics beyond the SM. One of the cornerstones of the SM is the CPT theorem that links C (charge), P (parity) and T (time) symmetries: according to this theorem, all physical processes are invariant under the simultaneous transformation of all three symmetries.

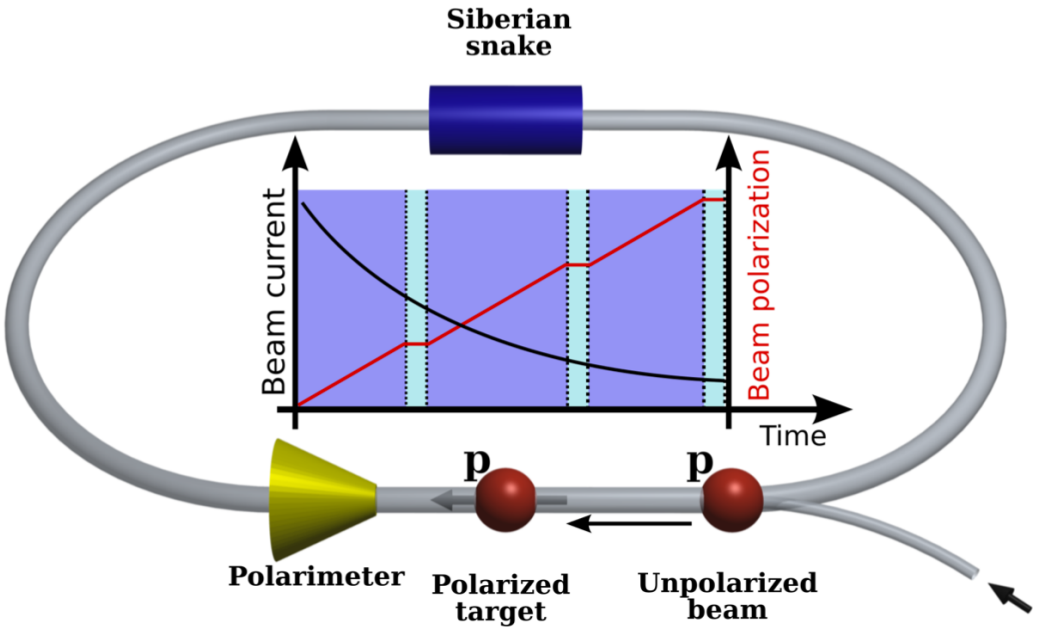

Figure 1.7: One cycle scenario for longitudinal spin-filtering. The measurement of the polarisation (light-blue) and polarization build-up by spin filtering (magenta) are alternated because they can not be be done simultaneously.

However, individual symmetries and combinations of two can be violated (see 1.8). For example the CP-symmetry and hence, assuming the CPT theorem, the T- symmetry is violated in weak interactions [24]. All the known CP-violating processes, discovered up to now, can be accounted for in the SM by introducing a phase in the Cabibbo-Kobayashi-Maskawa quark-mixing matrix of electroweak interactions [25]. In Quantum Chromodynamics the CP-violating process can be parametrized by a so called "θ-term" [26], the smallness of which, inferred from the neutron Electric Dipole Moment (EDM) limit, is not yet understood at all. It must be emphasized that a much larger CP violation is necessary to explain the BAU and thus our very existence in the world. This is why searches for T-V and CP- V have such an outstanding importance in the scientific programs at different experimental facilities all over the globe – TIVOLI will play a unique role among these searches, since the experiment will enable us to improve the current upper limit of the "time reversal violating, parity conserving" (T-VP-C), or "T - odd, P-even" strength by one to two orders of magnitude. The primary objectives of TIVOLI are: 1. To search for T-symmetry violation at the Cooler-Synchrotron COSY-Jülich using a polarized proton beam and an internal tensor-polarized deuterium target. This quest will make use of a

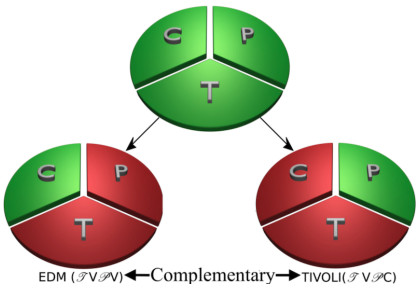

Figure 1.8: Assuming the validity of the CPT theorem, the TIVOLI project addresses one of the most fundamental challenges in modern physics, namely the baryon asymmetry of the Universe (BAU), in an approach which is independent, and yet complementary to searches for Electric Dipole Moments (EDM). While EDMs test interactions that violate Time Reversal Invariance and Parity simultaneously (T-VP-V), the TIVOLI experiment will investigate those interactions which violate Time Reversal Invariance, while obeying P-symmetry (T-VP-C).

novel method to measure the total cross-section in an internal target experiment [27]; 2. To provide the needed theoretical developments (see theory section below) and thus create the proper framework for the interpretation of the new data as well as a comparison with complementary results, e.g., from EDM searches. This combined effort will advance the understanding of T-V processes in a baryonic reaction and shed light on the mystery of the Baryon Asymmetry of the Universe.

1.3.2 Test of time reversal invariance

In contrast to the search for Electric Dipole Moments (EDM) [28], the existence of which would be a manifestation of the violation of parity (P) and time reversal (T) symmetries, it is proposed to perform a P-even, T-odd [4] null test of time reversal invariance with an accuracy of 10^{-6} at COSY (TIVOLI[1] experiment).

The parity that that conserves the time reversal is the total cross-section asymmetry $A_{y,xz}$. This value is measured with the help of a polarized proton beam with the energy of 135MeV and an internal tensor polarized deuteron target from the PAX source of the atomic beam.

In 1965 Okun [29], Prentki and Veltman [30], and Lee and Wolfenstein [31] postulated time reversal violating and parity conserving pure hadronic interactions as a source of CP-violation in kaon decays.

The term millistrong CP-violation (MSCPV) has been coined for such in-

[1]Time Invariance ViOlationf Interactions

teractions, and as far as CP-violations in weak decays are concerned, predictions from MSCPV would be similar to those from the Kobayashi-Maskawa mechanism adopted in the Standard gauge Model (SM) of weak interactions. While in the SM the CP-violation is confined to flavor changing transitions, MSCPV is flavor conserving. Henceforth it predicts time-reversal violation in a much broader variety of processes, including nuclear and strong interactions, nuclear β decays, and T-violating mixing of multipoles in nuclear γ transitions [32].

The strength of MSCPV can be estimated to be about 10^{-3} based on CP-violation in kaon decays and dimensional analysis. MSCPV predicts neutron EDMs of $d \approx 3 \cdot 10^{-26}$ e cm [33], about seven orders in magnitude larger than the SM predictions.

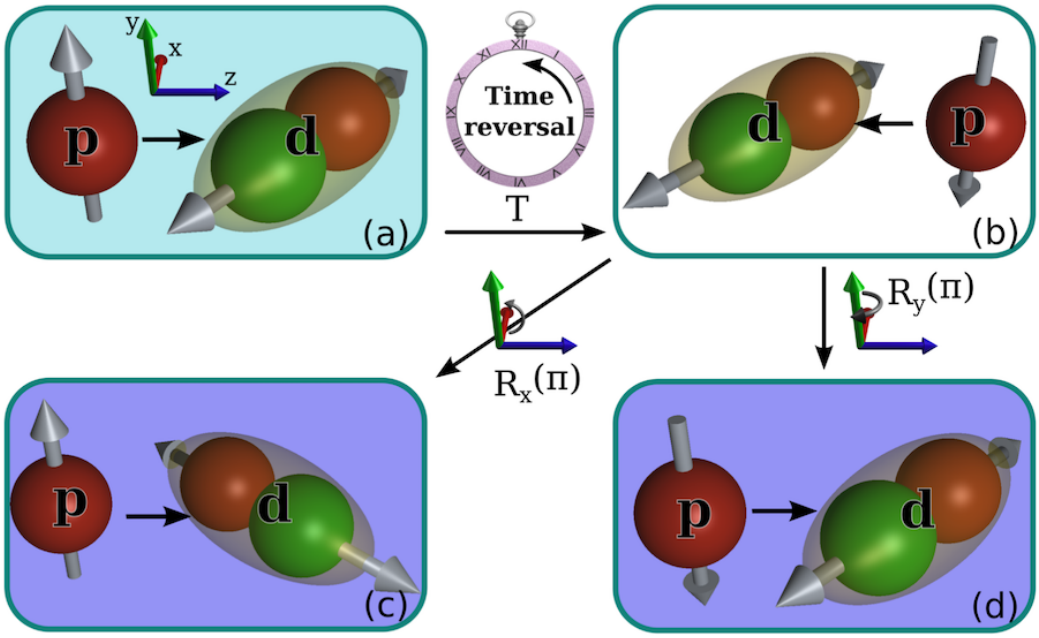

Figure 1.9: Either a proton or a deuteron spin-flip prepare in-principle demonstration of a time-reversed situation. (a) shows the basic system. (b) shows the time reversal operation is applied (momenta and spins are reversed and the particles are exchanged). In order to have a direct comparison between situation (a) and (b), two rotations $R_y(\pi)$ or $R_x(\pi)$ by 180° about the y- or x- axis are applied, leading to the situations (c) and (d), respectively. Time reversal operation allows these operations, since it is invariant under rotations.

Parity-conserving MSCPV has symmetry properties distinct from that of the QCD θ- term and can not be incorporated into the SM. Whether MSCPV

can be associated to CP-violation beyond the SM, called upon by the large unexplained baryon asymmetry of the Universe [34] is an intriguing open issue.

For the TIVOLI experiment at COSY, there is in fact one observable available, namely the total spin-correlation parameter $A_{y,xz}$ in proton-deuteron scattering with polarized beam and target, that would vanish in the absence of some T -odd P -even interaction [35]. By the generalized optical theorem, the imaginary part of the forward p-d elastic scattering amplitude with these spin orientations is linked to the integral cross section of the corresponding double polarized p-d interaction. At COSY this could be studied by arranging the proton beam polarization along the perpendicular direction with respect to the ring plane while keeping the tensor polarization of the deuteron in the (horizontal) ring plane at an angle of 45 (in the c.m. frame) between the beam and the radial direction.

The principle of the experiment is illustrated in the c.m. frame in Fig. 1.9, where it is shown that the combined application of the time-reversal and rotation operators leads to the same initial configuration, but with signs of the polarizations of either the proton or deuteron being reversed. Time-reversal invariance therefore means that the total cross section measured with configuration (c) or (d) should be identical to that obtained using (a). The ability to invert either of these polarizations allows a useful check of the systematics of the experiment.

The measurement of such a $\vec{p}\vec{d}$ total cross section in a transmission experiment with an external beam is much less efficient with respect to a storage ring, given the loss in statistics in a single pass configuration. In addition, in a storage ring, one can measure the total cross section simply by measuring the lifetime of the beam as it passes through the target [36–38].

1.3.3 Experimental approach for time-reversal test

The experiment is intended to be performed at 135 MeV.

Any proton energy for the TIVOLI measurements of $A_{y,xz}$ could be used, but there are good arguments for choosing $T_p = 135MeV$. Beyer actually predicted [39] that the sensitivity to T-violating forces should be maximal for T_p of the order of 125 MeV. On the practical side, high-quality polarimetry data for proton-deuteron elastic scattering are available at 135MeV [40]. In addition, at this energy the electron cooler can continuously cool the COSY beam over the complete cycle of measurements. It should also be noted that only one depolarizing resonance has to be crossed to arrive at this energy. The TIVOLI experiment could be carried out at the PAX internal target station. Using the new high precision beam current measurement system, COSY will

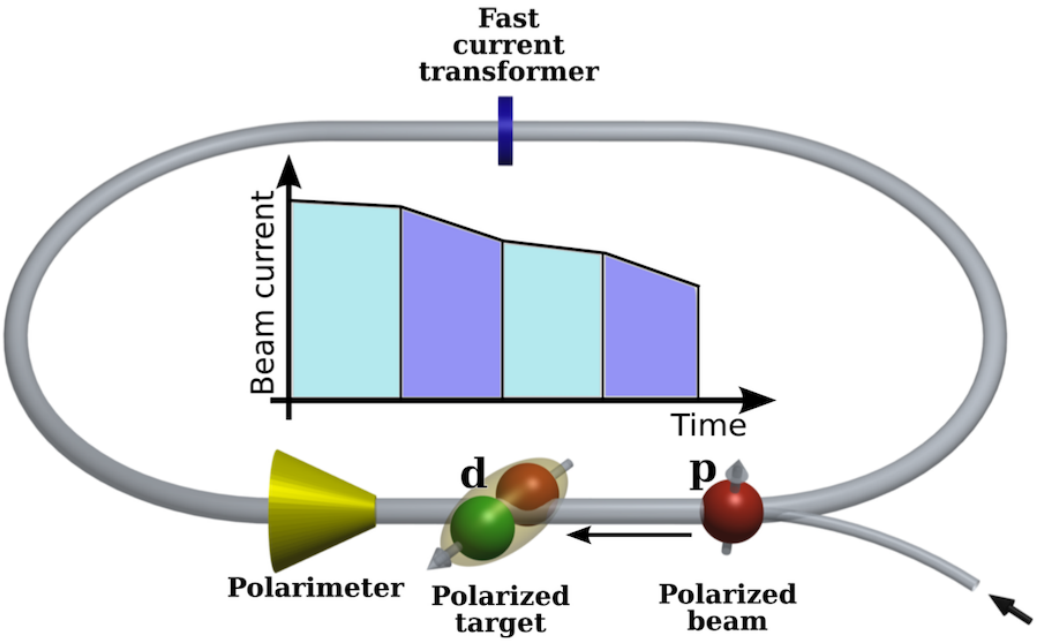

Figure 1.10: Time reversal invariance will be obtained by detecting the difference in the beam lifetime between the situations a) and c) or d), shown in Fig. 1.9. The scheme depicts main components of the experimental setup for the TIVOLI experiment: polarized beam from the injector cyclotron, polarized deuteron target from ABS, polarimeter and beam current sensor.

serve as accelerator, storage ring, and ideal zero-degree spectrometer and detector for the TIVOLI experiment.

The experiment is planned as a null transmission experiment in the storage ring using the T-violation sensitive observable $A_{y,xz}$ available in double-polarised pd scattering. A polarised proton beam, together with a tensor polarised deuterium gas target located the PAX interaction point, will be used for the experiment. The $A_{y,xz}$ observable will be determined from the difference of beam lifetimes measured for two independent beam-target spin polarisation states (see Fig. 1.10).

For this reason, the experiment puts stringent requirements on the precision of beam lifetime determination and consequently the resolution of the beam current measurement device. A resolution of $\Delta I/I = 10^{-}4$ integrated over one second of beam current measurement will allow us to improve the present upper limit on the T-violation by an order of magnitude in one month of measurement time [41].

Chapter 2

Experimental setup

The spin-filtering experiments and tests of time reversal invariance mentioned in Chapter 1 are performed at the COler SYnchrotorn of Research Centre Jülich. To perform these activities dedicated interaction point was designed and realized. In order to maximize the number of events in experiments one needs to increase density of target. Interaction point includes special target storage cell with diameter of approximately 1 cm to increase density of gas target and the same time reduce spoiling of vacuum in the COSY ring, low-β section with additional quadrupole magnets to squeeze the beam into the target cell, magnetic guide field system with field about 1mT to operate the orientation of the target polarization.

The accelerator facility COSY is described in Sec. 2.1. In Sec. 2.3, the PAX installation is explained, consisting of a low-β insertion, an atomic beam source (ABS), an openable storage cell and a so-called Breit-Rabi Polarimeter (BRP). The beam polarimeter, PAX detector system, which will be used to measure the polarization of the proton beam at the PAX target position, is briefly described in Sec. 3.1, and fully described in Chap. 3.

2.1 COSY

COSY is a so called COoler SYnchrotron that provides unpolarized and transversely polarized proton and deutoron beams. Synchrotron and storage ring COSY at Forschungszentrum Jülich are exploited by Institute for Nuclear Physics (IKP). Accelerator setup (Pic. 2.1) consist of JULIC(JUelich Light Ion Cyclotron), which accelerates ions of H up to 300MeV/c and ions of D up to 600MeV/c, negative ion sources of polarized and unpolarized ions H and D, and the ring with a circumference 183.4 m itself. The pre-accelerated ions are stripped off their electrons and remaining protons or deuterons are

injected into COSY (stripped injection) [42], where an acceleration of the particles up to 3.65 GeV/c can be achieved.

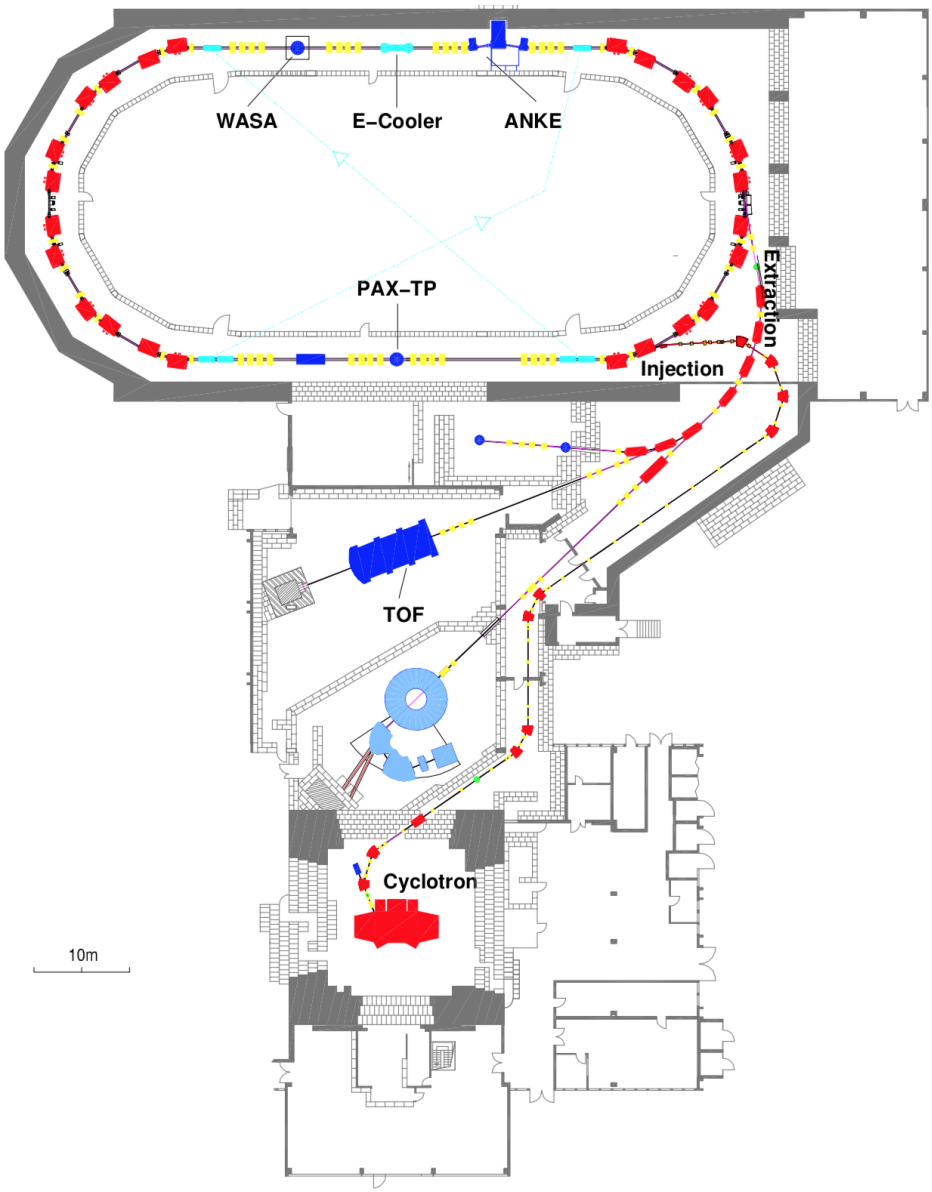

Figure 2.1: Floor plan of the COSY facility. The beam is pre-accelerated in the cyclotron JULIC before injection into COSY. Indicated in the straight sections are the internal experiments WASA, ANKE and PAX, as well as the electron cooler. For the external TOF experiment, the beam can be extracted after acceleration to the required energy.

For the purpose of shrinking the transverse equilibrium phase space and momentum spread two cooling system are used [43]. 100 keV electron cooling is available up to a momentum of 600 MeV/c and the stochastic cooling is applied in the momentum of the beam in the range from 1.5 GeV/c to 3.7 GeV/c. Cooled unpolarized proton beams, required for spin-filtering and time-reversal experiments, have been achieved with intensities up to $2 \cdot 10^{10}$ circulating protons in the ring with single injection and up to $5 \cdot 10^{10}$ protons with stacking injection [44]. Table 2.1 shows the maximum and typically used fillings of the COSY ring and where applicable the maximum and typical degrees of polarization for the different types of beams [44].

Beam	Maximum Filling [particles]	Typical Filling [particles]	Maximum Polarization [%]	Typical Polarization [%]
p	$1.4 \cdot 10^{11}$	$1.4 \cdot 10^{11}$	-	-
$\vec{p}$	$1.2 \cdot 10^{10}$	$1.0 \cdot 10^{10}$	85	70 - 80
d	$1.3 \cdot 10^{11}$	$1.3 \cdot 10^{11}$	-	-
$\vec{d}$	$6.0 \cdot 10^{9}$	$6.0 \cdot 10^{9}$	75	70

Table 2.1: Maximum and typically achieved fillings (number of particles stored in the ring) and degrees of polarization of COSY for different beam types

For unpolarized beams the maximum number of particles in the ring is in order of $1.2 - 1.4 \cdot 10^{11}$. The polarized beams have roughly 15 times less intensity for protons, and 20 times less particles for deuterons. The circulating beam is used in internal experiments, such as PAX, JEDI, tests of both of cooling etc., or extracted and delivered to the external target locations.

2.1.1 COSY lattice and low-β section

COSY is symmetrical accelerator with two 180° arc sections connected with two straight sections. The system could be tuned as telescopes with a 1 : 1 imaging with 2π phase advance. Each of the arcs is composed of three mirror symmetrical unit cells consisting of four dipole magnets (O), two horizontally focussing quadrupole magnets (F) and two horizontally defocussing quadrupole magnets (D).

Each of the six unit cells has a DOFO-OFOD structure. At COSY the two inner quadrupole magnets of a unit cell (F) are interconnected to the inner pair of the opposite unit cell located in the other arc. Such a group is called a quadrupole family. Since the same is true for the outer quadrupole magnets (D) of each cell, six quadrupole families are formed (QU1-6). A symmetric operation of all unit cells leads to a sixfold symmetry of the betatron functions

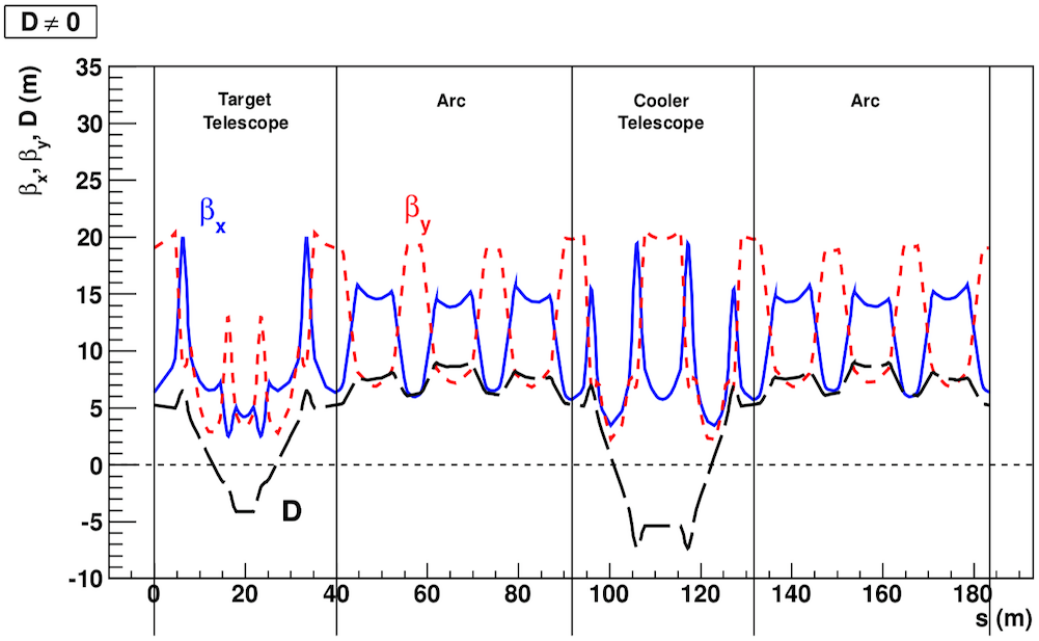

Figure 2.2: Optical functions (β_x, β_y) and dispersion D with standard settings ($D \neq 0$). Three similar unit sells cause a symmetric behavior in each of arcs.

[45]. Betatron functions describe the transverse vibrations of a particle in the focusing magnetic fields of an accelerator.

For the purpose of use dense polarized hydrogen storage-cell gas target low-β section is required. Low-β section allows to squeeze the betatron amplitude at the target position to about 0.3mm. In order to implement the low-β section, four quadrupole magnets from the decommissioned CELSIUS ring were installed in one of the COSY straight sections. Only minor modifications required to switch on the new PAX quadrupole magnets of the standard COSY operation settings at injection energy. The commissioning has shown, that the PAX optics caused neither additional acceptance restrictions nor shorter lifetimes. According to [23] a measurement of the β-functions at the positions of the new quadrupole magnets coincides well with the calculated values o about 0.3 m at the center of the target. Picture 2.2 shows behavior of the β-functions β_x, β_y and dispersion D for the typical COSY settings used for injection, while 2.3 shows behavior of β-functions β_x, β_y and dispersion D, where dispersion in strait sections is equal 0 because of broken sixfold symmetry specific settings of six arc quadrupole families, and is used as an advantage for the operation of the storage cell.

Based on the COSY lattice using the standard magnet settings, the optical functions were calculated with the methodical accelerator design (MAD)

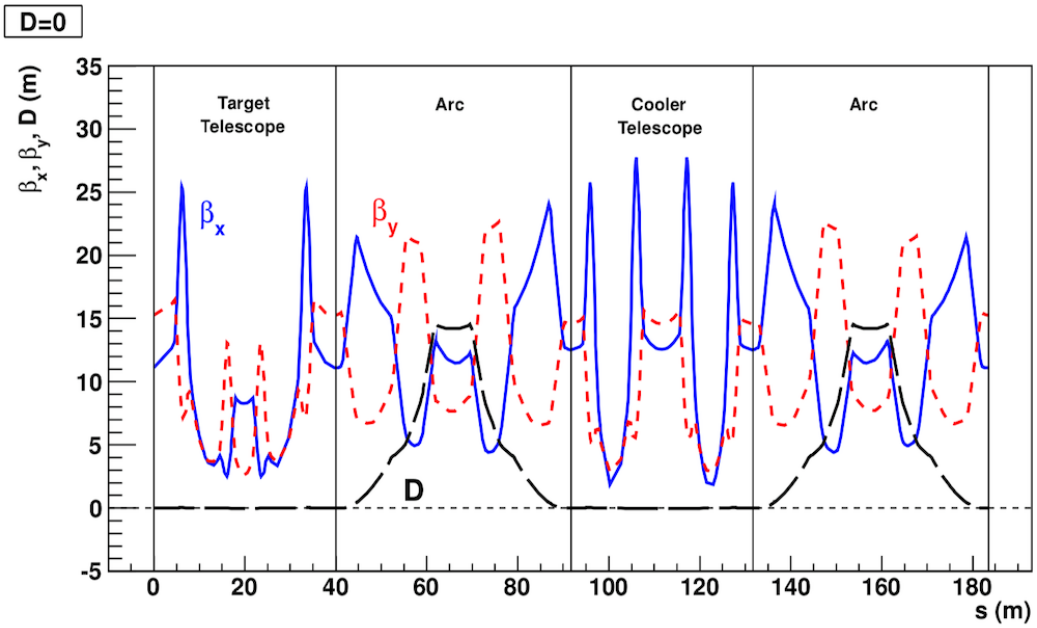

Figure 2.3: Betatron functions and dispersion for a $D = 0$ setting in the telescopes. As a result sixfolding symmetry breaks and the resulting optical functions show a twofold symmetry.

program, version 8 [46]. The results obtained with the PAX magnets switched ON and OFF are shown in Fig. 2.4, showing that β_x and β_y at the target point can be reduced by more than 1 order of magnitude. The minimal reached values are $\beta_{x,y} \approx 0.3m$. Reduction of β-functions at the interaction point, however, leads to increasing of β-functions up- and downstream, and reaching values of about 33 m (see Fig. 2.4, right panel). Therefore, excellent vacuum conditions also have to be maintained in these regions to avoid adversely affecting the beam lifetime (see Sec. 3.7).

2.2 COSY instrumentation

2.2.1 Beam current transformer

The purpose of a beam current transformer (BCT) is to measure the current of the circulating ion beam. The BCT electronics is based on the DCCT principle (DC current transformer) and could be set to deliver 1 V or alternatively 100mV output signal for 1mA of beam current [47]. Continuously recorded beam current from BCT determine the basis for the measurement

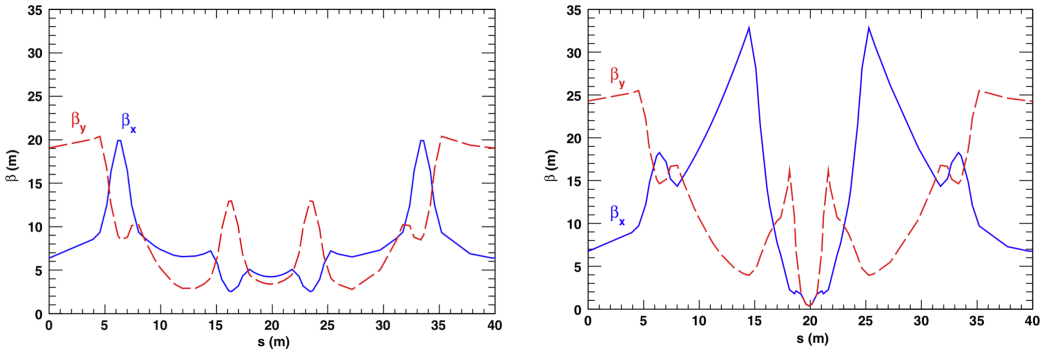

Figure 2.4: Calculation for β-function for standard COSY settings with $D \neq 0$ with PAX magnets switched OFF (left panel) and ON (right panel). Right panel indicates that the minimum of $\beta_{x,y} \approx 0.3m$ is reached at the target point at s = 19.87m. s = 0 is located at the beginning of the target straight section.

of the beam lifetime.

2.2.2 Beam position monitor

The beam position monitor (BPM) consist of two electrodes, providing sensitivity along the x and y directions. Design of electrodes is a cut from stainless tube, which matches to the size of the beam pipes, and placed in the straight and arc sections of COSY. Voltage induced on the electrodes by passing through of a bunch of charged particles, and depends of the distance between the beam and the electrodes. The position is determined from the voltage difference at the two electrodes $\Delta = U_1 - U_2$ divided by the voltage sum $\sum = U_1 + U_2$.

2.2.3 Movable frame system

A precise knowledge of the acceptance angle is required at the PAX target position. To this purpose a frame system (see. Fig. 2.5) was installed at target position before the experimental activity with target cell. It consists of three frames of $25mm \cdot 20mm$ and the tube of 9.6 mm inner diameter. The frame system is moved perpendicular to the beam allowing it to touch each frame individually, and observing the beam lifetime determinate the acceptance in three different positions along the target, i.e. the beginning, the end and the middle of the storage cell. The tube is used to precisely align the proton beam at the target prior to the installation of the storage cell [48].

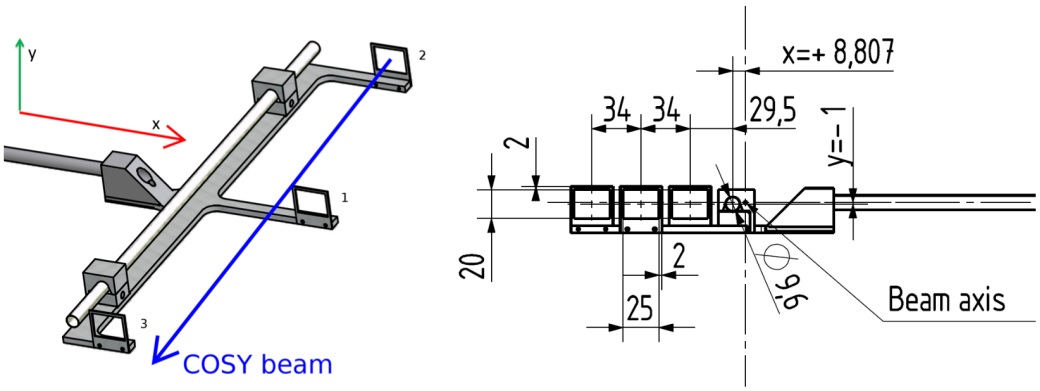

Figure 2.5: Movable system with three frames of orifice cross section. All the dimensions are given in mm.

2.2.4 Ionisation profile monitor

A fast and reliable nondestructive beam profile and position measurement is provided by an ionization profile monitor (IPM), developed in cooperation with the Gesellschaft für Schwerionenforschung mbH, Darmstadt, Germany (GSI). The stored beam interacts with residual gas and generates ions which are guided to a position-sensitive detector by transverse electric fields. The ion detection is based on an arrangement consisting of micro-channel plates, where secondary electrons are produced, a phosphor screen to produce light, and a CCD camera to detect the light. The system can record the beamwidth during the cycle with a resolution of 0.1mm [49].

2.2.5 H^0 monitor

Electron cooler monitored by H^0 monitor using the recombination of a small fraction of the protons and the electrons to neutral hydrogen atoms. Since those H atoms are not deflected by dipoles, they will immediately get lost at the end of a straight section. For beam diagnostics based on recombination a H^0 monitor is used and placed at the end of the cooler straight section in order to optimize electron cooling of protons. This consists of a multiwire proportional chamber, which measures the H^0 profile and scintillators for the determination of the intensity.

2.2.6 COSY vacuum system

All the experiments performed at particle accelerators in order to minimize particle looses caused by interaction with residual gas require high vac-

uum conditions. Typical average specified pressure at COSY to operate is $10^{-10} mbar$ [50] The accelerator ring is divided into eight vacuum sections by gate valves, in a manner such that each straight section and each bending section is subdivided into two subsections and each subsection forms an independent vacuum system, including different pumps, gas analyzers and pressure gauges. The system is completely remote controlled and provides vacuum safety interlock.

Both of experiments considered in this thesis are using internal gas target, what increases the load on the vacuum system of COSY ring. For the purpose of preserving the beam from significant loses outside of the target cell dedicated pumping system (see Sec. 3.7) is designed and realized.

2.3 PAX experimental setup

2.3.1 Atomic beam source (ABS)

Before experiments at COSY ring ABS was used in the HERMES experiment [51] [52]. For the spin-filtering studies of PAX experiment it was modified. A schematic drawing and a three-dimensional drawing of the Polarized Internal Target (PIT) is displayed in Fig. 2.6. Intensity from ABS is $I = 3.3 \cdot 10^{16} s^{-1}$ [53].

The dissociator dissociates hydrogen molecules into atoms in a gas discharge. The gas throughput is usually in a range between 0.5 and 3 mbar l/s, and results gas pressure in a range between 0.3 and 3 mbar. The discharge is sustained by plasma source, which consist of the field applicator and the discharge vessel. The microwaves in dissociator impact on free electrons in discharge which, in turn dissociate the molecules of hydrogen.

It has four chambers equipped with turbomolecular pumps to provide differential pumping and limit attenuation of the polarized atomic beam by residual gas and the deflected hyperfine states. The total pumping speed amounts to approximately 10^4 l/s, providing a pressure of 10^{-6} mbar in the last chamber close to the target chamber [54].

The working principle is in detail described in [55].

2.3.2 Breit-Rabi polarimeter and Target gas analyser

Breit-Rabi polarimeter gas analyser serves to measure and monitor the total target polarization. It counts the atoms as well as the molecules that constitute the target, taking into account as well the recombination of target atoms into molecules on the cell surface as a minor process.

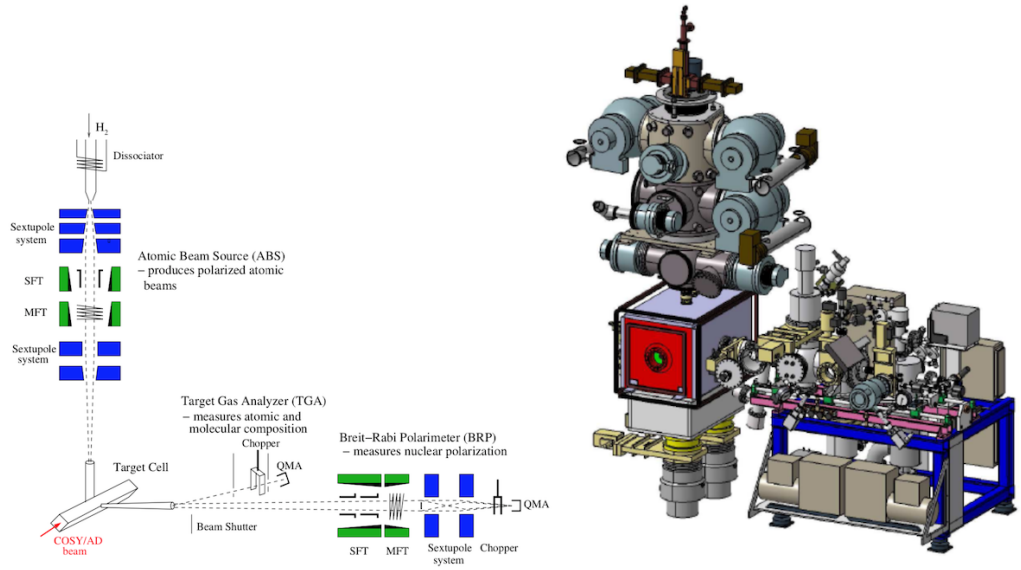

Figure 2.6: Left: Schematic drawing of the Polarized Internal Target with the ABS feeding the storage cell, the BRP, and the Target Gas Analyzer. Right: Three dimensional drawing of the ABS and the BRP.

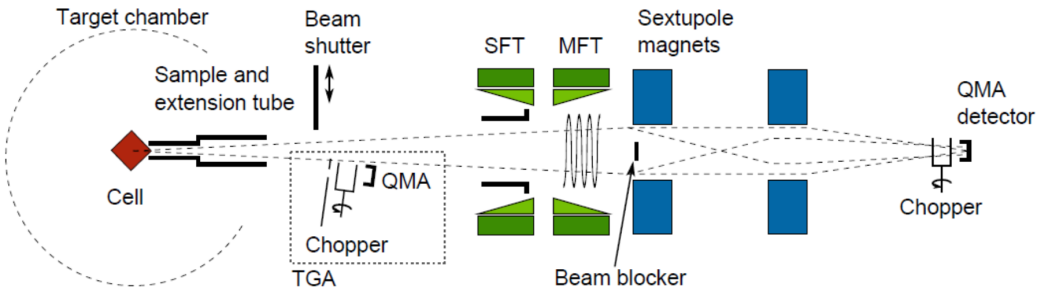

Figure 2.8: Schematic representation of the Breit-Rabi polarimeter and the target gas analyser it contains.

A feeding tube lays in horizontal plane and attached to the storage cell to extract a small fraction of less then 10%

2.3.3 Holding field

In order to provide a magnetic field of 1mT for the definition of orientation of the target polarization at storage cell and allow to reverse it in short sequence a magnetic guide system has been developed by the Zentralabteilung Technologie (ZAT) of FZJ [56] ($B_{y\uparrow}$ and $B_{y\downarrow}$). Small orbit differences in the arcs

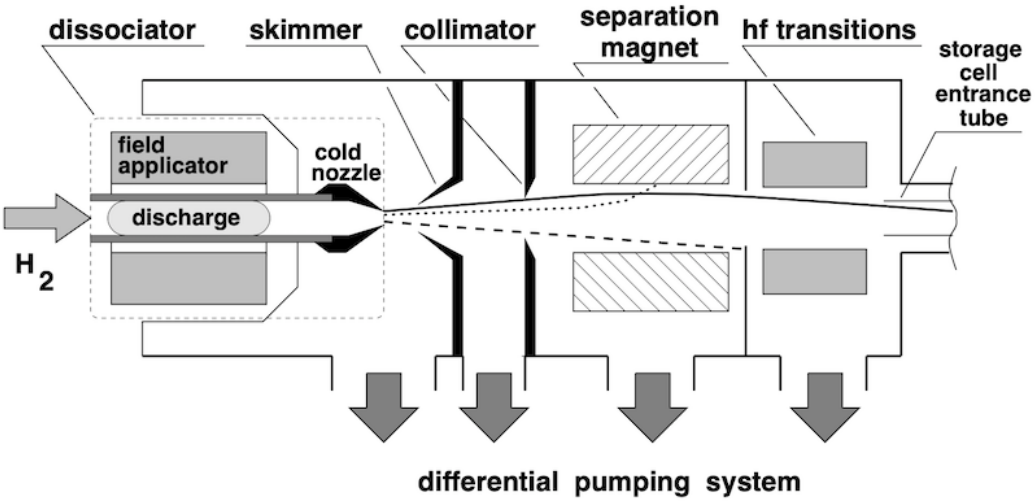

Figure 2.7: Schematic of polarized atomic beam source. Strong magnetic field applied to produce a nuclear polarized hydrogen beam. Atoms with electron spin $m_S = +1/2$ and =-1/2 and molecules are depicted with continuous, dotted and dashed lines respectively.

of $\Delta x \leq 0.9$ mm and in the straight section of $\Delta x \leq 0.2$ mm were observed, resulting satisfactory stability of the beam position in the accelerator.

The largest orbit displacements occur in the arcs, where the dispersion reaches values of $D \approx 15$ m (see Fig. 2.3). A system of coils (Fig. 2.9) that provides fields along x-, y-, and s- direction has been mounted in the target chamber. The system consist of three sets of Helmholtz coils, which providing magnetic holding fields in transverse x, y and longitudinal s directions. For the reason of compensation the magnetic field from holding coils and space optimisation and functionality, additional coils have been mounted on the edges of the chamber 2.9 The polarization of the gas atoms is known to be fully reversed within about 10 ms after switching the polarity of the magnetic field [57]. Both of holding field and compensation coils requires only a single power supply.

Test of the magnetic field B_y in the center of the target chamber was performed using a Hall sensor. Result of the test has shown a good agreement with the calculated magnetic field of 1.0 to 1.1 mT inside the storage cell and yields $B_{y\downarrow} = 1.08 \pm 0.03$ mT and $B_{y\uparrow} = 1.10 \pm 0.03$ mT, pointing downward and upward respectively. The calculations were performed in Amperes program [58] and a vertical magnetic flux density B_y displayed in 2.10.

The quality of the magnetic compensation scheme was determined using the dispersion-free setting (D = 0) of the telescopes by measuring the

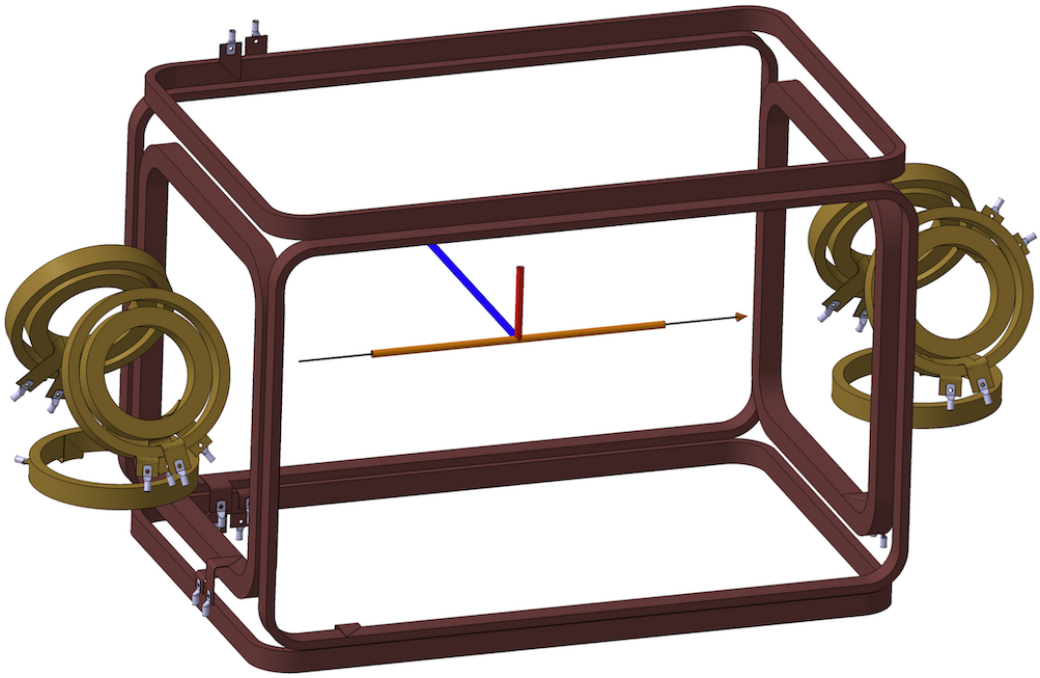

Figure 2.9: Technical drawing of the magnetic guide field coils. The large coils provide holding field along x, y and s directions. The small coils provide compensation for the incoming and outgoing beam for either horizontal x and vertical y orientations.

horizontal orbit difference $\Delta x = x_{B_{y\uparrow}} - x_{B_{y\downarrow}}$ for reversed vertical magnetic holding fields ($B_{y\uparrow}$ and $B_{y\downarrow}$) using the beam position monitors (see 2.2.2). Small orbit differences in the arcs of $\Delta x \leq 0.9$ mm and in the straight section of $\Delta x \leq 0.2$ mm were observed, resulting satisfactory stability of the beam position in the accelerator.

The largest orbit displacements occur in the arcs, where the dispersion reaches values of $D \approx 15$ m (see Fig. 2.3).

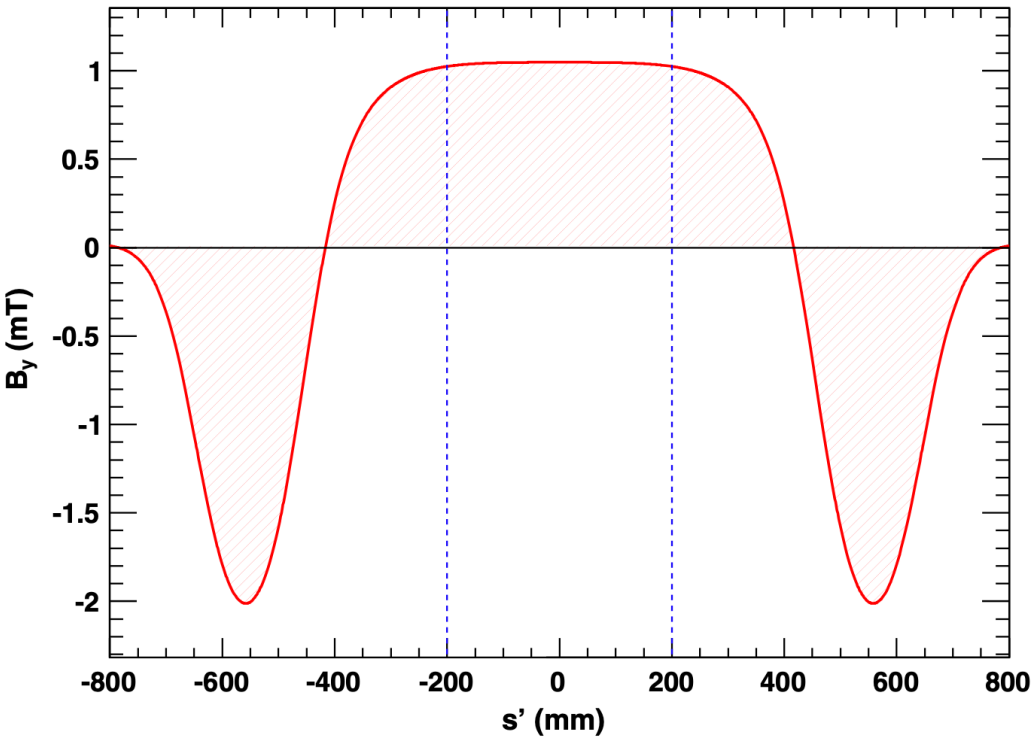

Figure 2.10: Vertical magnetic flux density B_y along the s' direction for the coil configuration of Fig. 2.9 calculated in MAD. The magnetic field about 1 mT located in the target cell region s' = -200 to +200 mm, indicated the vertical dashed blue bars.

Chapter 3

Detector setup

3.1 Detectors system

In order to perform the planned experimental activities, our group has realized a silicon vertex detector to serve as a beam and target polarimeter in proton-(anti)proton and proton-deuteron internal gas target experiments in the 30 MeV to 200 MeV beam energy range.

All of the components of the detector have been selected for high vacuum operation and were prepared and tested one by one to be compatible with in the 10^{-9} mbar range.

The detector composed of four identical quadrants combined in a diamond-shaped configuration. Target cell is located inside of the system, and has special insertion mechanism for independent from quadrants installation. It allows to inject polarized or unpolarized H or D target atoms and molecules. A picture 3.1 shows 3d view of the system, and picture 3.2 shows realized detector setup, mounted at the flange for PAX-chamber.

The detector system is used to measure the polarization of either the target or the beam or both. To perform such activity one needs to observe tracks and deposited energies from particles, deuterons or protons, which passed through the system, or stopped in it.

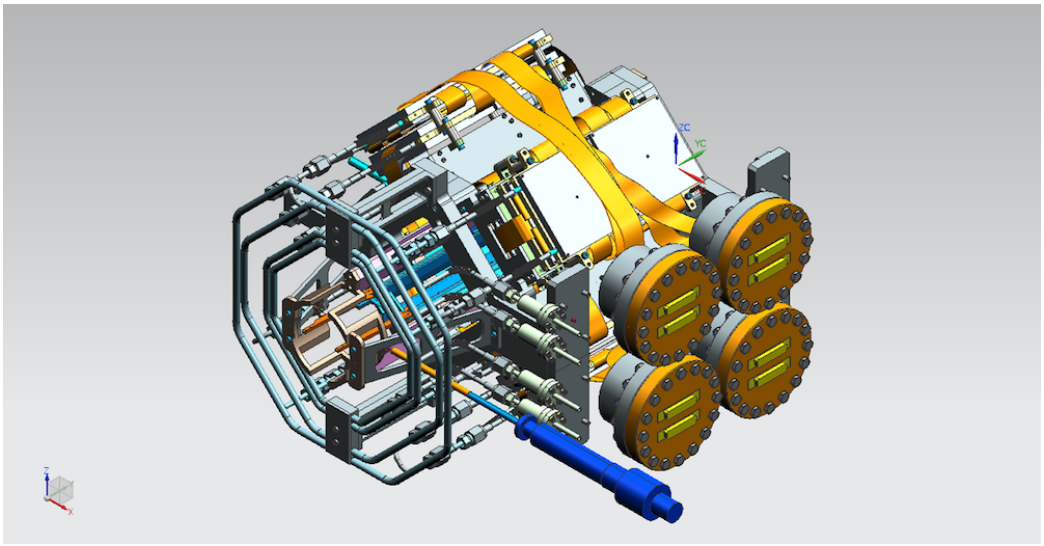

Figure 3.1: 3D view of the vacuum part of detector system. On the left side cooling pipes are depicted, with blue color actuator for openable storage cell is defined, yellow depicts electrical connections such as flat cables and flanges with feed-through DB50 connectors.

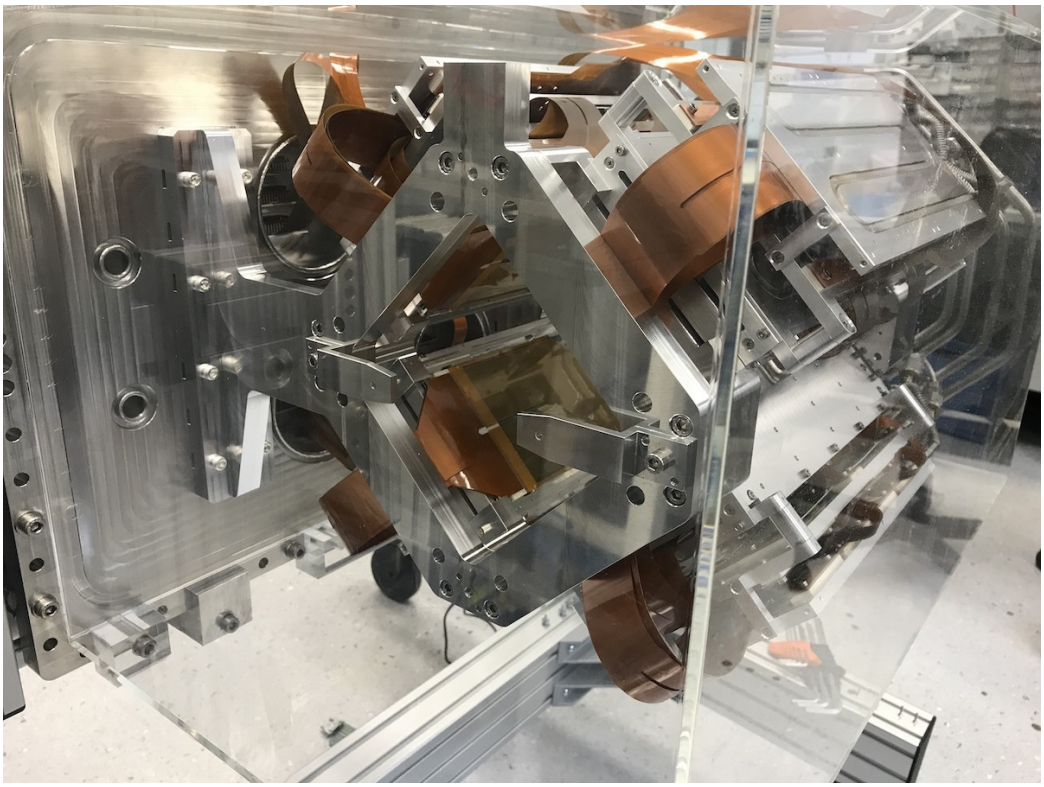

Figure 3.2: Photograph of the detector setup located at the vacuum flange and covered with protective plexiglas box.

All the parts of detector system and its tests, such silicon sensors, openable storage cell, cooling system, vacuum system, front-end and back-end electronics parts and assembly design, as well as working principle of a silicon strip detecor and required tests of parts of the system are considered in next sections.

3.2 Working principle of microstrip sensor

A solid state detector is a detector with a basis element $p - n$ junction and basically represented as a diode, with applied reversed depletion voltage.

A microstrip detector represents a solid state flat detector with common bulk material n-type (or p-type, but for ease of reference I will only consider n-type, explanation for p-type detector could be obtained by exchanging p+ and n+) and multiple isolated strip electrodes. When a particle gets into a semiconductor, ionization results in the formation of non-equilibrium carriers of the charge - electrons and holes amount of order 10^4, which, under the influence of electric fields, move to the electrodes. As a result, a current pulse occurs in the electrical circuit connected to the semiconductor detector. An amplifier (see Sec. 3.9) converts current pulse into a voltage pulse, the amplitude of which is proportional to the energy release of the particle in the semiconductor.

Typical density of electrons and holes in n-type silicon detector is $N_e \approx 10^{15} cm^{-3}$ and $N_h \approx 1 - 5 \cdot 10^{12} cm^{-3}$ respectively.

At the picture 3.3 depicted DC coupled strip detector (in our case it is applied to PAX detector type TTT2) a process of appearance of electron-hole pairs.

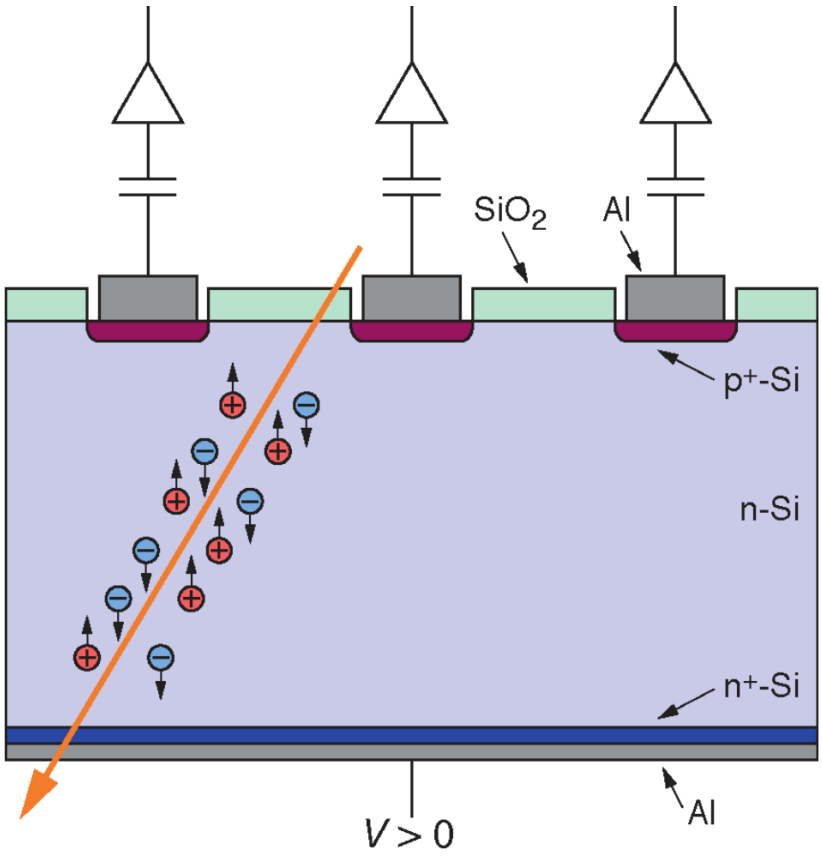

Figure 3.3: Working principle of a mictrostrip detector and production of electron-holes pairs. Aluminum electrodes directly connected to the detector strips.

Double sided microstrip detector have strips on both sides of the crystal placed perpendicular to each other, what allows to get information of both energy and position of particle interaction.

Picture 3.4 depicts AC coupled double sided strip detector with integrated coupling capacitances in standard planar process. (in our case it is applied to HERMES type TTT1)

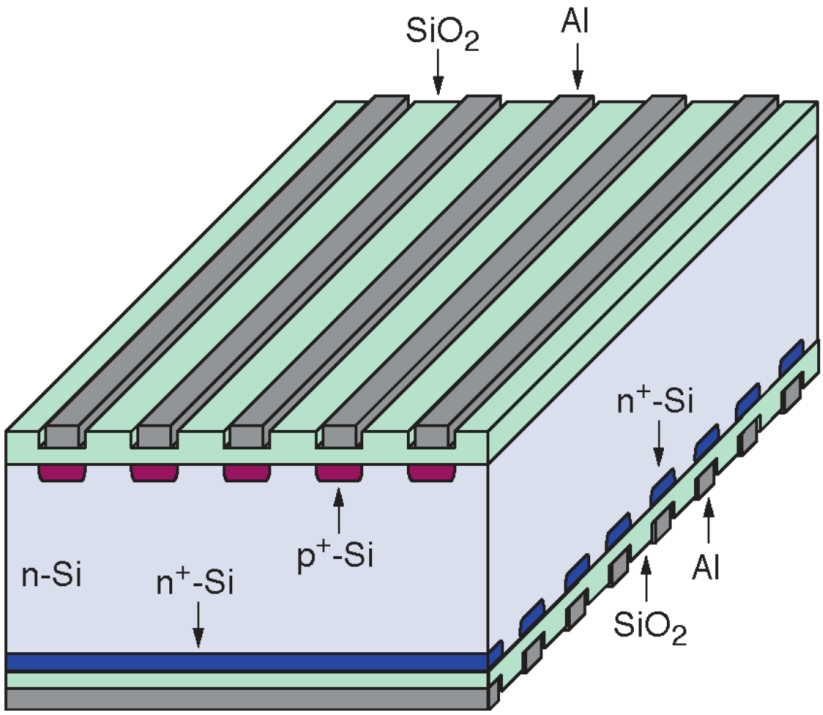

Figure 3.4: Scheme of a double sided strip detector. Aluminum electrodes are DC-isolated from detector strips by SiO_2.

3.3 The silicon sensors of the PAX-detector

Detector system uses three different types of sensors, all of them produced by Micron semiconductor Ltd in England [59], arranged one after each other:

- recoil detectors from HERMES experiment (3.5)
- $300\mu m$ thick PAX detectors (3.6)
- $1000\mu m$ thick PAX detectors

First two layers serves for particle tracking. The aim of the third layer is to increase the stopping power and to extend the detector applicability to the possible identification of deuteron-breakup events in the low energy domain.

The HERMES sensors [60] are two silicon wafers type TTT1 [59], thickness $300\mu m$, which glued together into a holding frame made of Shapal-M, which thermal expansion coefficient is very similar to that of silicon. Total area of each wafer is $99 \times 99 mm^2$, an active area of $97.3 \times 97.3 mm^2$ and a

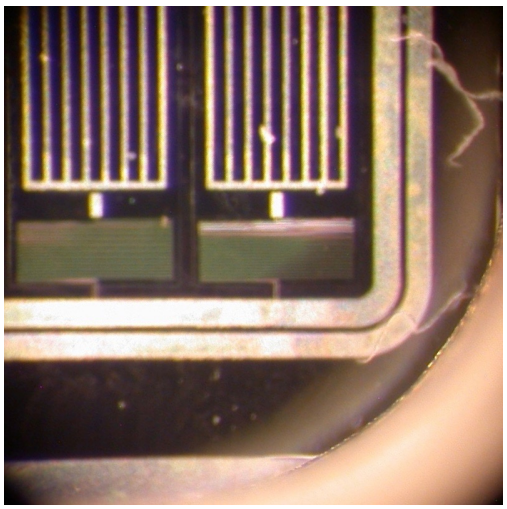

Figure 3.5: The microscopic photo of the structure of the one of HERMES detector.

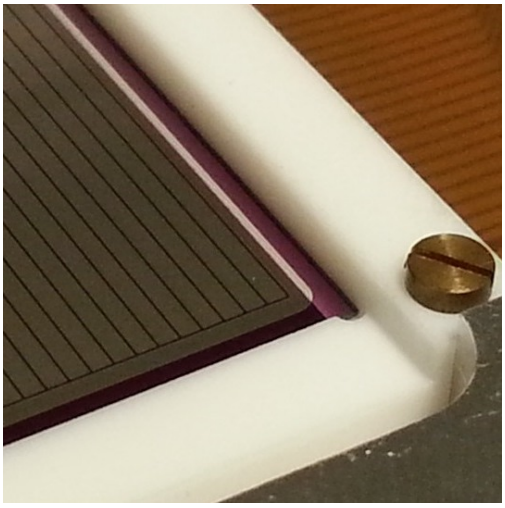

Figure 3.6: The photo of the structure of one of the PAX detector, which has no complicated structure.

pitch of $758\mu m$, when width of one strip is $702\mu m$. Geometry of the HERMES sensors is depicted at Fig. 3.7.

Detectors came from DESY in transport boxes and were not ready for using. Electronic board, which were used in previous experiment are not fit for the PAX experiment, and adaptation boards should be issued. Ceramic plates with kapton cables were designed and ordered to purpose of connecting detectors to preamplifier boards, used in the experiment. Detectors and adaptation boards were installed in specially designed and produced aluminum frames, then with the ultrasonic welding machine were bonded between each other. Some mistakes were made and corrected, for example: aluminum was polished, and the vacuum glue, joint frame and adaptation board, could not resist normal usage: one detector was almost lost.

Another big part of the work with HERMES detectors consisted of a selection of detectors in a good condition - during HERMES experiment detectors were in use, and got some traces of use. All of the detectors have and amount of damaged strips: some strips do not work at all, some strips generate very big noise. Such strips are excluded form trigger.

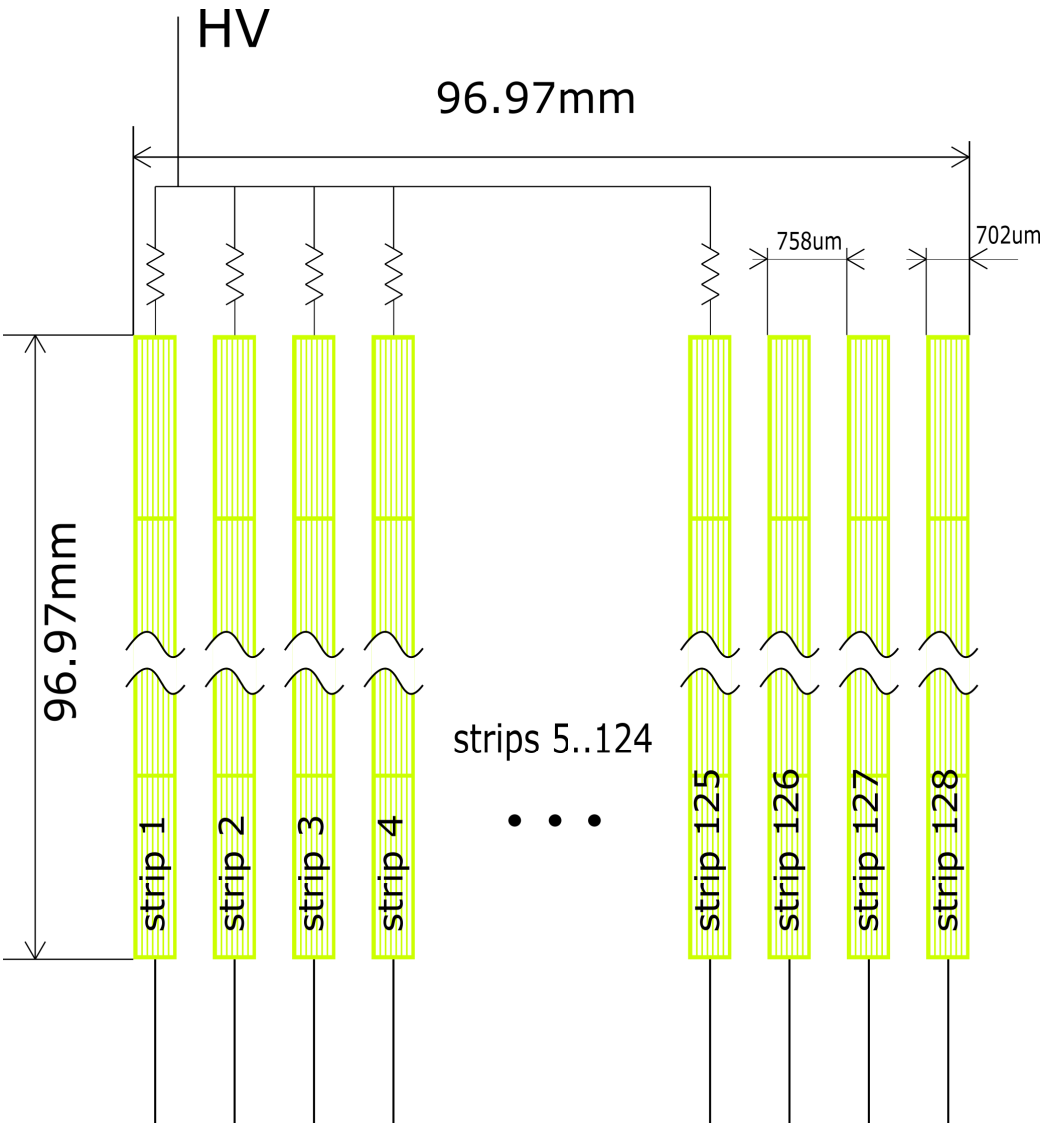

Figure 3.7: Geometry and connection scheme for both sides of the HERMES detector.

For the test purposes dedicated vacuum chamber was designed and produced. It consists of the pipes diameter 200mm (See 3.4).

The picture 3.8 shows the result of test of one of the detectors, irradiated with α-particles from ^{241}Am source. Right part of the picture shows the detector with both types of the damages. Left part is just shadowed with kapton-foil of the detector. After certain amount of tests it was concluded, that defects would show themselves even in shadowed part.

In the beginning of the selection activity we had eight detectors, and as a

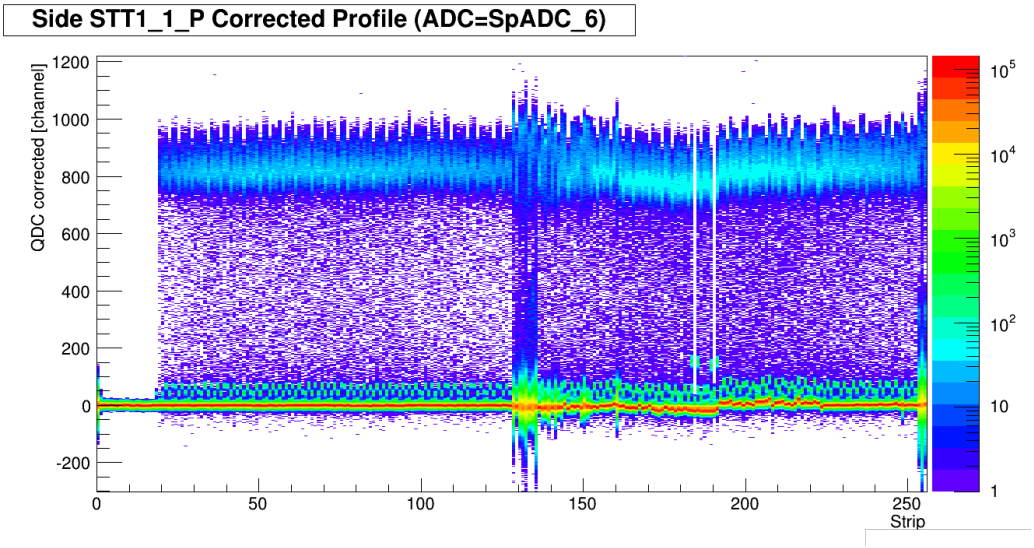

Figure 3.8: Defect strips of the HERMES detector. The strips number 184, 190 do not work, the strips number 128-135, 253-254 have a lot of noise. The beginning of the detector (0-19) was shadowed during the test from α-particles by kapton-foil of the detector.

result of this activity we got set four working detectors, and one spare for the spare quadrant. The amount of strips, excluded from trigger was between 3 and 10 strips for each side.

The $300\mu m$ thick PAX sensors are silicon wafer type TTT2 [59], glued into a holding frame made of Shapal-M, but in this case only one wafer in one frame. Thermal expansion coefficient of the frame is again very similar to that of silicon. Total area of each wafer is $102 \times 102 mm^2$, an active area of $100.42 \times 100.42 mm^2$ and a pitch of $760\mu m$, when width of one strip is $700\mu m$. Geometry of the PAX sensors is depicted at Fig. 3.9.

The PAX detectors were issued especially for this experiment, and need to be tested only to be sure, that there are no defects. The test were conducted in the same vacuum chamber and the same source of α-particles ^{241}Am. The results of the test showed, that no one defected strip was found. The example of the test result is present in A.2.

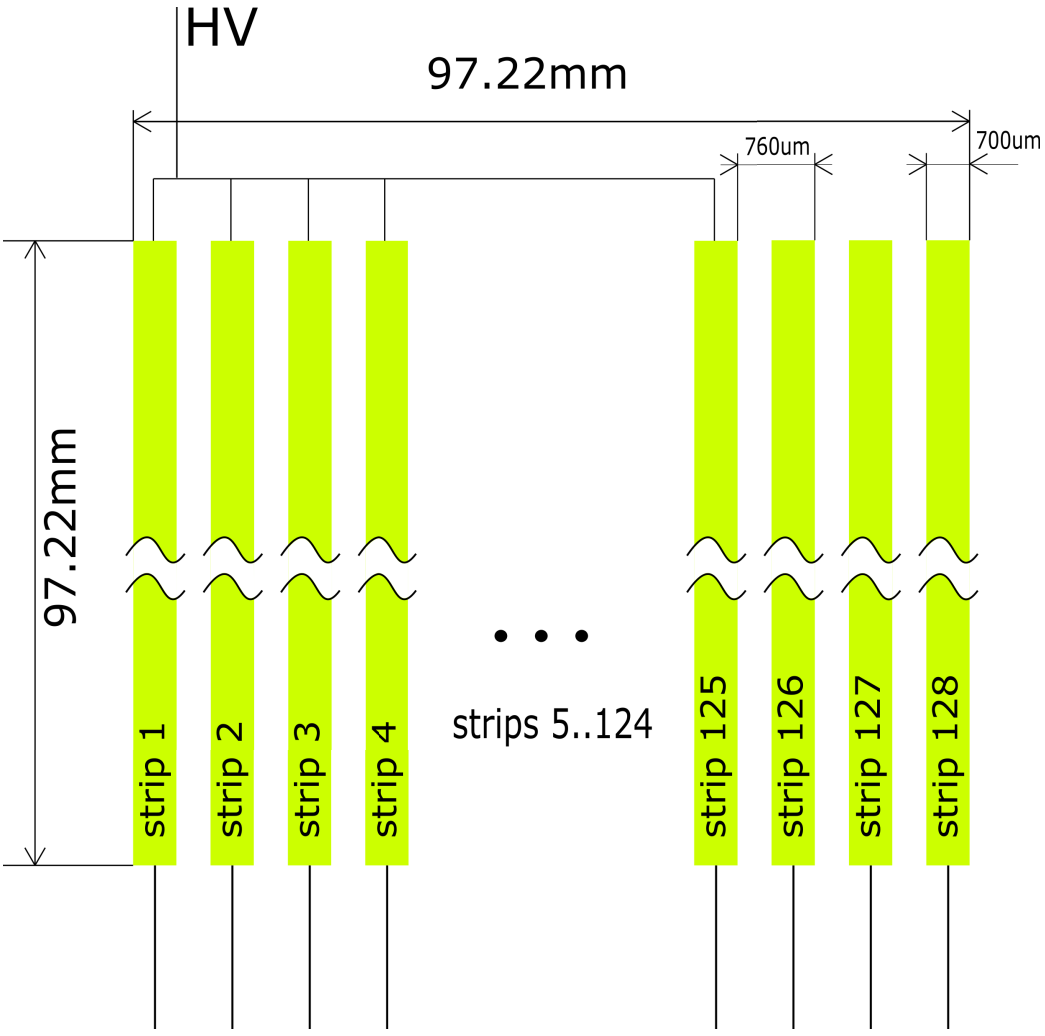

Figure 3.9: Geometry and connection scheme for both sides of both 300μm and 1000μm the PAX detector.

The 1000μm thick PAX sensors are made as 300μm thick wafers type TTT2 [59], glued into a holding frame made of Shapal-M, but in this case only one wafer in one frame. Thermal expansion coefficient of the frame is again very similar to that of silicon. Total area of each wafer is $102 \times 102 mm^2$, an active area of $100.42 \times 100.42 mm^2$ and a pitch of 760μm, when width of one strip is 700μm.

3.4 Quadrant assembly

The most responsible part of my work was quadrants assembly. Following pictures (3.10 3.11 3.12 3.13) shows short story of assemble procedure. Each quadrant has approximately one hundred of pieces, and assembled according to drawings, designed at Ferrara University. Because the assembly has sensible ceramics and silicon sensors each screw should be tightened with reasonable torque, and the same time the quadrant should have good thermal conductivity. First, aluminum parts are assembled with loosen screws, and only than, when every part take a right place one should tighten the screws. The last step after assembling quadrants is them installation to the support construction, mounted on a vacuum flange.

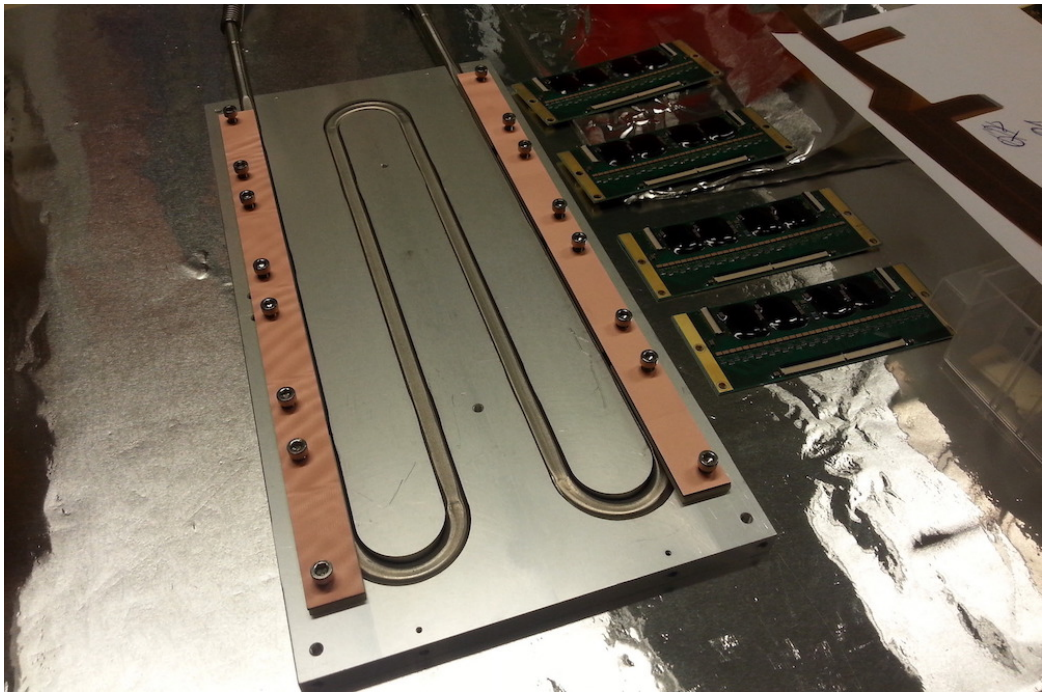

Figure 3.10: Cooling plate and four PCBs.

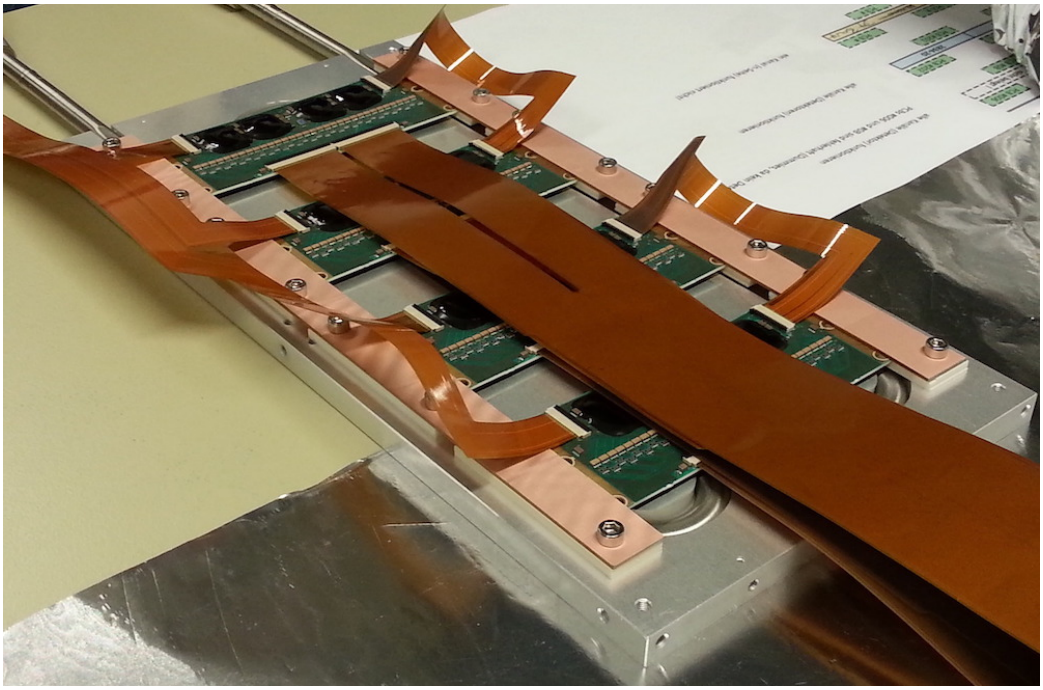

Figure 3.11: Assembled cooling plate with PCBs.

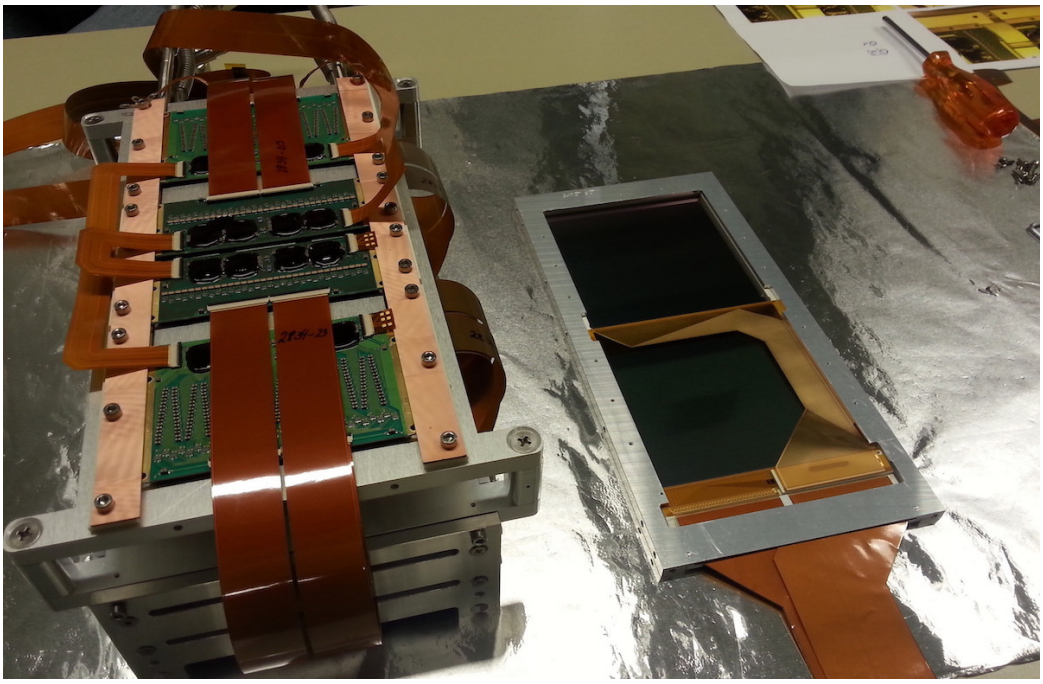

Figure 3.12: Preassembled quadrant.

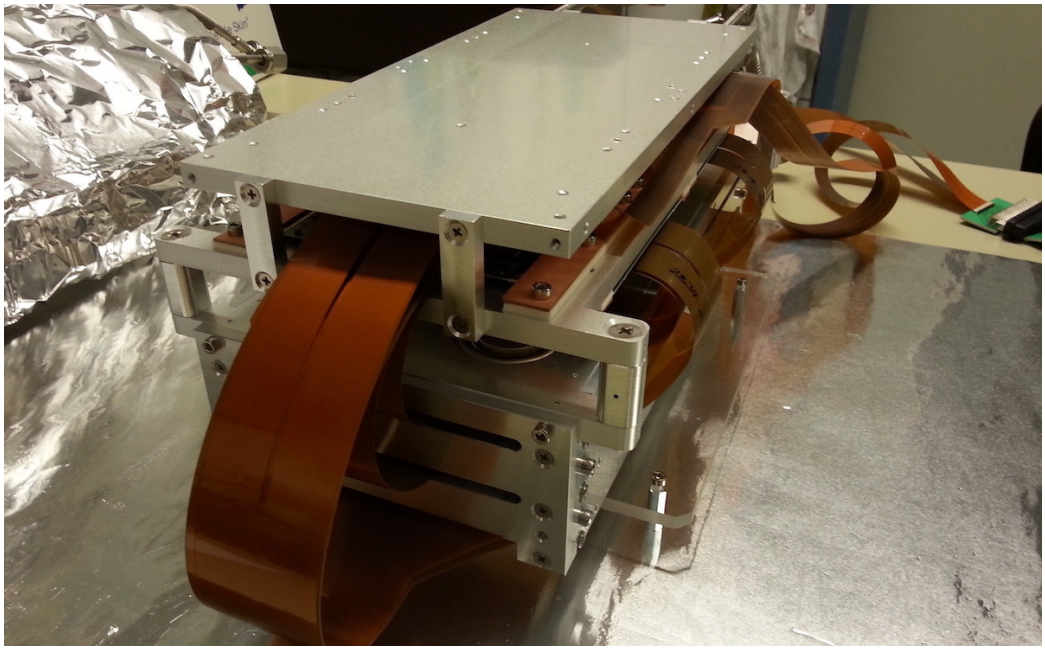

Figure 3.13: Assembled quadrant.

3.5 Openable storage cell

In order to increase gas density in the interaction point openable storage cell was designed (see 3.14) and produced by INFN-Ferrara mechanical workshop. The cell walls are covered with a $5\mu m$ Teflon foil which is known to reduce depolarization and recombination [61]. Distribution of the density of gas in storage cell, assuming linear decrease of the gas density from the center to the open ends is given by formula:

$$d_t = \frac{1}{2} \cdot \frac{l \cdot I}{C_{tot}} atoms/cm^2 \tag{3.1}$$

where $I[s^{-1}]$ is the intensity of the injected gas from the ABS, l [cm] the total length of the storage tube, and C_{tot} the total conductance of the storage cell. The conductance $[l/s]$ of a circular tube of diameter d_i [cm] and length l_i [cm] is given by formula:

$$C_i = 3.81\sqrt{\frac{T}{M}} \cdot \frac{d_i^3}{l_i + 1.33 \cdot d_i} \tag{3.2}$$

where T [K] is the temperature and M [u] the molar mass.

The sum of all conductances with respect to the cell center gives the total conductance C_{tot}. Geometrical parameters of the storage cell tube are l = 400mm, d = 9.6mm, parameters of the feeding tube are l = 100mm, d = 9.6mm, parameters of the extraction tube to the target polarimeter are l = 380mm, d = 9.6mm, and the total conductance expressed as $C_{tot} = 2 \cdot C_{1/2cell} + C_{extract} = 12.15 l/s$. An intensity from ABS injected into the feeding tube $I = 3.3 \cdot 10^{16} s^{-1}$ results an areal density expected of $d_t = 5.45 \cdot 10^{13} cm^{-2}$.

A target density of

$$d_t = (5.5 \pm 0.2) \cdot 10^{13} atoms/cm^2 \tag{3.3}$$

was deduced from the shift of the orbit frequency of the coasting beam caused by the energy loss in the target gas during the spin-filtering experiment.

The target chamber for PAX experiments at COSY was installed at PAX interaction point (PAX-IP) in 2016 with the detector system to perform experiment.. The purpose of the openable storage cell is providing high target density up to $5 \cdot 10^{13} atoms/cm^2$ during target gas injection and the same time increasing accelerator acceptance for the beam during injection and setting up of the working parameters of the particle accelerator. The storage cell is opened at beam injection, and closed after beam has been cooled and its emittance and size are consequently reduced. The gas is injected into the cell after it come to the close position.

Geometrical parameters of the cell are 40cm long and 1 cm diameter in closed position. Cell is a T-shaped pipe. Polarised gas can be injected into the cell through a tube installed in the upper part of the cell. A sample of the target gas diffuses through a side tube into a diagnose system, that measures the atomic polarisation (Breit-Rabi polarimeter [62]) and the atomic fraction (Target Gas Analyser [63]). The cell is realized with an aluminum foil of $50 \mu m$ thickness. To avoid depolarisation of the target gas the sell is covered with polytetrafluoroethylene [61].

A dedicated insertion mechanism allows for replacement of the cell without interference with the detector. The assembly of the four quadrants and the cell is accomplished by using a dedicated motor driven rotatable support structure on which the detector flange is mounted.

3.6 Cooling system

In order to ensure the best signal-to-noise ratio of the sensors and front-end electronics and to protect them from overheating in vacuum, a liquid cooling system has been designed and implemented. Cooling of the detector system

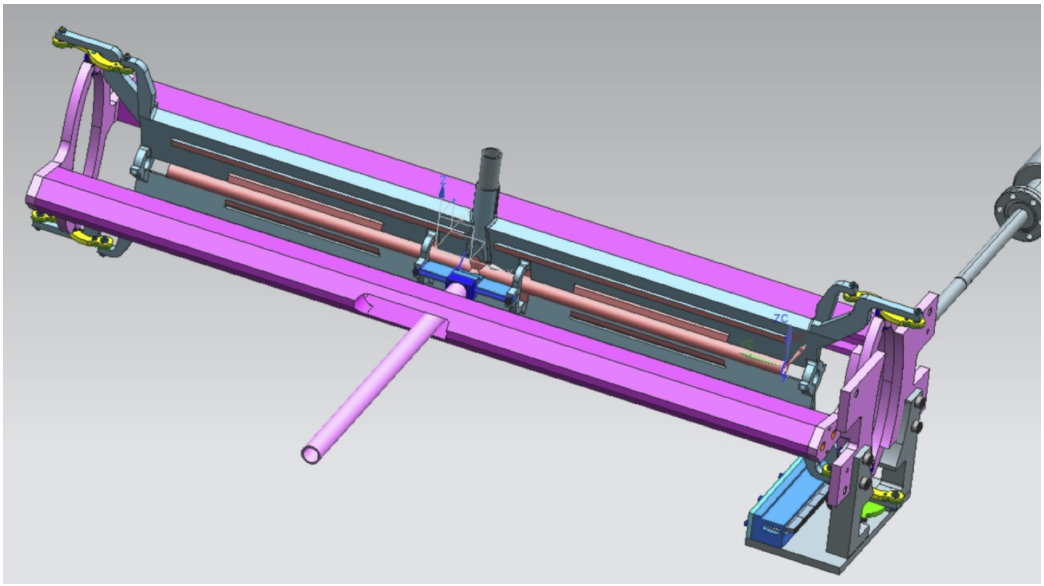

Figure 3.14: Storage cell in the closed position. The polarized or unpolarized atomic beam is injected into the cell throug a tube in the upper part of the cell (blue color). Sample of the target gas diffuses into the direction of the BRP system through a side tube (pink color).

is provided by Integral T 1200 LAUDA cooling modules [64]. Taking into account that cooler part of system condenses more water and other substances on itself, different temperatures for the silicon sensors and electronics is desired, As soon as silicon sensors are the most vulnerable to the damage during contacting any substance, higher temperature mode should be applied for the sensors. Basing on this statements and the fact, that preamplifier boards produce 15 W of heat per quadrant design of cooling system includes two circuits, and to LAUDA modules respectively. Such solution allows to choose the "right" temperature for the sensors, and make electronics part the "coolest" in the system. Parameters of temperature settings are based on thermal expansion coefficients of protection epoxies for the chips (see Sec. 3.9) to be in safe range of expansion. and having values of 5 °C for the sensors and 0 °C for the front-end electronics. To prevent freezing in system as cooling liquid is used mixture of alcohol and water in "vodka" ratio: 40% of alcohol, 60% of water. Each quadrant is equipped with thermocouple type K to have the feedback.

After mounting, the cooling system was tested with helium leak detector. The system was connected to leakage vacuum system, which measures partial pressure of helium, helium nozzle source was brought to possible leak

locations, but no leakage was found after several assembly procedures.

Cooling system provides thermal stability not only during normal operation, but also it prevents detector from overheating during reactivation of NEG pumps (see 3.7). Test for NEG pumps showed, that temperature in vacuum chamber rises up to 70 °C. The test was conducted without detector system, closed blinds, with two thermocouples K type, and sensors on NEG pumps.

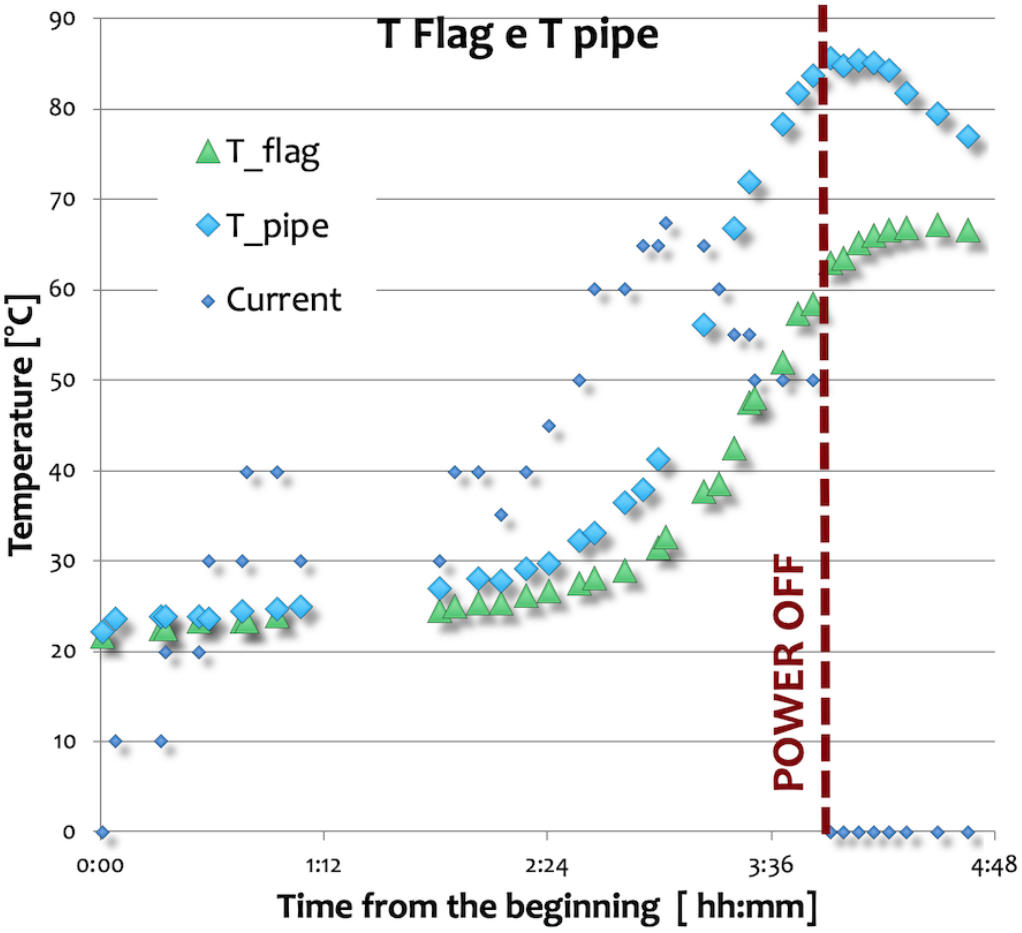

Figure 3.15: Dependence of the temperature of the vacuum chamber from time.

Graph 3.15 depicts the temperature of the pipe, and the temperature of the "flag", placed at the closest point of absent detector. The thermocouples had no cooling, and had good thermal insulation to walls of the vacuum chamber. Taking these facts into account, it can be concluded, that detector system would not be damaged during reactivation process of NEG pumps.

Additional feature of the cooling system is auxiliary function to provide deep vacuum. LAUDA modules supports big temperature range $-25+120\,^{\circ}\mathrm{C}$ [65], and one can "bake" complete detector system up to $40\,^{\circ}\mathrm{C}$. Such procedure helps to evaporate water from all the surfaces and especially from inside of kapton-cables, because they absorb water from air during assembling process.

3.7 Vacuum system

The expected polarization build-up in spin-filtering experiments at COSY is known to be small and the measurements confirms the calculation and shows that it takes 20000s at 49.3MeV to reach 1% beam polarisation.

For the successful measurement we need to achieve reasonable beam intensity after filtering. Considering the facts that the experiment is conducted on the internal gas target, a significant part of particles is removed by filtering and the same time should last for a relatively long time, strict requirements for vacuum condition should be applied in COSY in general, and particular at the interaction point, as soon as experiment requires feeding hydrogen or deuterium gas.

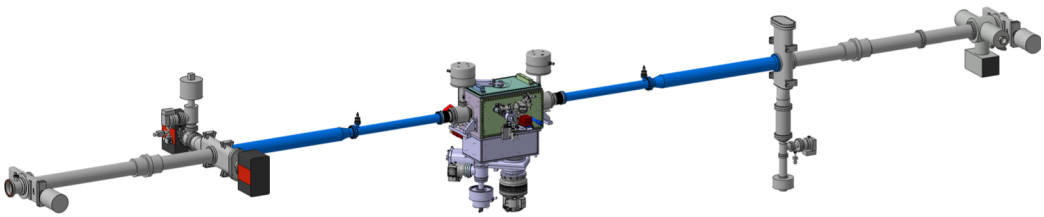

Figure 3.16: Schematic representation of PAX section. Blue depicts NEG pipes.

In conjunction to the COSY vacuum system, that is divided into eight vacuum sections by gate valves and that provide operating pressure 10^{-10} mbar [50], PAX interaction point has its own complex vacuum system, PAX vacuum section depicted at 3.16, and has following features:

- 10 SAES getter pumps GP 500 MK5 Non-evaporable getter (NEG), each providing a nominal pumping speed of 1200 l/s for H_2 [66];
- 1 HiPace 1800 turbo pump with a nominal pumping speed of 1700 l/s for H_2 installed below the target chamber [67];

- flow limiters are installed on inlet and outlet of a beam-pipe, have an inner diameter of 19 mm and a length of 80 mm, and reduce the target gas flow into the neighboring sections;
- 2 NEG coated pipes on inlet and outlet of target chamber with a nominal pumping speed of $2 \cdot 5000$ l/s for H_2

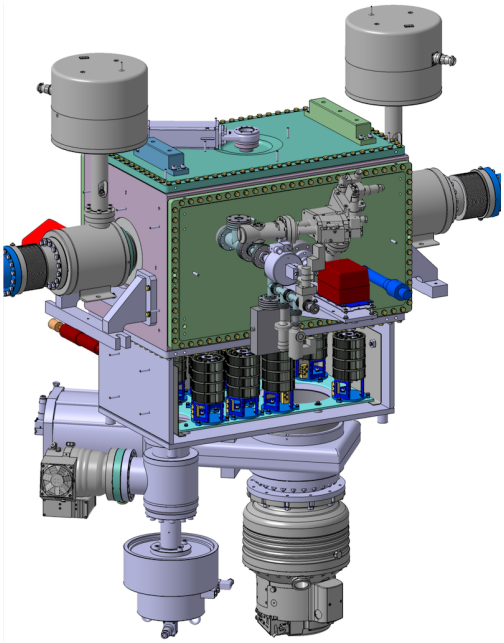

Figure 3.17: 3D view of the PAX chamber. Fast shutters placed on inlet and outlet of chamber for emergency case, 10 NEG pumps are observable in "transparent" wall, turbomolecular pump creates necessary pressure for NEG pumps to operate.

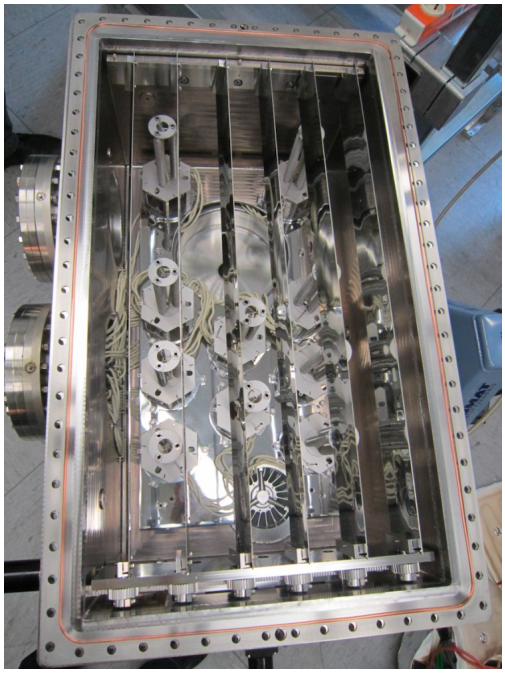

Figure 3.18: Photograph of opened chamber with missing NEG cartridges, only heatable supports are mounted, and opened blinds, mentioned in 3.6

Auxiliary devices to prevent increasing of the pressure in accelerator are "diaphragms" on the sides of the vacuum chamber, preventing flow of the gas to accelerator.

For the reason of small mechanical sizes and the same time high pumping capacity and speed NEG pumps are used, with a total speed of 12000 l/s for H_2. Special reactivation procedure is prescribed for the NEG pumps and should be taken into account. Non evaporating getter's main part is coating surface based on the ST 707 getter material, alloy, which consist of 70%

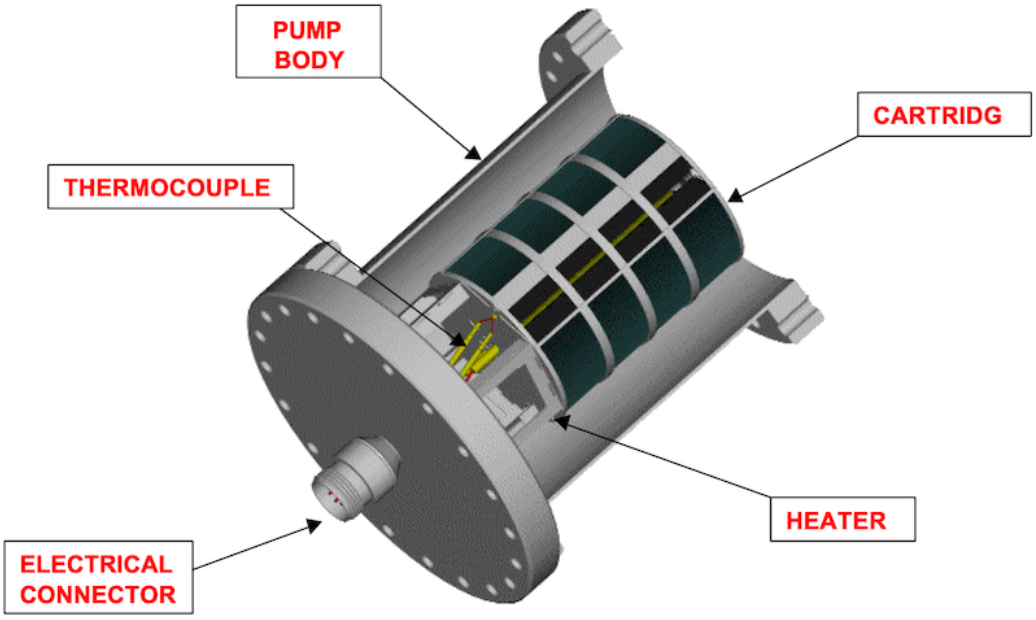

Figure 3.19: Schematic representation of one NEG cartrige

Zirconium, 24.6% Vanadium and 5.4% Iron [68]. Active surface of one getter is $14290cm^2$. Heater is made of a tantalum wire spiral wound on a alluminia element and equipped with a K type thermocouple. Picture 3.19 depicts these parts. During normal operation of getters the surface of alloy becomes covered by passivation layer of mainly carbides and oxides, which should be eliminated to start the gettering action and allow gas molecules to reach with the alloy.

To accomplish this, the getter is heated under vacuum to a sufficiently high temperature for a short time. This process, called reactivation, see 3.20, causes the passive film to difuse into the bulk of the getter, making the surface active for sorbtion.

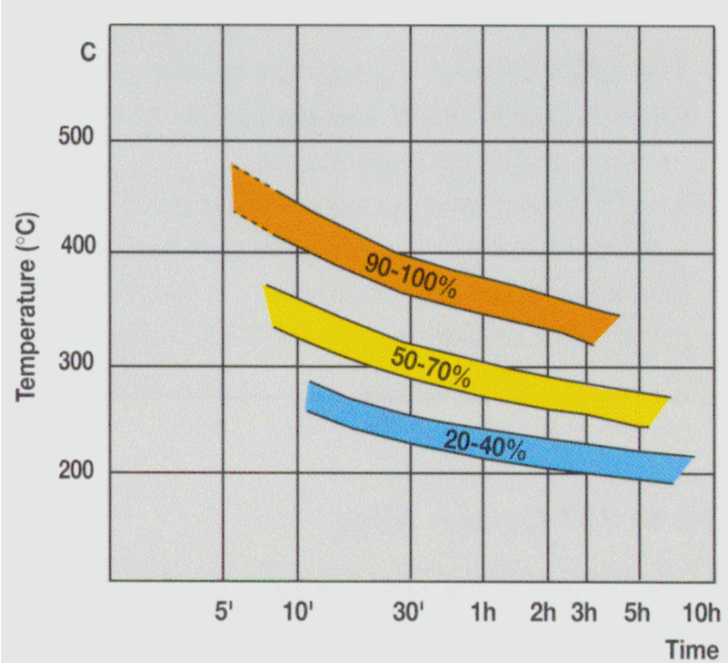

Figure 3.20: Activation conditions and gettering efficiency

As soon as NEG pumps during activation are heated up to 550 °C, additional temperature tests of the vacuum chamber are desired. Picture 3.21 depicts the temperatures of the "coolest" and "warmest" pump. As it was said in part of cooling system detector system during pumping heated up to 40 °C. This procedure helps to evaporate water from the kapton-cables of detector system, and may

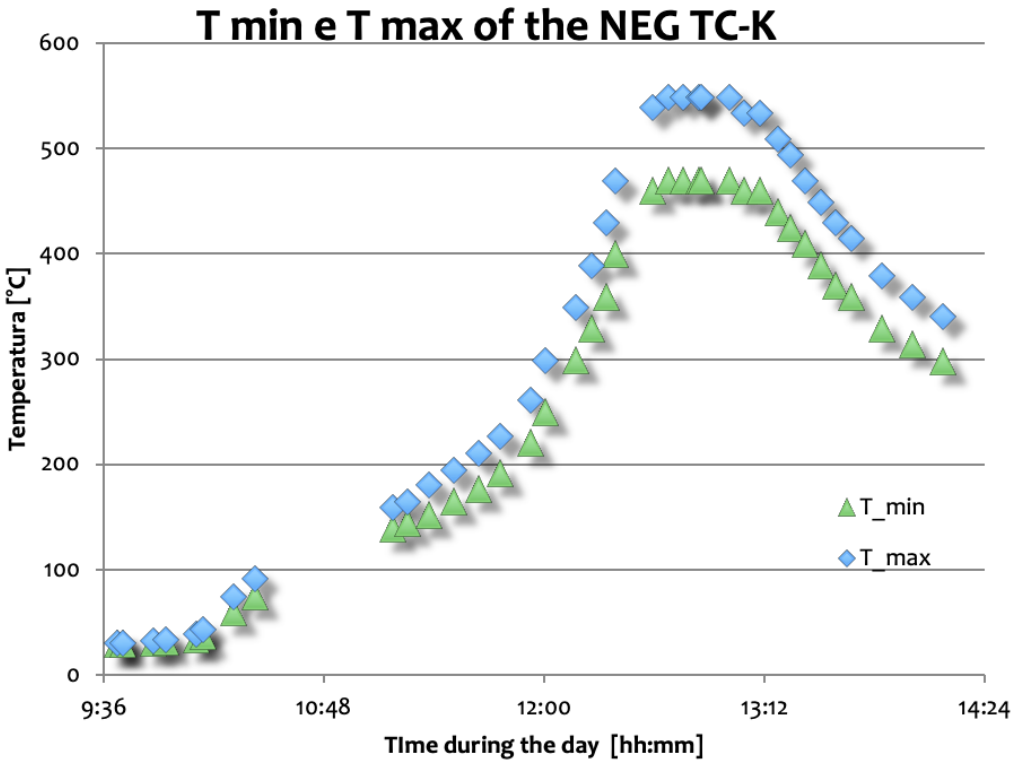

Figure 3.21: Dependence of the temperature of the NEG heater from time.

Turbo-pumps serves as usual pump for vacuum applications.

All components of the detector have been selected to be high-vacuum compatible. Before installation inside the COSY ring for the commissioning work, the completely assembled detector has been tested to reach a pressure in the 10^{-9} mbar range.

3.8 Electronic readout

Readout system of the PAX experiment is the legacy of the readout system of the ANKE experiment. Vertex ADC modules, depicted at 3.22. en-vacuum electronics for the PAX experiment follows electronics for ANKE and carries the readout chips with 11MeV linear range, and time resolution better then 1ns, sufficitent to provide a fast signal for triggering. The interface card outside the vacuum provides power supplies, control signals, trigger pattern threshold and calibration pulse amplitudes to the front-end chips. The vertex readout module developed at Jülich comprises a sequencer together with a 12 bit ADC with 10 MHz sampling; it allows common-mode correction for

hardware zero-suppression to reduce the output flow to 0.1 MByte/s with less than $50\mu s$ dead time. A programmable trigger and a pre-scaler module have been developed to provide a flexible trigger logic.

Figure 3.22: Photograph of one vertex ADC module.

3.9 Preamplifier boards

With number of channels for single detector side of 128, and total number for detector system of 5120 channels it become obvious, that integrated read-out electronics have to minimize the amount of vacuum feed-throughs and number of single amplifiers. For this purpose, using experience of ANKE experiment [69], dedicated preamplification boards have been designed in FZJ and produced in Italy.

The front-end preamlifier boards use VA32TA2 integrated circuit (IC) chip designed and produced by the company IDEAS[1]. The chip based on two chips - VA32HDR preamplifier chip and TA32cg trigger chip, which are combined at a single die and allows to reduce amount of the "bonds". Reasons for using exactly this chip are: partial reuse of already designed and developed soft- and hardware of DAQ of the ANKE experiment and accumulated experience of work with such ICs.

Good vacuum properties of PCBs are based on materials of boards and epoxy protection of chips. As the material of substrate of the PCBs used ROGER 3003 laminates. The specified PCB thickness is 0.8mm. The chips and bonds are protected from mechanical damage with EPO-TEK H70E-2 and 509FM-1-LB epoxies ([70]). First one is used for fabrication of "dam" (common part of fig. 3.23), second one is used to fill the rest. Such steps are necessary for better vacuum conditions.

[1]Integrated Detector Electronics AS, https://ideas.no.

The VA32TA2 chips are placed on PCB, ultrasonically "bonded" to the tracks of the PCB with thin aluminum wire 17μm thick. As soon as facility has two different thickness of sensors, and different amount of charge is produced from strips of sensors, consequently needed different dynamical range for different thickness of sensors, and two different types of PCBs are were designed and produced (Pic. 3.23, 3.24).

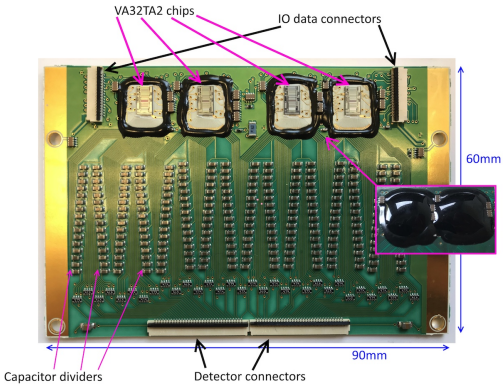

Figure 3.23: PCB for thick detectors

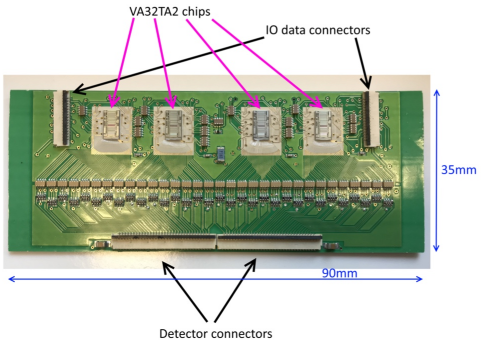

Figure 3.24: PCB for thin detectors

The uncommon part of the PCBs is scheme of connection of input capacitors. For thin detectors used usual CR-filter with capacitors in assemblies, for thick detectors used capacitive divider in special form - it sends part of signal not to ground (Pic. 3.25, 3.26), but to neighbouring channel to avoid charge loss and noise ground.

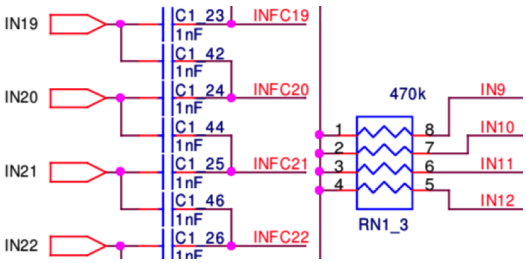

Figure 3.25: Part of scheme of the PCB for thick detectors

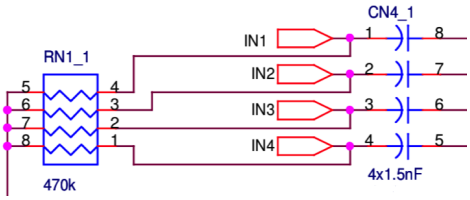

Figure 3.26: Part of scheme of the PCB for thin detectors

The chip consist of 32 identical parallel channels low-noise/low power high dynamic range charge sensitive fast triggering circuit of the VATA family. Each channel can be logically split in an amplitude and a trigger part. First, charge came on the input pad amplified in preamplifier stage. Then it is split into two branches - an amplitude part and a trigger part. It has simultaneous

sample-and-hold facility for proper readout and calibration facility for checking each channel individually. The preamplifier-shaper subcircuit provides a multiplexed current and voltage readout with a global 5-bit DAC trimmed reference. The chip includes for each channel a fast CR-RC shaper followed by a level-sensitive discriminator. The trigger signals from each channel are wire-or'ed together onto one common trigger output. To reduce threshold-spread, the chip has 4-bit trim-DACs on each discriminator and an additional global threshold 5-bit trim DAC. All biases are internally generated with each being optionally adjustable externally from corresponding overriding pads. It's possible to test a channel while the rest of the channels are performing direct measurement [71].

Picture 3.27 illustrates the block-scheme of the chip.

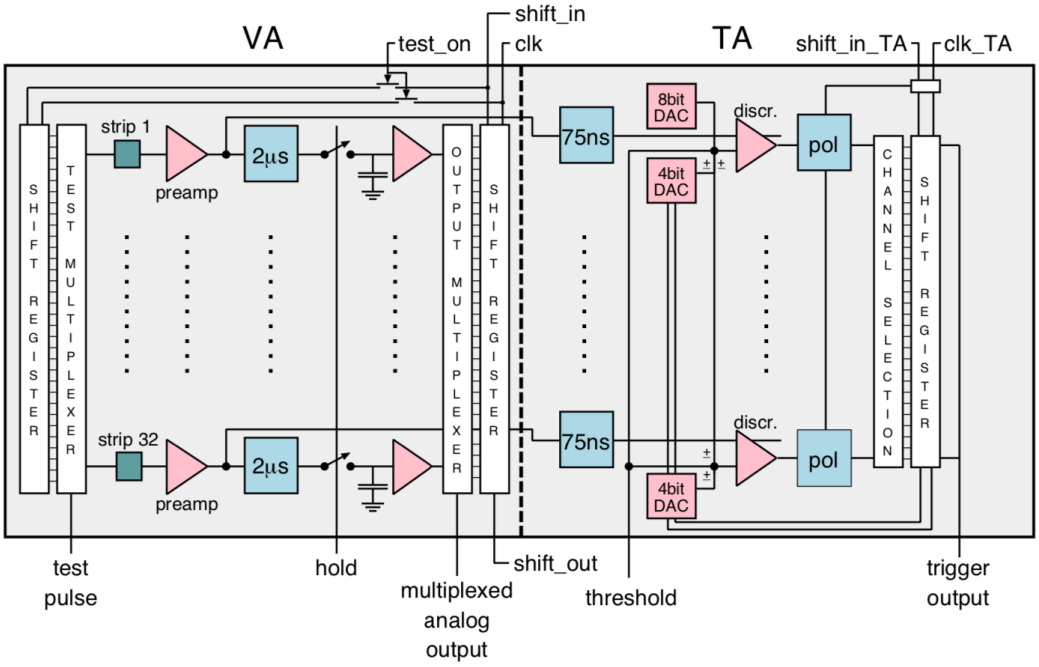

Figure 3.27: Principal block-scheme of the VA32TA2 amplifier chip

In the amplitude part of the chip - slow part - the signal is fed to the slow shaper. Once a readout cycle is started by applying the "hold" signal (time line IV in the figure 3.28), the output of each of the 32 slow shapers is stored in the sample and hold facility. With both the "shift_in" (time line V) and the "clk" (time line VI) signal active one bit is inserted into the read-out register which switches the first channel of the output multiplexer to the output bond pads. By clocking the "clk" control signal the bit is moved though the register switching the channels step by step to the output. According to the

specifications, the maximum clock frequency is 10MHz, although only 5 MHz have been confirmed by the measurements. Each channel is therefore for a minimum time of 100ns applied to the output of the chip. The output of the shift register is in addition provided on a "shift out" bond pad allowing to build a daisy-chain of chips. Up to ten chips can be connected to a daisy chain allowing a maximum number of 320 inputs (restriction of vertex ADC) to be read out. In the detector system two preamplifier boards are used in serial, that means 8 chips and 256 channels are read by each vertex ADC. To build a chain of chips, the control signals have to be provided to all chips simultaneously and the output of the shift register of a chip has to be connected to the "shift_in" input of the next chip in the chain.

In the trigger part of the chip, the fast branch, the signal from the preamplifier stage is shaped with a peaking time of 75 ns. The output of this fast shaper is compared with a threshold giving the opportunity to obtain a trigger signal from the chip. The individual threshold for each channel is made up of an external voltage, per chip offset voltage and a per channel offset. Both the per chip and per channel offset voltages can be controlled by an additional slow control shift register. It is also possible to mask out certain channels from the trigger pattern. The shift register is controlled by two signals similar to the control lines of the read-out shift registers inside the amplitude part of the chip. These signals are the "clk_TA" and "shift_in_TA".

When used in a daisy chain it is likely that the average output level of the chips varies over a wide range. In order to minimize that range each chip has an additional 7 bit DAC that allows the shift of the average output level of each chip individually. The DAC is an extension of the slow control shift register and is also controlled by the "clk_TA" and "shift_in_TA" signals. Figure 3.28 shows the timing diagram of a read-out sequence. I is physical trigger, generated by TA part of chips and processed by trigger board, II is accepted trigger available on the output of trigger module and connected to Vertex ADCs. The running sequence generates all the necessary control signals for the read-out of the front-end chips (IV, V and VI) III is the coincidence of both discriminator outputs and 10 MHz reference clock, IV is accepted trigger, V is hold/VETO signal for VATA, used to freeze measured amplitudes in VA part VI is shift_in signal for activation read-out register, VII is clock for moving bit through the register switching channels step by step, VIII is so called "DTbyShaper (dead time by shaper) signal is the coincidence of both discriminator outputs and a 10 MHz reference clock which allows the determination of the introduced dead-time with a resolution of 100 ns (time line III), IX is counted DTbyShaper, X is 10MHz reference clock, counting enabled by VETO signal, XI is reference clock - 10MHz.

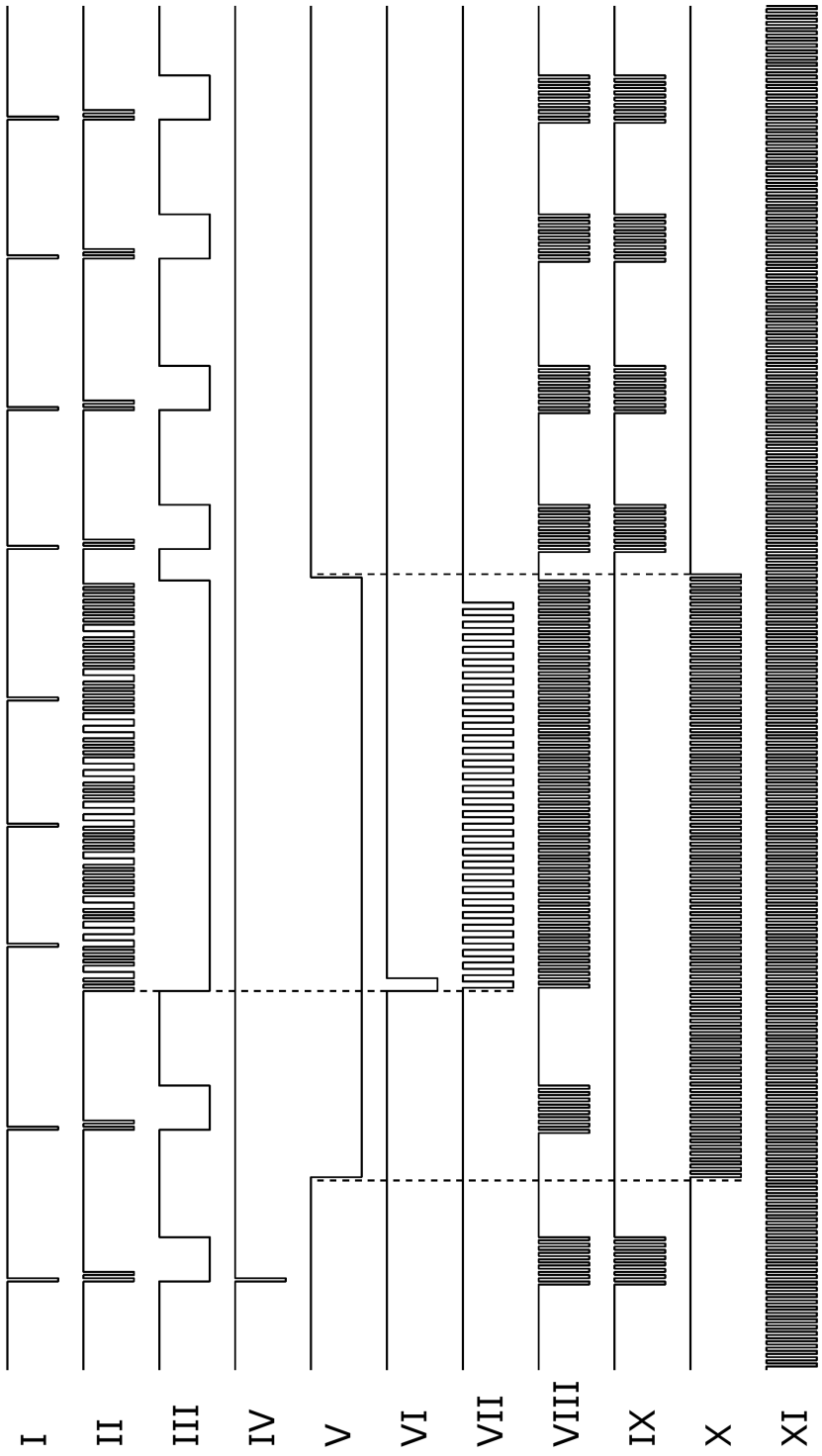

Figure 3.28: VA32TA2 timing. Where I is physical trigger, II - VA/TA trigger response, III - shaped trigger response, IV - accepted trigger, V - hold/VETO, VI - shift in, VII - clock (5 MHz), VIII - DT by Shaper, IX - DT by shaper (counted), X - DT by VPG, XI - reference clock (10 MHz).

:

3.10 Repeater boards

Another important electronic part of the project is Repeater Card (RC) (Fig. 3.29) designed and produced at FZJ. The board is a continuation of previous version, used at ANKE experiment. The requirements to the RC are mostly dictated by VA32TA2 chip. Repeater card has next modules with functions:

- HV_Power part of RC consist of LM317 and LM337 linear regulators. The VA32TA2 chip requests ± 2 volts power supply, while supply voltages are ± 5 volts. For each, analogue and digital power supplies, independent regulators are used.
- The LVDS part serves for translating LVDS signals from long line from scaler to logic level signals, suitable for use in VA32TA2 chips and DAC part of the RC.
- Analog Outputs part serves for amplification of analogue differential signal from VA32TA2 chips for delivery it though long coaxial cables to the Vertex ADC.
- VA_LVDS part serves to translate trigger signal from VA32TA2 chips for its delivery to the Trigger module of the detector system.
- DAC module serves for the conversion of the digital signal into analogue to manage the different parameters of VA32TA2 chip, such a level for the discriminator threshold, different bias voltages and etc.

My work with this boards was to find mistakes in design as soon I got the design as a legacy from previous colleague. These mistakes prevented normal operation of the repeater card:

- lines of output of LM317 were connected to ground, that lead to inoperability of RC;
- tracks in one of differential LVDS lines were confused, and this issue manifested itself only on long 30 mete cables, since long cable makes shift of 100ns;
- two manage line from digital to analog converters (DAC) were confused, that lead to swap of fields in software used for setting parameters of VA32TA2 chips.

Figure 3.30 illustrates points where these mistakes were found.
Detailed schematics of RC is presented in appendix A.1

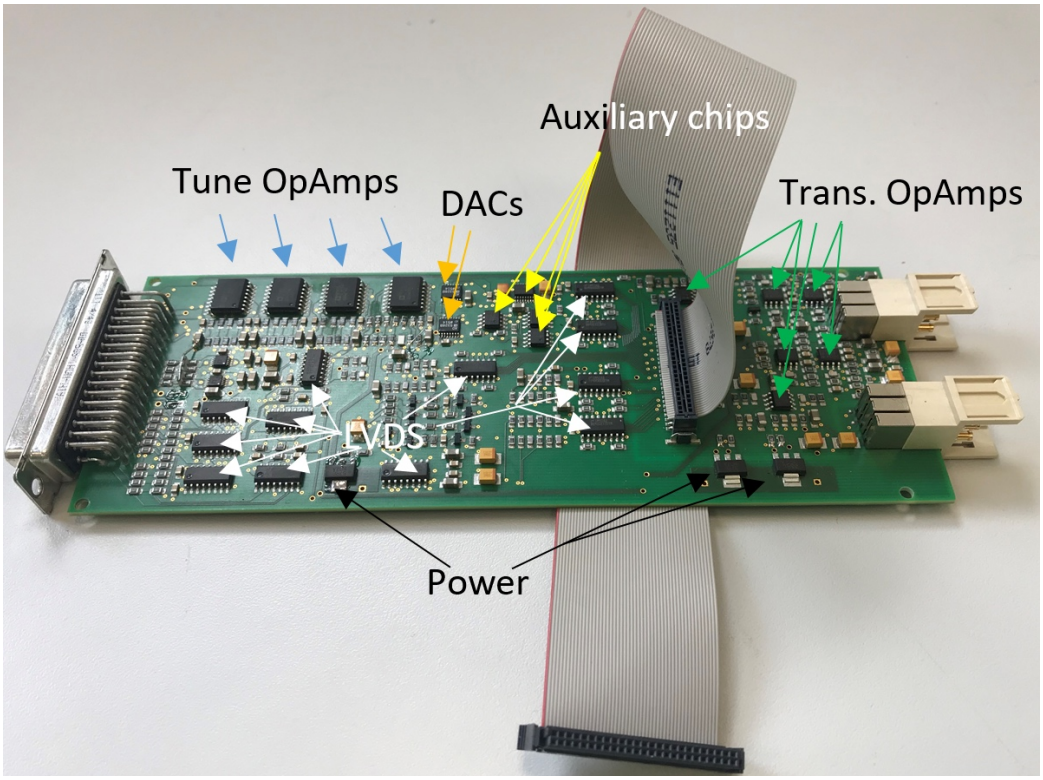

Figure 3.29: Photo of working repeater card

3.11 Vertex modules

The analogue to digital converter module - Vertex-module for MATE3 and va32 - has been designed and realized by the Zentralinstitut für Systeme der Elektronik (ZEA-2) of the Forschungszentrum Jülich 3.31. Each module is designed to read both sides of one silicon sensor. The card consists of two identical units with galvanically isolated ADC, LVDS inputs/outputs and three independent memory blocks. One board can read a maximum of 1024 channels. The module has possibility to configure its parameters with dedicated software. The VA32TA2 chips are configured serially via LVDS line. The module has input trigger line to start readout-sequence. In the FPGA two completely separated programmable sequencers for the VA32TA or MATE3 timing are available. Each channel presents three independent and completely separated addressable memory areas. The blocks are used to store sequences and parameters for the needs of Common Mode. Common Mode is base shift level for all the channels, and need to be corrected because of its drift. The connection to the LVDS bus is also done via the FPGA [72].

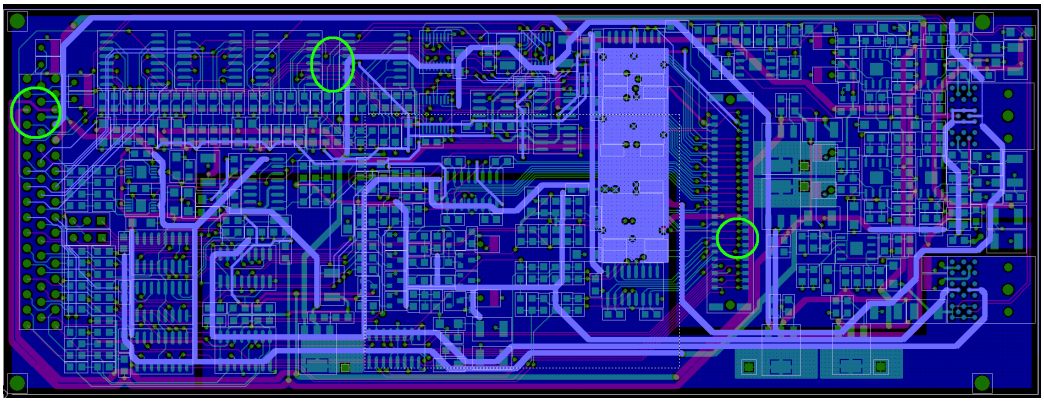

Figure 3.30: Board view of the repeater card, where green circles shows severe mistakes in design.

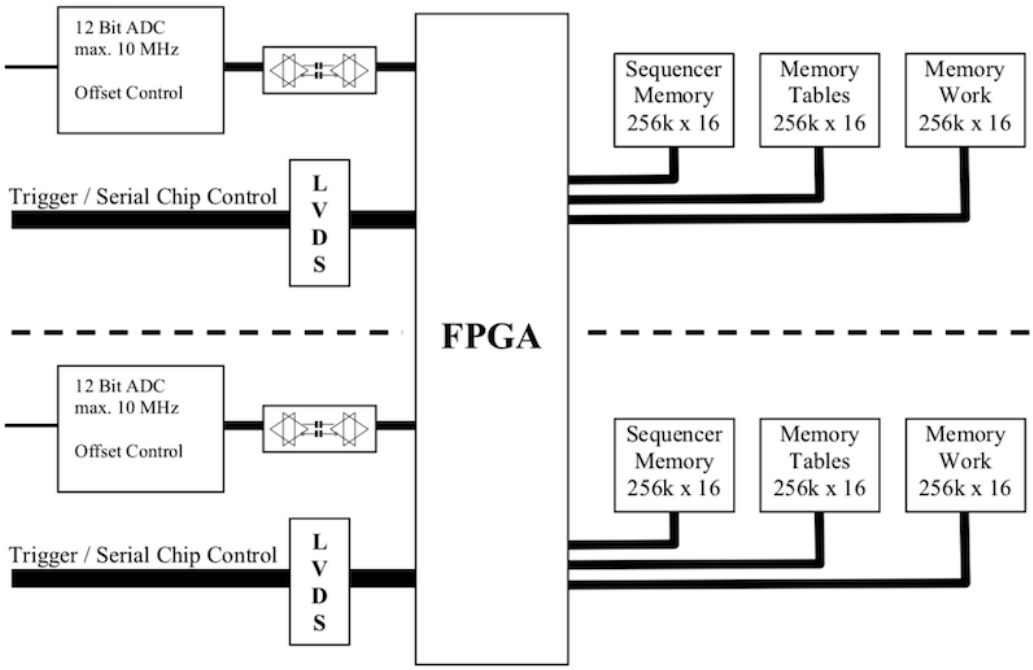

Figure 3.31: Internal block-structure of the VERTEX-Module for MATE3 and VA32. FPGA has two independent sequencers for VA32TA/MATE3 timing. Each channel has 3 independent memory blocks, which are used for storage sequencer code, for storage common mode/threshold tables and as working memory.

3.12 Telescope trigger

The trigger board was designed and realized by the electronic workshop of the University of Ferrara and INFN of Ferrara and depicted at Fig. 3.32 It is used with dedicated control board with SPI line and with dedicated software, were one can choose desirable trigger scheme.

The board has eight trigger inputs, four trigger outputs, compatible with Vertex ADC modules; Veto, Gate, Strobe and clear inputs, and ECL outputs compatible to the counting devices of the complete system.

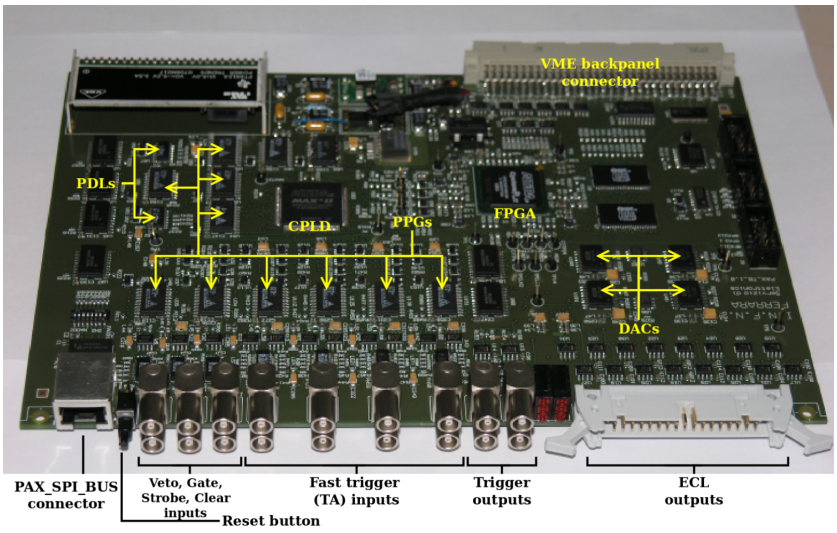

Figure 3.32: View of ready trigger board.

Taking into account the pd elastic scattering (see chapter 5) and the fact of standard configuration with four quadrants, the trigger signal from the detector system is the coincidence of the individual signals from the intermediate $300\mu m$ sensors of opposite quadrants (1 and 3, or 2 and 4). The detection threshold is thus the energy loss in the first layer plus the trigger threshold of the second layer, since the particle has to pass the first layer before it can even generate a trigger signal. For protons the detection threshold is then about 9.5 MeV, for deuterons It is in the order of 12.6 MeV. With a trigger threshold of about 150 keV and the fact that only particles which pass the first detector and deposit enough energy in the second layer can be considered in the track determination. The used trigger scheme could be reduced to the half of initial scheme due to the absence of two quadrants, as it was made during first beam-time. Only 1 and 3 quadrants were present, and only coincidence signal from then lead to trigger generation.

3.13 MPOD

Wiener MPOD crate [73] (Fig. 3.33) is used for generating power supply voltage for the Repeater Cards, and for generating high voltage bias for sensors operation. The crate is remotely controlled with 10/100 Ethernet. It works with low voltage (LV) and high voltage (HV) power supply modules, which are used in mixed configuration. The PAX detector setup uses 2 LV modules - OMPV.8008L, and 2 HV modules - iseg EHS 8010n-K [74], each module has 8 galvanically isolated voltage, individually controlled and monitored outputs. Each channel is independently configurable and has its own settings for voltage/current limits, ramping speed, and etc. Dedicated software was realized in Ferrara, and tested in FZJ.

Main work with MPOD was to identify suitable parameters and modules. LV modules worked as expected, first of all were tested with resistive load. HV modules were selected from three other types we had. For some reason HV modules EHS 8001p and EHS 8001n had common problem - both modules dropped voltage (current respectively) to 0, when current limit was reached, what is not acceptable in our application.

Figure 3.33: Photograph of MPOD crate and the modules high and low voltage supply

3.14 Assembly

One logical unit - complete electronic path - is shown on the 3.34. It serves to work with the set of two silicon sensors. One logical unit reads out 512 channels of the sensors, the signal goes through one feed-through DB-50 connector on CF 160 flange. Each CF 160 flange contains three feed-throughs. The logical unit contains four preamplifier PCBs, repeater card, which is connected to the power-supply with high-voltage supply, to the Vertex ADC module, to the trigger board. For digital control of the preamplifier boards used 30 pin LVDS flat line.

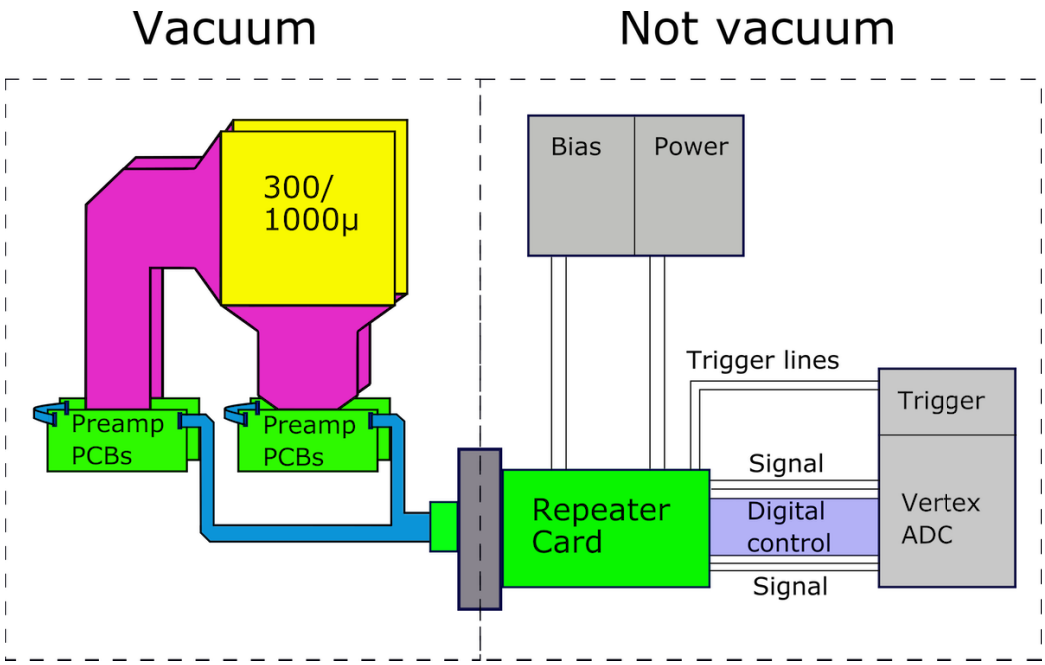

Figure 3.34: Simplified scheme of the one complete electronic path..

High and low voltage supplied by MPOD crate with four modules, two for bias-voltage, and two for 5 Volts low voltage.

Chapter 4

Test benches

All the components of the detector system were manufactured almost pies by piece. As opposed to mass production, a manufacturer can guarantee only 90% of working product and often test costs at manufacturer side are is incomparably higher than the cost of parts. Therefore in most our cases it is more reasonable to order a double number of parts, and perform a detailed inspection of all the components. Moreover, every assembly step must also be tested. Dedicated test benches were designed and realized to solve these problems.

4.1 PCBs test bench

Test bench for PCBs used National Instruments module USB-6001 and corresponding Virtual Instrument program (VI) in LabView. The task of the given test bench was check of the general working capacity of PCBs. The test bench used test mode feature of the preamplifier chips, and allowed to test each preamplifier channel at any time without connection of real signal to inputs of PCBs [71]. The first VI got the triggering threshold in units of digital-to-analogue converter setting threshold. The VI works in following sequence:

- PCB initialization - 175 bits are loaded in each chip, also analogue levels are set.
- Sequential search of threshold level on zero DAC values of each channel by method of half division in conditional units. Since the test signal value is set during initialization, this procedure should be repeated for each channel several times (7 on average) until a threshold is found.

Result of the measurement is presented in following picture 4.1:

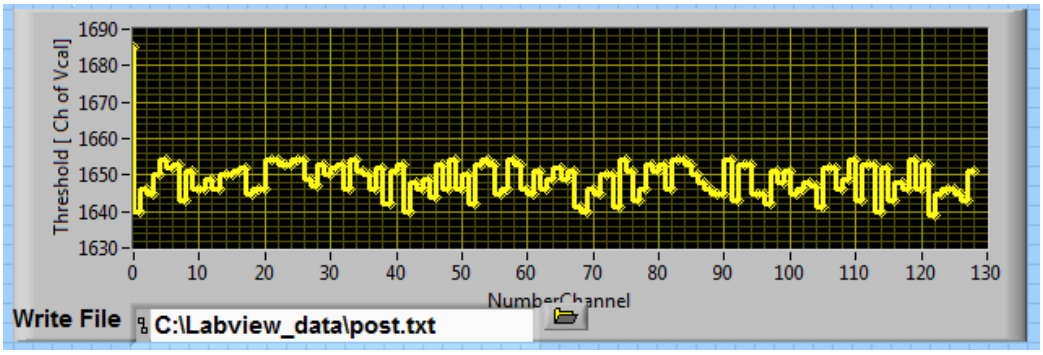

Figure 4.1: Window of LavView VI, demonstrating triggering threshold in each channel.

The second VI checked response of each amplification channel to the test signal, and the result was a difference between the amplitude of the zero and test signals. The VI works in following sequence:

- PCB initialization - 175 bits are loaded in each chip, also analogue levels are set.
- First each output voltage of each channel is measured without input signal, then test signal is applied and output voltage is measured again.
- Resulting difference is observed

Result of the measurement is presented in following picture 4.2, and demonstrates faulty PCB, where one chip doesn't amplify anything:

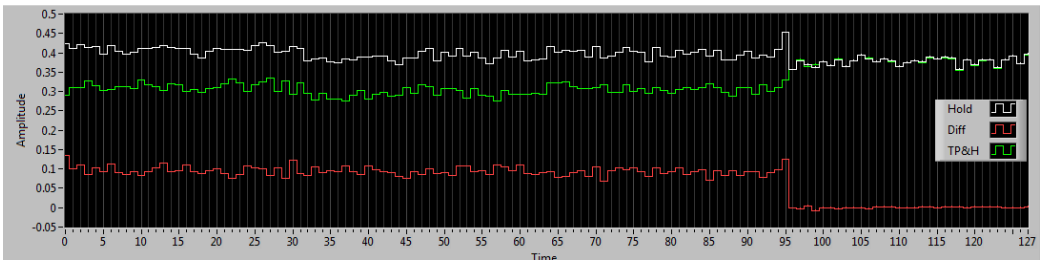

Figure 4.2: Window of LavView VI, demonstrating output voltage amplitude without test signal (green), amplitude with test signal (white), and the difference (red).

However, such test bench could not identify all the possible faults in PCBs, such as absence of contact between input of the chip and input of the PCB, but sifts out most of the faulty PCBs. The following sections will give more labor-intensive, but more productive method.

4.2 Quadrant test bench

Quality test for the silicon sensors was realized in vacuum chamber using ^{241}Am α-source. Dedicated T-piece was designed and ordered. Special rails were also produced at mechanical workshop in FZJ (Pic. 4.3). Detectors were tested one by one in case of HERMES sensors, or 2 units together in case of PAX sensors. The result of test of unsatisfactory HERMES sensor depicted at picture 3.8. It shows the energy deposit in units of ADC To perform the test vacuum chamber should be under the pressure in the range of $10^{-5} - 10^{-6}$ mbar. To create such pressure one Pfeiffer Vacuum TSH 071 Turbo Cube [75] is used, and it takes at least six hours, depending on initial moisture of the components, to reach it.

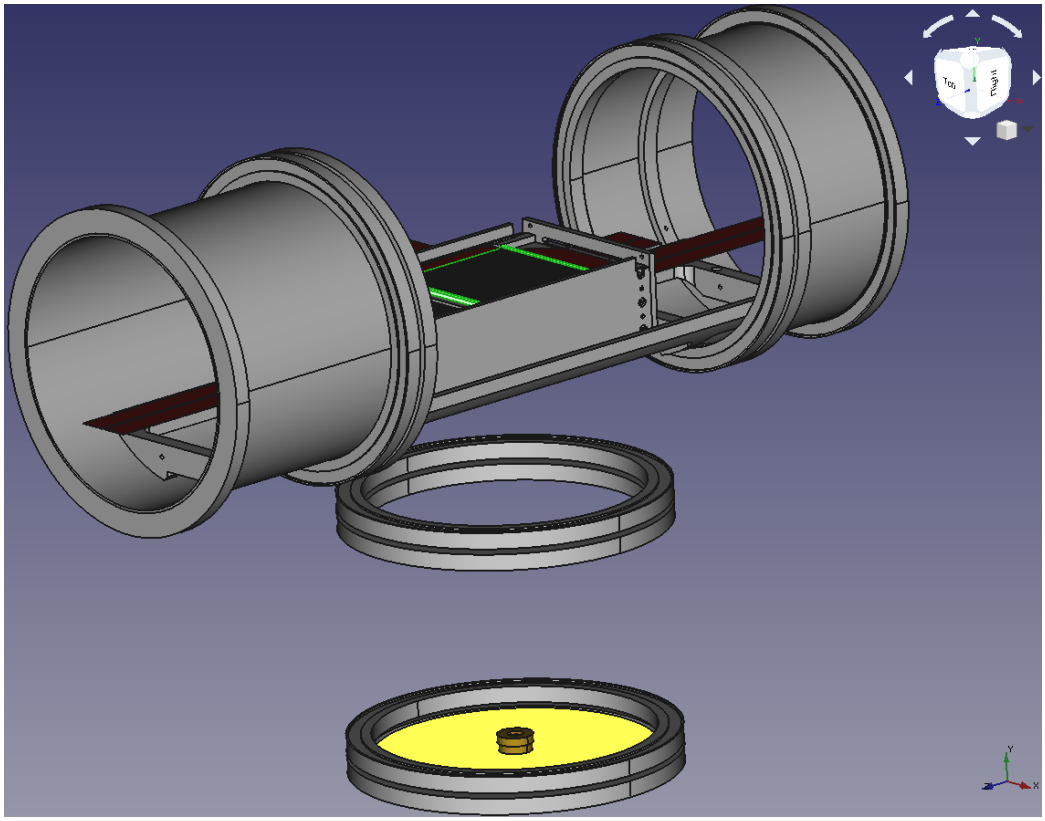

Figure 4.3: 3D view of the test chamber with transparent T-piece. One of the sensors in quadrant marked green. On the yellow bottom α source is placed.

After all the sensors and other parts were tested, the same test bench was used to perform test of already assembled qudrants. But in this case, only first lair of the sensors could be irradiated with α particles, while another

two are covered by first one. To perform such test ^{152}Eu-gamma source was used. However, efficiency of the sensors to high-energy gammas tends to be zero, only some counts per second were acquired from the qudrant, thus, it need some days to get reasonable amount of counts in each of 1280 channels of quadrant. At the same time, one can not see, if channel has good characteristics. Only obtainable information from this test is workability of channels.

Together with detectors PCBs were tested, however, we had to test approximately 150 PCBs and it became obvious, that such method will waste a lot of time, and together with it will jeopardize sensors with unnecessary switching operations. Kapton cables withstand approximately 100 insertions, see 4.4. Dedicated test bench for PCBs was used. A drawing of vacuum chamber is presented in A.3. A result of two PAX sensors is presented in A.2. It shows α-spectra in each channel, and these data were used to calibrate the detector system.

4.3 Detector and PCBs test bench

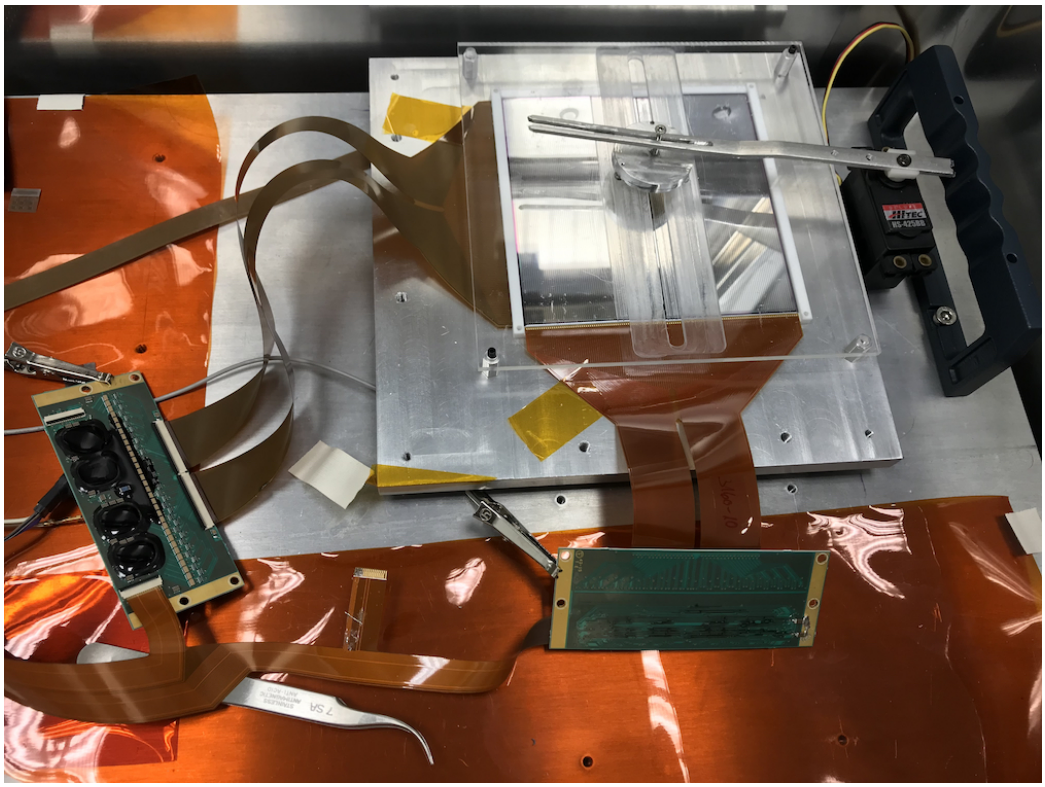

Figure 4.4: Photograph of the moving mechanism for α-source.

Originally, the test bench was used, as intended, to test both detectors and PCBs, but later it became clear that such test bench with moving parts could pose a danger to sensors. The detector used for this bench is faulty sensor, supplied by manufacturer [59] for free. Picture 4.4 shows photo of the test bench.

Idea of the test bench is the same like in 4.2 to use ^{241}Am α-source as particle source, but in the air. Because the α-particles only travel a few centimeter in the air, and do not have well-defined energy, they do not give sharp peak of energy deposit in the sensor, however uniform picture of energy deposits in channels could tell the quality of complete PCB.

In the beginning of this test procedure couple of PCBs were tested in vacuum, then in this test bench.

Since α-particles only travel a few centimeters in the air, moving mechanism for α source was assembled with plexiglass plate with slit in it, hobby servo motor and Arduino.

The code for the device was taken from example folder of Arduino IDE, and modified to move the source in given range.

The sensor has set of completely not working channels from both sides, however the numbers of channels are different, and by connecting a PCB to first, and then second side of the sensor will give full picture of channels in it.

4.4 Kapton-cable test bench

Kapton cables, used to connect PCBs between each other and to the output flange. Dedicated device, based on several analog-to-digital converters and I2C to USB converter (Pic. 4.5), and LabView VI were used to check the resistance of each line in kapton cable. The device forms voltage divider with 100 Ohm resistors serially connected to each of channel of kapton-cable, applies voltage to the divider and measures output voltage on to calculate resistance. Normal measurement resulted approximately 2 Ohm for channel.

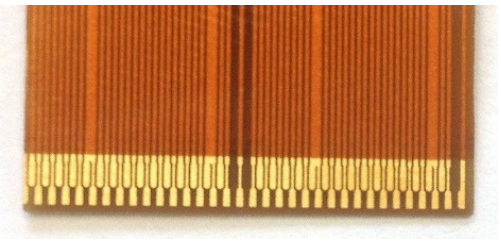

Figure 4.6: Photograph of defect kapton cable

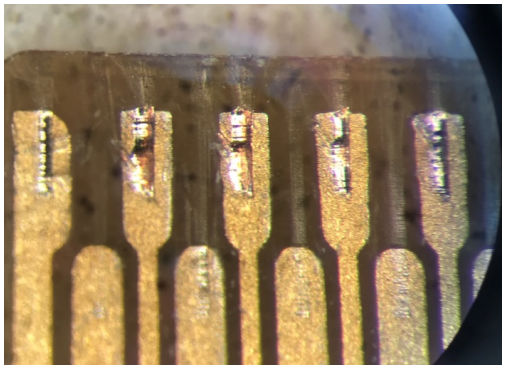

Figure 4.7: Microscopic photograph of defect contacts of kapton cable

During the tests, it was determined that kapton cable could withstand approximately 100 insertions. Because of relatively soft gold-plated contacts further use is fraught with connection variability. With microscopic picture (Pic. 4.7) one can observe carves in the cable.

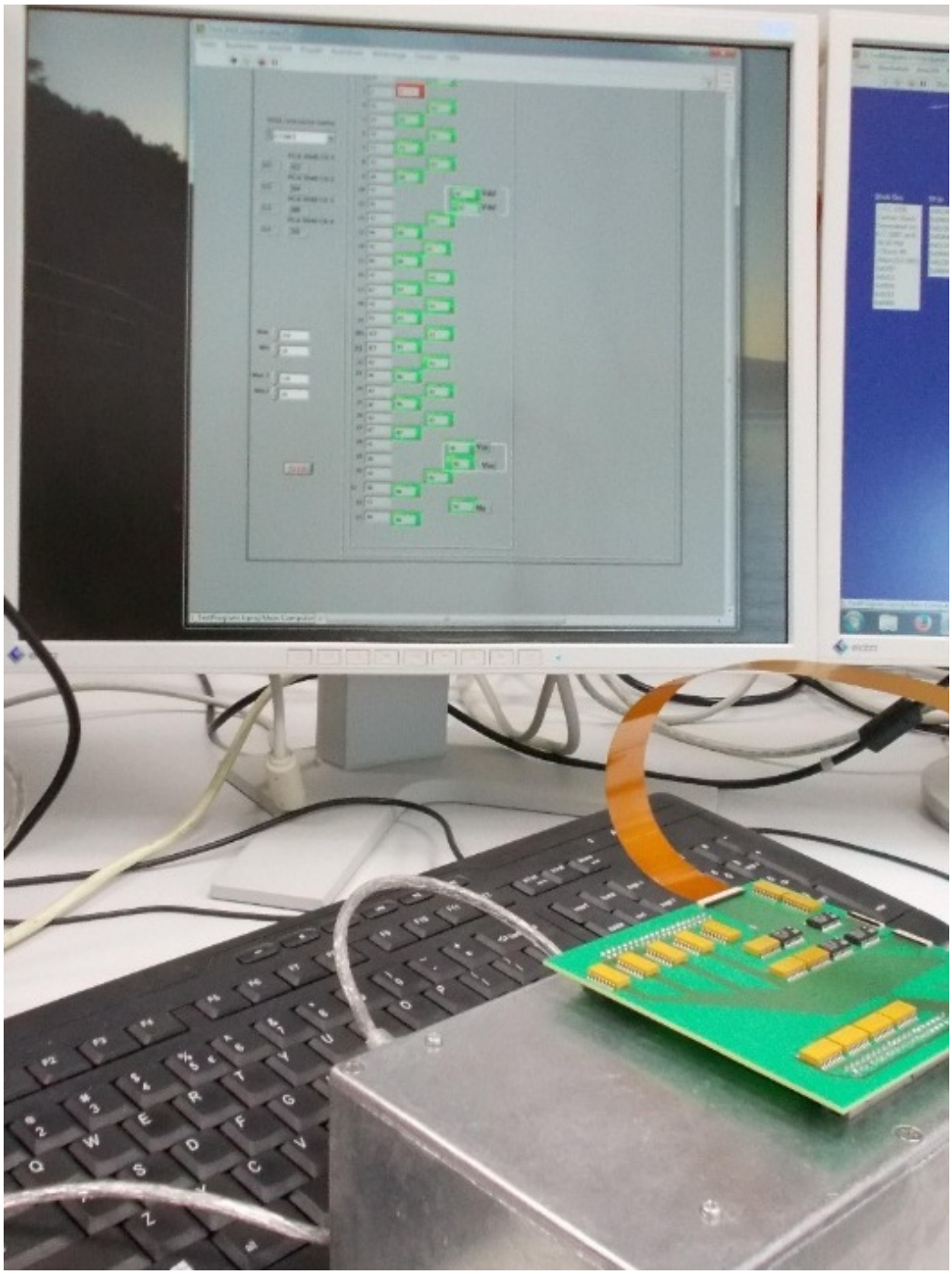

Figure 4.5: Photograph of test bench for kapton cables.

Chapter 5

Detector commissioning at COSY

As a first step, two quadrants of the detector were calibrated and tested at an external test bench. After that the detector was assembled with the two quadrants and installed in the low$-\beta$ section 2.1.1 at the PAX interaction point 2.3 of the COSY ring.

The vector polarized deuterium target and an unpolarized proton beam at an energy of $T_P = 135$ MeV were used for the commissioning. The beam passed through the storage cell of the target, which was filled with transversely polarized atomic deuterium from the atomic beam source 2.3.1. The vertical direction of the polarization was flipped every 5 seconds to reduce the systematic uncertainties of measurement.

The goals of the commissioning run was to check the ability of the detector to reconstruct the particle trajectories, measure their energy deposits, identify the particles and processes, and eventually to define the target polarization. Since the longitudinal vertex coordinate could be reconstructed in each event, this run provided an unique opportunity to study the distribution of the target gas polarization along the storage cell. Beside that, the background conditions of the experiment as well as the detector efficiency were to be studied.

The experiment was conducted at a beam energy below the pion production threshold of $T_{\text{thresh}} = 207$ MeV, hence the dominant processes were the pd elastic scattering and the deuteron breakup. The $pd \to pd$ reaction, with both final state particles detected, was also by far the cleanest one to select, and was primarily used for the detector performance study as well as for the target polarimetry.

5.1 Energy measurement and particle identification

The energy deposit of a particle in the detector is described by the Bethe-Bloch formula:

$$-\frac{dE}{dx} = \frac{4\pi n z^2}{m_e v^2} \cdot \left(\frac{e^2}{4\pi\epsilon_0}\right) \cdot ln\frac{2m_e v^2}{I}, \tag{5.1}$$

where v is the velocity of the incoming particle, ϵ_0 is the vacuum permittivity, m_e is the electron mass, n is the electron density, z is the atomic number and I is the average ionization energy.

Comparison of the energy deposited in different layers of the detector allows for the $\Delta E/E$ particle identification provided that the particle stops in the second or third layer. In Fig. 5.1 one can see the loci of protons and deuterons that were stopped in the third layer and of those that passed it. To avoid thickening of the lines, the plot was obtained in a narrow range of the laboratory polar angle around 70°. Analogous dependencies were observed for the combination of the first and second layers.

The energy resolution of the detectors was obtained from the tests of the sensors in vacuum test bench during initial tests of all the components of the experiment. For α-particles from ^{241}Am it amounted to $\Delta E/E \approx 2\%$.

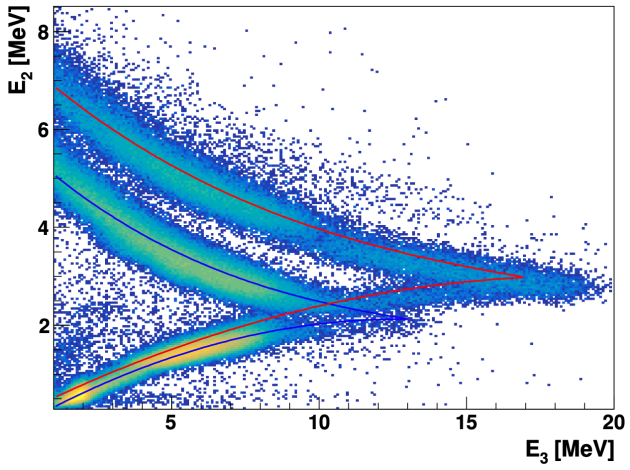

Figure 5.1: Energy deposit in the second layer vs. one in the third for the tracks with $60° < \Theta < 80°$. The two upper bands contain deuterons and protons stopped in the third layer, with the deuteron band above. The lower rising band contains the particles passing through the third layer. The curves show position of the bands in the simulation: red for deuterons, blue for protons.

The energy loss in the detector was calibrated with the use of a GEANT-based simulation [76]. By comparing the $\Delta E/E$ dependencies derived from the simulation with the correlations of the measured charges, the calibration parameters were derived. In the $pd-$elastic scattering, measurement of the polar angle of one of the ejectiles yields the polar angles and energies of the both final state particles. In the events where the final proton or deuteron stopped in the detector, the correlation of the angle and the deposited energy of the stopped particle allowed a clean selection of the process. Such events with a well defined energy of the ejectiles served as additional input to the calibration procedure. The energy loss E was described by a polynomial of the measured charge Q, with individual calibration made for each side. The $E(Q)$ dependence was found to be linear for most of the sides, with two exceptions, where one had to use cubic polynomials.

5.2 Track and vertex reconstruction

As described in 3.3, each layer of the detector consists of two stripped sensor sides, with strips oriented respectively along the beam axis on one side and orthogonally on the other. Thus, each layer can measure a two-dimensional coordinate on a track. The average number of strips in a track hit was about two in the first two layers and four in the third thick layer, and a track coordinate was reconstructed as a weighted average according to the charge distribution in the strips fired. The clusters of strips on the two sides of each layer were combined into two-dimensional hits provided that the energy deposits in the clusters were close enough. Such 2D-hits were required in at least two of the three layers in the same detector for construction of a track, thus allowing for an inefficiency in one of the layers.

The track curvature due to the holding field of the target was negligible compared to the strip width and the effects of multiple scattering in the sensor material, thus straight line trajectories were drawn between the layers. By extending such a straight line to the beam axis, one could find the longitudinal and transverse coordinates of the interaction point with an RMS accuracy of about 2 mm. A distribution of the reconstructed vertex coordinates is shown in the left panel of Fig. 5.2. The transverse coordinates are clustered around 0 while the longitudinal ones are distributed along the storage cell. The beam direction coincides with the direction of Z axis and the visible asymmetry of the distribution reflects the change of the detector acceptance along this axis.

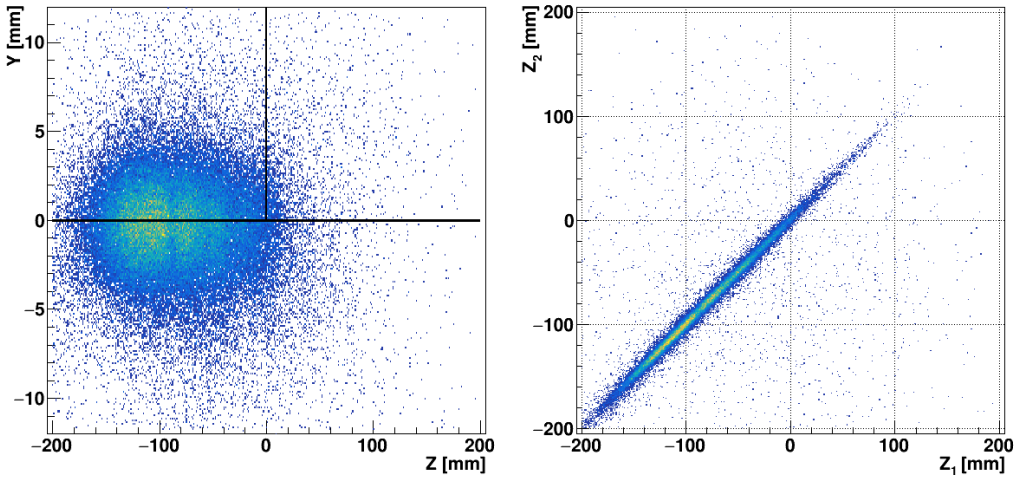

Figure 5.2: Reconstructed vertex coordinates. Left panel: longitudinal (Z) vs. transverse (Y) coordinates for each track. The vertical line shows the position of the storage cell feeding tube, the horizontal one depicts the cell. Right panel: longitudinal coordinates of two tracks in two-track events.

Reconstruction of the vertex coordinates provided a powerful background rejection criterion. The transverse coordinates were required to stay close to zero, with the resolution comparable to the beam diameter. The Z coordinates were distributed along the storage cell, but had to match for the two particles detected in coincidence, as it is shown in the right panel of Fig. 5.2.

The detector efficiency was studied by using *pd*-elastic scattering. For that, a track was reconstructed by using two out of three layers, and the probability was determined to find a hit in the third layer at the position defined by the track. Given the lower multiple scattering compared to deuterons, only the proton tracks were used. The energy deposit of the protons were 0.6 MeV in the two 300μm layers and 2.0 MeV in the 1 mm thick layer. All detectors showed an efficiency above 99%.

5.3 Identification of *pd*-elastic scattering

The process possesses characteristic dependence between the polar angles and the energies of the two ejectiles. Thus, for the kinematic identification of the reaction it was sufficient to measure two of these four observables. This could be achieved in two cases:

– when trajectories of the both final proton and deuteron were reconstructed,

– when one of the ejectiles stopped in the second or third layer.

The former case is demonstrated in Fig. 5.3. Here, energy of the both particles was too high for stopping in the detector. The cuts of the energy loss selecting the punch-through particles were applied. The correspondence of the azimuthal angles (see Fig. 5.3(a)). of the two particles as well as of the longitudinal coordinates of the vertex served as additional selection criteria. Despite the non-ideal vacuum conditions in the target chamber during the beam time (no sensible dependence of the total detector rate could be detected with and without injection of polarized gas into the cell), the coincidence $pd-$elastic events could be cleanly selected with a background level of only 1.5 %.

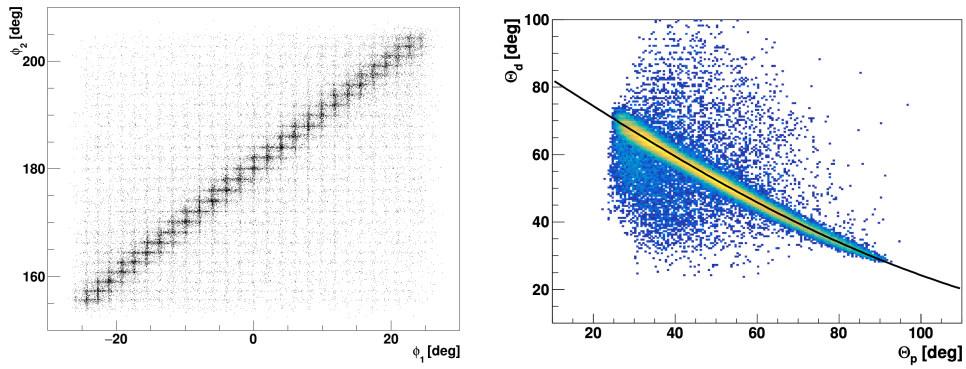

(a) Azimuthal angles.

(b) Laboratory polar angles, events selected by pd-elastic azimuthal correlation.

Figure 5.3: Angular correlations in two-track events. The energy loss cuts are applied to select protons and deuterons passing through the third layer.

In the case when one of the particle stopped, it could be identified via $\Delta E/E$. The total kinetic energy of the particle was reconstructed along with the track angles. The process was then selected by the missing mass criterion. This scenario covered the regions of small emission angles of the final proton or deuteron.

5.4 Measurement of the target polarization

In order to determine the target polarization, the vertical direction of the target holding field was flipped every five seconds. The cross section for the interaction of an unpolarized proton beam incident on a transversely vector polarized deuterium target is given by:

$$\frac{d\sigma}{d\Omega}(\theta,\phi) = \frac{d\sigma_0}{d\Omega}\left[1 + \frac{3}{2}QA_y^d(\theta)\cos\phi\right] \tag{5.2}$$

where $d\sigma_0/d\Omega$ is the unpolarized cross-section, $A_y^d(\theta)$ is the deuteron vector analyzing power, Q is the target polarization, θ and ϕ are the polar and the azimuthal scattering angles, respectively. Precise *pd*-elastic analyzing power exists exactly at $T_p = 135$ MeV [40].

The target polarization has been determined using the so-called cross-ratio method [77]. The method provides a cancellation at the first order of the false asymmetries caused by differences in acceptance and efficiency of the two detectors, and in the integrated luminosity accumulated for the two polarization directions. The cross ratio δ is defined through of the rates $Y(\theta,\phi)_{R,L,\uparrow,\downarrow}$ in the left (L) and right (R) detectors for data samples with spin up ($\uparrow$) and down ($\downarrow$) target polarizations,

$$\delta = \sqrt{\frac{Y_{L,\uparrow}(\theta,\phi)\cdot Y_{R,\downarrow}(\theta,\phi)}{Y_{L,\downarrow}(\theta,\phi)\cdot Y_{R,\uparrow}(\theta,\phi)}} = 1 + \frac{1+\frac{3}{2}QA_y(\theta)}{1-\frac{3}{2}QA_y(\theta)} \tag{5.3}$$

Then, the asymmetry is defined as:

$$\epsilon = \frac{1-\delta}{1+\delta} = \frac{3}{2}QA_y\left\langle cos\phi\right\rangle, \tag{5.4}$$

where $\langle cos\phi\rangle$ is an average over the detector acceptance. In Fig. 5.4 the acceptance-corrected observed asymmetry ϵ corrected for is presented for the *pd*-elastic reaction. The events were selected by the vertex criterion, angular correlations and cuts on the energy loss. The remaining low background was accounted individually for in each angular bin and for each polarization direction. The resulting polarization of $\langle Q\rangle = 46.2 \pm 1.0\%$ is the average value over the storage cell.

Dependence of the polarization on longitudinal coordinate Z of the production point is shown in Fig. 5.5, where the origin corresponds to the position of the feeding tube of the storage cell, and the axis is directed along the beam flow. The values in each bin are obtained in the same way as in Fig. 5.4. The range of Z-coordinates shown is defined by the detector acceptance. One can see that no polarization loss is observed away from the feeding tube. This result could be obtained only from the measurement presented since the Breit-Rabi polarimeter only samples the gas from the center of the cell.

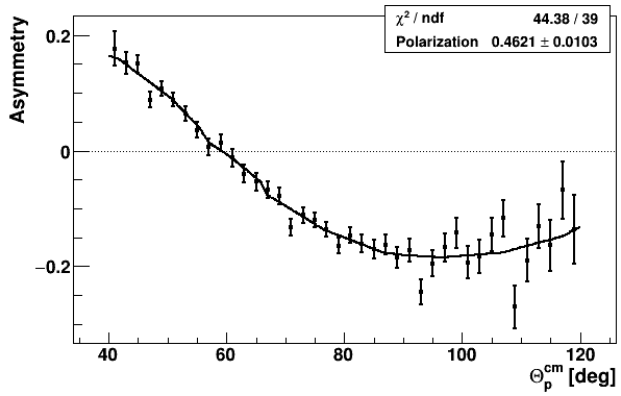

Figure 5.4: Experimental asymmetry in *pd*-elastic scattering as a function of proton center-of-mass polar angle. The curve shows interpolated A_y^d data from Ref. [40] scaled to fit our data.

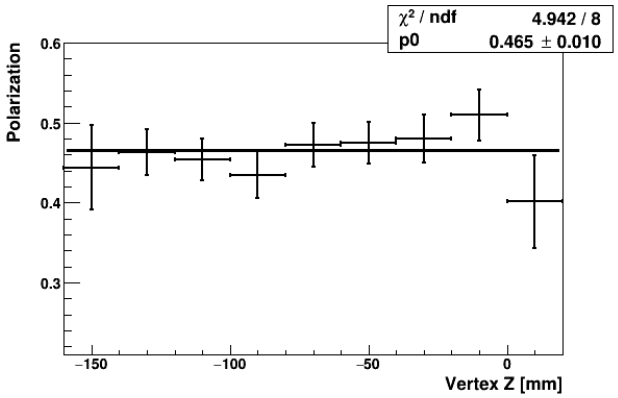

Figure 5.5: Target polarization estimated as a function of the longitudinal vertex coordinate Z along the storage cell. The full line presents fit with a constant.

Conclusion

The PhD thesis work was performed in the frame of PAX Collaboration at Institut für Kernphysik in Forshungszentrum Jülich.

The physics motivation to the development of dedicated PAX detector is based on problems of Drell-Yan production in proton-antiproton collisions, with both particles polarized, and Time Invariance Violation Interactions.

The detector is intended to be used as a polarimeter for longitudinal spin-filtering experiment at Cooling Synchrotron COSY.

The aim of my thesis was to develop the procedure of assembling of a complete PAX detector system from scratch and of its failure diagnostics, to perform all possible tests for the operation of the system.

In frame of the thesis I also presented the results of the tests of the detector system with two quadrants during a beam-time with a polarized target and an unpolarized proton beam.

The most responsible part of my job was to assemble the quadrants and install them to vacuum flange.

In the nearest future the detector will be tested again with the full set of quadrants. The outcome of the studies of spin-filtering will be of utmost importance for the possible application of polarized antiprotons at the Facility for Antiproton and Ion Research in Darmstadt.

Appendix A

Appendices

A.1 Repeater card schematic

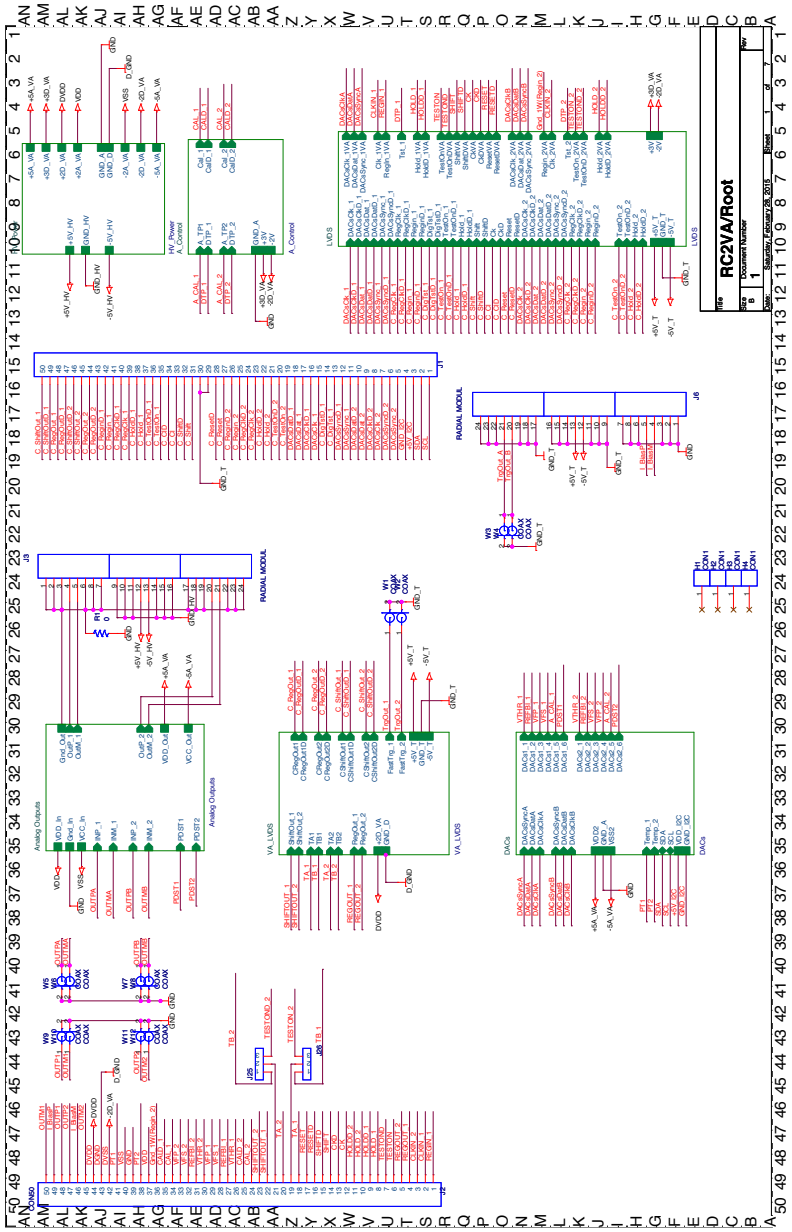

Figure A.1: Circuit diagram of Repeater Card.

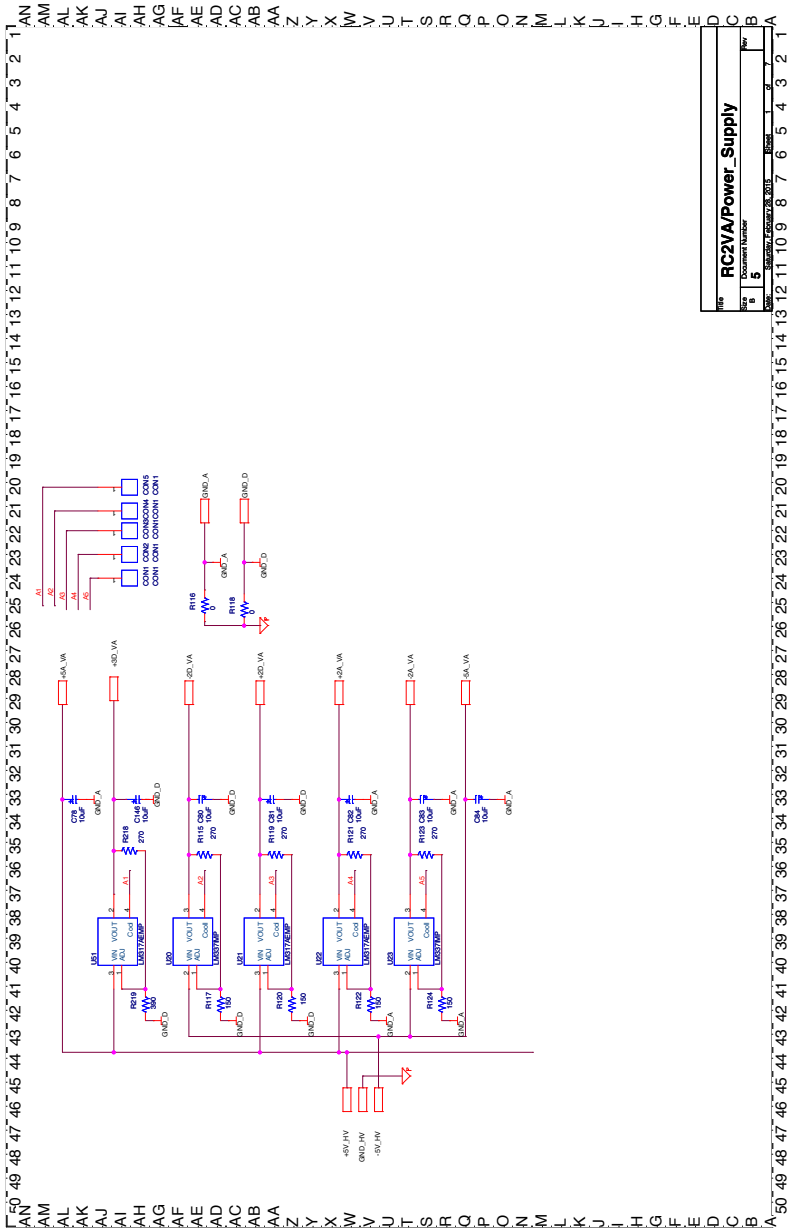

Figure A.2: Circuit diagram of Repeater Card.

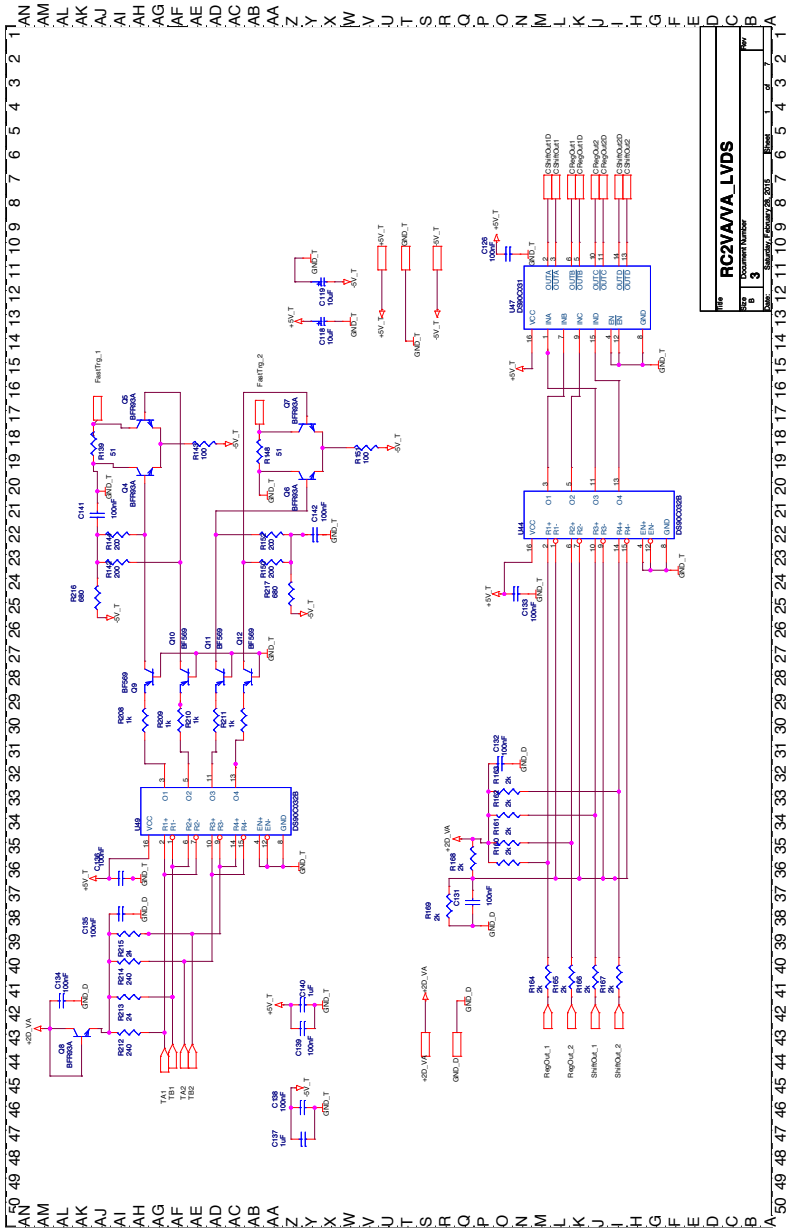

Figure A.3: Circuit diagram of Repeater Card.

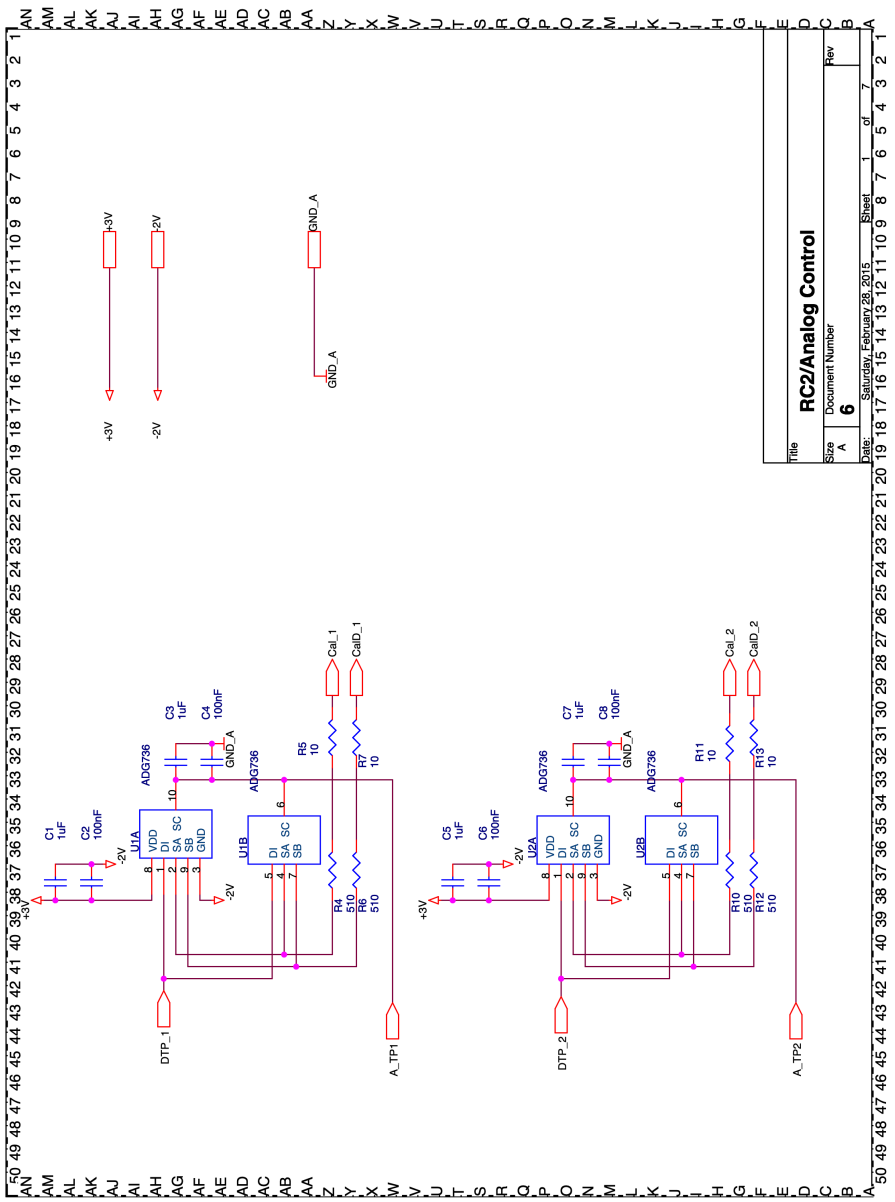

Figure A.4: Circuit diagram of Repeater Card.

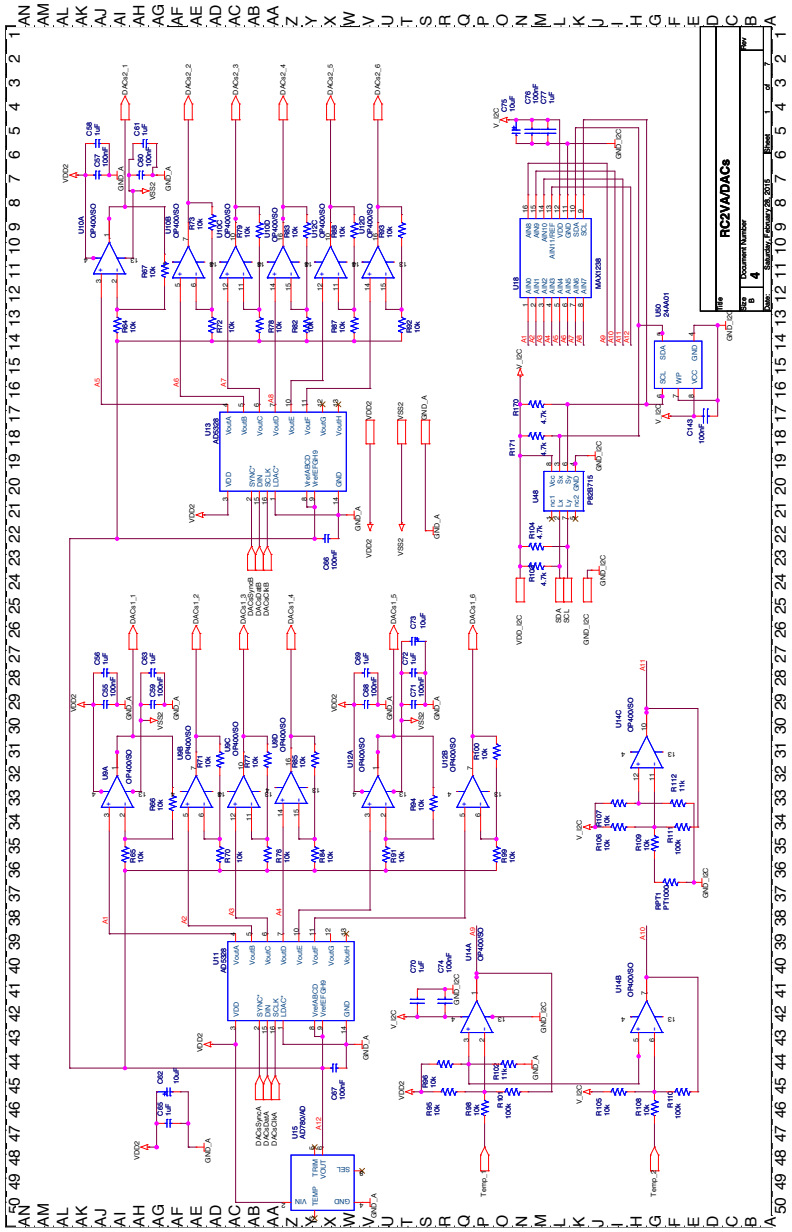

Figure A.5: Circuit diagram of Repeater Card.

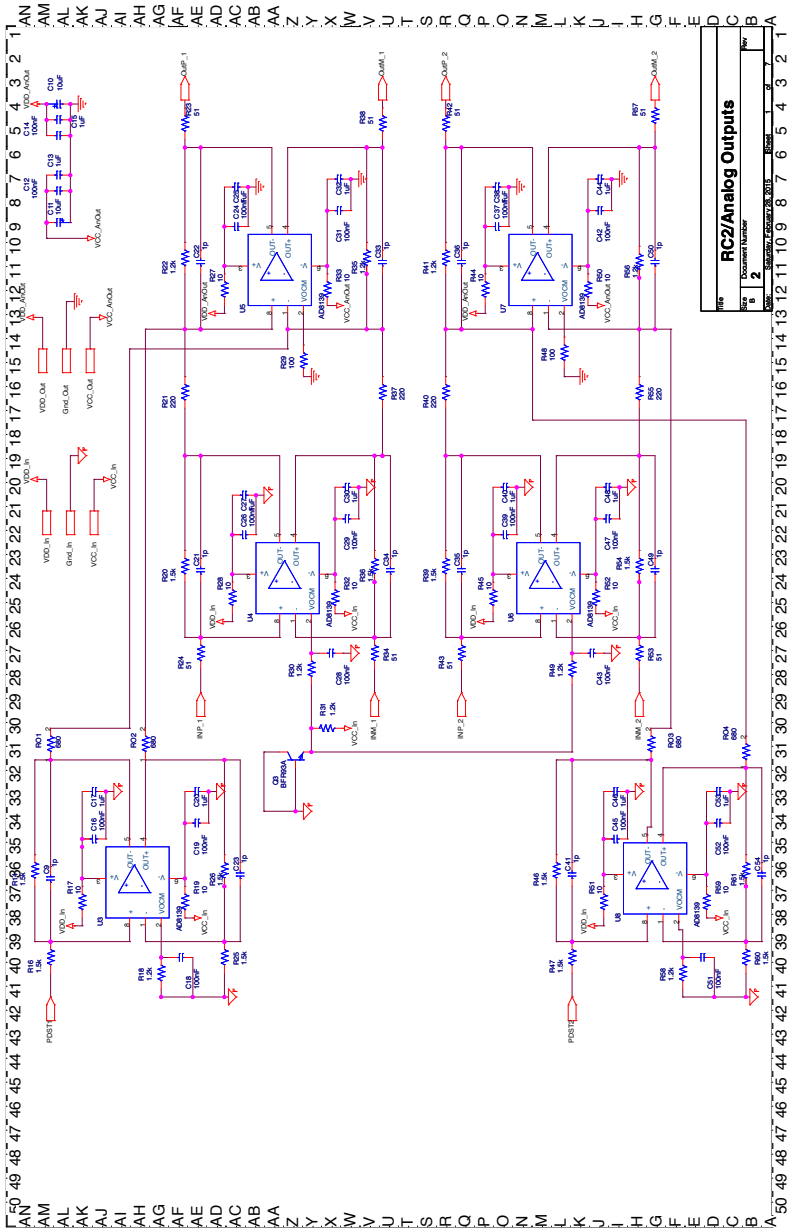

Figure A.6: Circuit diagram of Repeater Card.

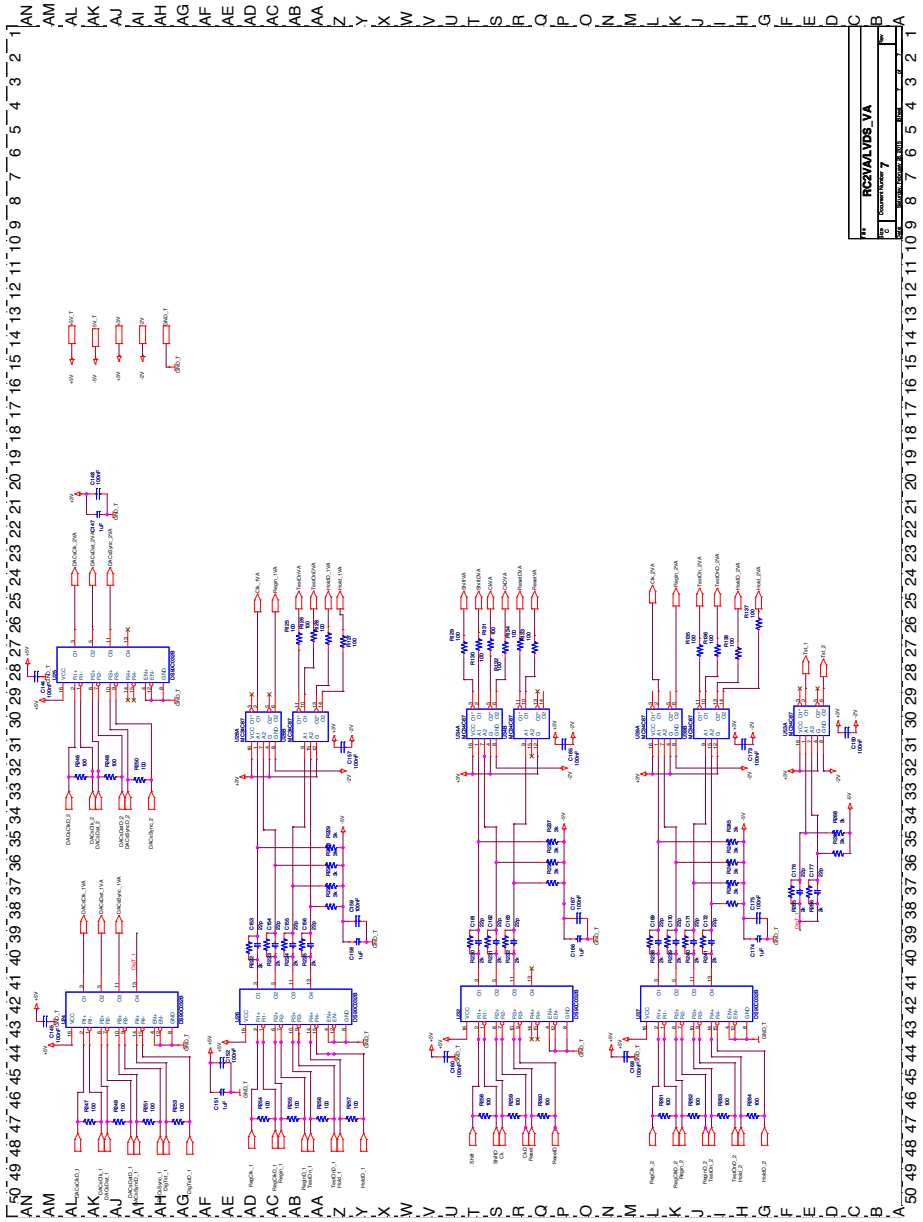

Figure A.7: Circuit diagram of Repeater Card.

A.2 Results of sensor tests

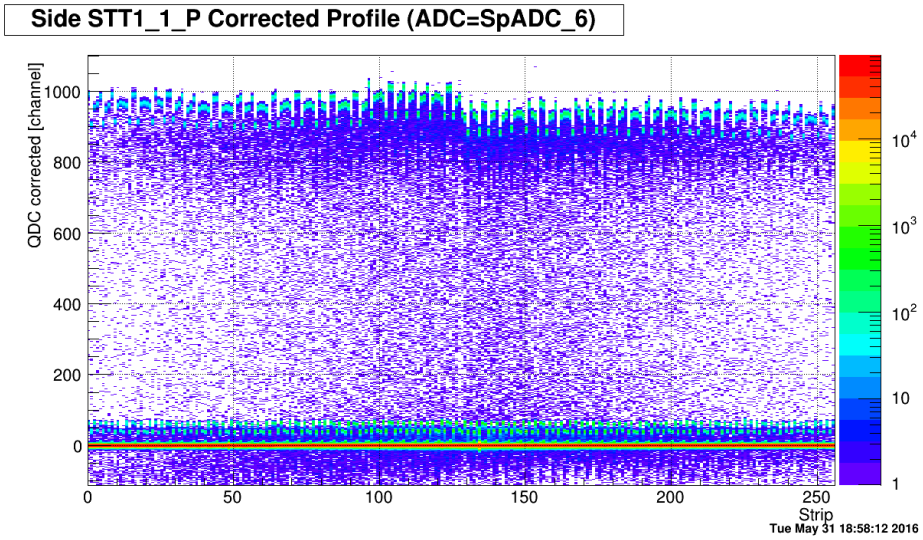

Figure A.8: Diagram of two suitable for experiment sensors. Irradiated with α-particles. P-side of sensor.

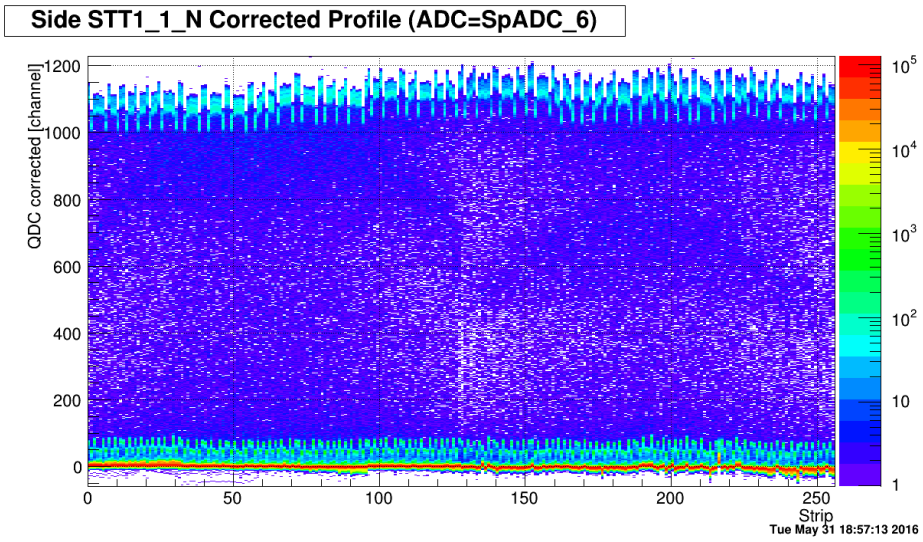

Figure A.9: Diagram of two suitable for experiment sensors. Irradiated with α-particles. N-side of sensor.

A.3 Test chamber for quadrants

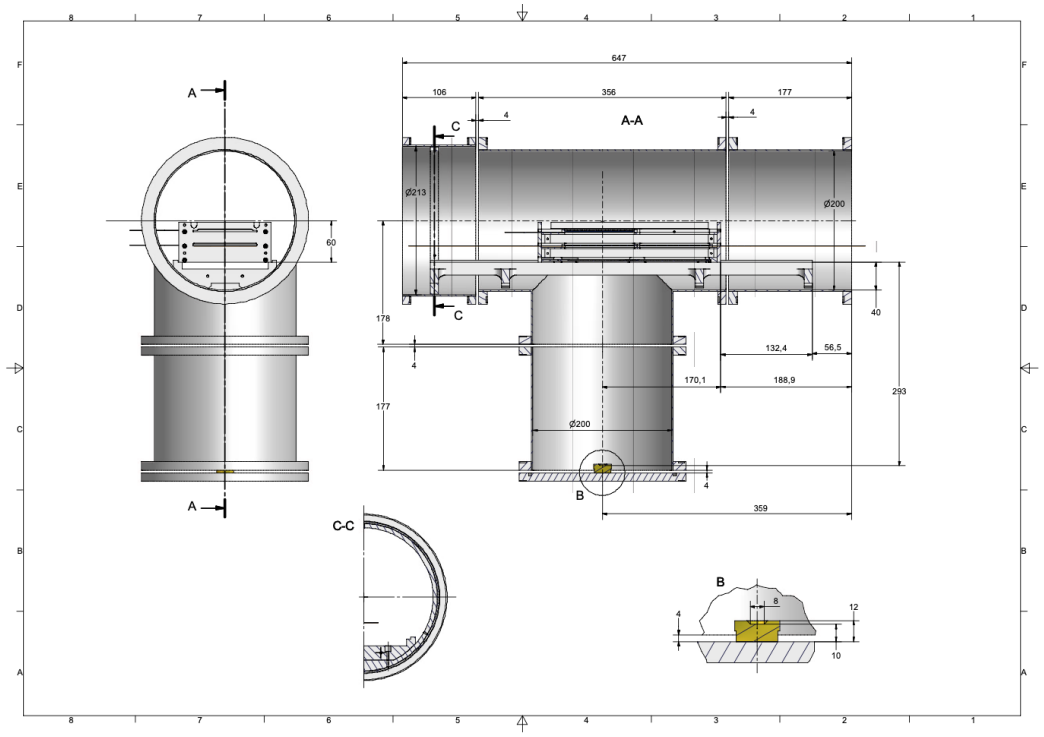

Figure A.10: Drawing of test chamber for quadrants.

Bibliography

[1] P. Lenisa and F. Rathmann, "Antiproton–Proton Scattering Experiments with Polarization," 2005.

[2] W. Augustyniak *et al.*, "Polarization of a stored beam by spin-filtering," *Phys. Lett.*, vol. B718, pp. 64–69, 2012.

[3] Y. Valdau, A. Aksentyev, D. Eversheim, and B. Lorentz, "The physics program of PAX at COSY," *Journal of Physics: Conference Series*, vol. 678, p. 012027, feb 2016.

[4] D. Eversheim, Y. Valdau, and B. Lorentz, "Test of time-reversal invariance at COSY (TRIC)," *Hyperfine Interactions*, vol. 214, pp. 127–132, Mar 2013.

[5] J. C. Collins, "Fragmentation of transversely polarized quarks probed in transverse momentum distributions," *Nucl. Phys.*, vol. B396, pp. 161–182, 1993.

[6] P. Lenisa and F. Rathmann, "Antiproton–Proton Scattering Experiments with Polarization (Technical Proposal)," 2005.

[7] A. Airapetian *et al.*, "Single-spin asymmetries in semi-inclusive deep-inelastic scattering on a transversely polarized hydrogen target," *Phys. Rev. Lett.*, vol. 94, p. 012002, 2005.

[8] E. S. Ageev *et al.*, "A New measurement of the Collins and Sivers asymmetries on a transversely polarised deuteron target," *Nucl. Phys.*, vol. B765, pp. 31–70, 2007.

[9] X. Qian *et al.*, "Single Spin Asymmetries in Charged Pion Production from Semi-Inclusive Deep Inelastic Scattering on a Transversely Polarized He3 Target at $Q^2 = 1.4 - 2.7\mathrm{GeV}^2$," *Physical Review Letters*, vol. 107, Aug 2011.

[10] M. Anselmino, M. Boglione, U. D'Alesio, A. Kotzinian, F. Murgia, A. Prokudin, and C. Türk, "Transversity and Collins functions from SIDIS and e+e- data," *Physical Review D*, vol. 75, Mar 2007.

[11] R. Seidl *et al.*, "Measurement of Azimuthal Asymmetries in Inclusive Production of Hadron Pairs in e+e- Annihilation at s**(1/2) = 10.58 GeV," *Phys. Rev.*, vol. D78, p. 032011, 2008. [Erratum: Phys. Rev.D86,039905(2012)].

[12] R. Seidl *et al.*, "Measurement of Azimuthal Asymmetries in Inclusive Production of Hadron Pairs in e^+e^- Annihilation at Belle," *Phys. Rev. Lett.*, vol. 96, p. 232002, Jun 2006.

[13] V. E. Fortov, "Relativistic Charged Particle Beams, Part of the Springer Series in Materials Science book series (SSMATERIALS, volume 216)," 2016.

[14] A. D. Krisch, A. M. T. Lin, and O. Chamberlain, "Polarized Beams at SSC. Proceedings, Workshop, Ann Arbor, USA, June 10-15, 1985. Polarized anti-protons. Proceedings, Workshop on Polarized Anti-proton Sources, Bodega Bay, USA, April 18-21, 1985," *AIP Conf. Proc.*, vol. 145, pp. pp.1–251, 1986.

[15] S. Chattopadhyay, D. P. Barber, N. Buttimore, G. Court, and E. Steffens, "Polarized antiproton beams - how? Proceedings, International Workshop, Daresbury, UK, August 29-31, 2007," *AIP Conf. Proc.*, vol. 1008, p. 1, 2008.

[16] T. O. Niinikoski and R. Rossmanith, "Selfpolarization of Protons in Storage Rings," *Nucl. Instrum. Meth.*, vol. A255, pp. 460–465, 1987.

[17] D. P. Grosnick *et al.*, "The Design and Performance of the Fnal High-energy Polarized Beam Facility," *Nucl. Instrum. Meth.*, vol. A290, p. 269, 1990.

[18] D. Oellers *et al.*, "Polarizing a stored proton beam by spin flip?," *Physics Letters B*, vol. 674, no. 4, pp. 269 – 275, 2009.

[19] P. Csonka, "Could we build polarized proton storage rings?," *Nuclear Instruments and Methods*, vol. 63, no. 3, pp. 247 – 252, 1968.

[20] J. Bystricky, F. Lehar, and P. Winternitz, "Formalism of Nucleon-Nucleon Elastic Scattering Experiments," *J. Phys.(France)*, vol. 39, p. 1, 1978.

[21] "ANKE Collaboration website accessible at: `http://collaborations.fz-juelich.de/ikp/anke/index.shtml`."

[22] J. Bystricky, F. Lehar, and P. Winternitz, "Formalism of Nucleon-Nucleon Elastic Scattering Experiments," *J. Phys.(France)*, vol. 39, p. 1, 1978.

[23] C. Weidemann *et al.*, "Toward polarized antiprotons: Machine development for spin-filtering experiments," *Phys. Rev. ST Accel. Beams*, vol. 18, p. 020101, Feb 2015.

[24] J. H. Christenson, J. W. Cronin, V. L. Fitch, and R. Turlay, "Evidence for the 2π Decay of the K_2^0 Meson," *Phys. Rev. Lett.*, vol. 13, pp. 138–140, 1964.

[25] M. Kobayashi and T. Maskawa, "CP Violation in the Renormalizable Theory of Weak Interaction," *Prog. Theor. Phys.*, vol. 49, pp. 652–657, 1973.

[26] R. J. Crewther, P. Di Vecchia, G. Veneziano, and E. Witten, "Chiral Estimate of the Electric Dipole Moment of the Neutron in Quantum Chromodynamics," *Phys. Lett.*, vol. 88B, p. 123, 1979. [Erratum: Phys. Lett.91B,487(1980)].

[27] D. Eversheim *et al.*, "COSY Proposal No.215, endorsed by the PAX Collaboration (Spokespersons: P. Lenisa and F. Rathmann). Accessible at: `https://apps.fz-juelich.de/pax/paxwiki/images/8/8c/215-TRI_Prop_sum.pdf`."

[28] H. Ströher, "Search for electric dipole moments using storage rings (srEDM). Advanced grant of the European Research Council, Proposal number: 694340, available from `http://collaborations.fz-juelich.de/ikp/jedi/public_files/proposals/Proposal-SEP-210276270.pdf`," 2015.

[29] L. B. Okun, "Note concerning CP parity," *Yad. Fiz.*, vol. 1, pp. 938–939, 1965.

[30] J. Prentki and M. J. G. Veltman, "Possibility of CP violation in semistrong interactions," *Phys. Lett.*, vol. 15, pp. 88–90, 1965.

[31] T. D. Lee and L. Wolfenstein, "Analysis of CP Noninvariant Interactions and the K0(1), K0(2) System," *Phys. Rev.*, vol. 138, pp. B1490–B1496, 1965.

[32] L. B. Okun, "The Violation of CP Invariance," *Sov. Phys. Usp.*, vol. 9, pp. 574–601, 1967.

[33] C. A. Baker *et al.*, "An Improved experimental limit on the electric dipole moment of the neutron," *Phys. Rev. Lett.*, vol. 97, p. 131801, 2006.

[34] W. Bernreuther, "CP violation and baryogenesis," *Lect. Notes Phys.*, vol. 591, pp. 237–293, 2002. [,237(2002)].

[35] H. E. Conzett, "Null tests of time reversal invariance," *Phys. Rev.*, vol. C48, pp. 423–428, 1993.

[36] A. A. Temerbayev and Yu. N. Uzikov, "Spin observables in proton-deuteron scattering and T-invariance test," *Phys. Atom. Nucl.*, vol. 78, no. 1, pp. 35–42, 2015. [Yad. Fiz.78,no.1-2,38(2015)].

[37] Yu. N. Uzikov and A. A. Temerbayev, "Null-test signal for T-invariance violation in *pd* scattering," *Phys. Rev.*, vol. C92, no. 1, p. 014002, 2015.

[38] Yu. N. Uzikov and J. Haidenbauer, "Polarized proton-deuteron scattering as a test of time-reversal invariance," *Phys. Rev.*, vol. C94, no. 3, p. 035501, 2016.

[39] M. Beyer, "Time Reversal Invariance in Multipole Mixing Ratios," *Nucl. Phys.*, vol. A493, pp. 335–349, 1989.

[40] B. von Przewoski *et al.*, "Analyzing powers and spin correlation coefficients for p+d elastic scattering at 135-MeV and 200-MeV," *Phys. Rev.*, vol. C74, p. 064003, 2006.

[41] A. Aksentyev, D. Eversheim, B. Lorentz, and Y. Valdau, "The Test of Time Reversal Invariance at Cosy (TRIC)," *Acta Phys. Polon.*, vol. B48, p. 1925, 2017.

[42] H. J. Stein, D. Prasuhn, H. Stockhorst, J. Dietrich, K. Fan, V. Kamerdjiev, R. Maier, I. N. Meshkov, A. Sidorin, and V. V. Parkhomchuk, "Present Performance of Electron Cooling at Cosy-Jülich.," 2004.

[43] A. Lehrach, "Strahl- und Spindynamik von Hadronenstrahlen in Mittelenergie- Ringbeschleunigern Habilitationsschrift Universität Bonn, ISBN 978-3-89336-548-7," 2008.

[44] B. Lorentz *et al.*, "Status of the Cooler Synchrotron COSY-Juelich," in *9th European Particle Accelerator Conference (EPAC 2004) Lucerne, Switzerland, July 5-9, 2004*.

[45] A. Lehrach, R. Gebel, R. Maier, D. Prasuhn, and H. Stockhorst, "Suppressing intrinsic spin harmonics at the cooler synchrotron COSY," *Nucl. Instrum. Meth.*, vol. A439, pp. 26–30, 2000.

[46] H. Grote and F. C. Iselin, "The MAD program (methodical accelerator design) version 8.4: User's reference manual," 1991.

[47] K. Unser, "A Toroidal DC Beam Current Transformer with High Resolution," *IEEE Transactions on Nuclear Science*, vol. 28, pp. 2344–2346, June 1981.

[48] K. Grigoryev *et al.*, "Machine studies for the development of storage cells at the ANKE facility of COSY," *Nucl. Instrum. Meth.*, vol. A599, pp. 130–139, 2009.

[49] P. Forck, "Minimal Invasive Beam Profile Monitors for High Intense Hadron Beams," *Conf. Proc.*, vol. C100523, p. TUZMH01, 2010.

[50] H. Stechemesser and V. Vau, "Layout and design of the vacuum system for the cooler synchrotron COSY at Julich," *Vacuum*, vol. 46, pp. 867–869, 1995.

[51] A. Nass *et al.*, "The HERMES polarized atomic beam source," *Nucl. Instrum. Meth.*, vol. A505, pp. 633–644, 2003.

[52] A. Airapetian *et al.*, "The HERMES polarized hydrogen and deuterium gas target in the HERA electron storage ring," *Nucl. Instrum. Meth.*, vol. A540, pp. 68–101, 2005.

[53] A. Nass *et al.*, "The HERMES polarized atomic beam source," *Nucl. Instrum. Meth.*, vol. A505, pp. 633–644, 2003.

[54] A. Nass, E. Steffens, L. Barion, M. Capiluppi, P. Lenisa, M. D. Stancari, H. Kleines, F. Rathmann, and J. Sarkadi, "The polarized target for spin filtering studies at COSY and AD," *AIP Conf. Proc.*, vol. 915, no. 1, pp. 1002–1005, 2007.

[55] N. Koch, *A Study on the Production of Intense Cold Atomic Beams for Polarized Hydrogen and Deuterium Targets*. PhD thesis, Erlangen - Nuremberg U., Theorie III, 1999.

[56] C. Weidemann, *Identification and Tracking of low Energy Spectator Protons*. PhD thesis, Universität zu Köln, 2007.

[57] F. Rathmann *et al.*, "Complete angular distribution measurements of pp spin correlation parameters Axx, Ayy, and Axz and analyzing power Ay at 197.4 MeV," *Phys. Rev.*, vol. C58, pp. 658–673, 1998.

[58] Integrated Engineering Software (IES). `http://www.integratedsoft.com`.

[59] Micron Semiconductor Ltd. `http://79.170.44.80/micronsemiconductor.co.uk/wp-content/uploads/2017/01/cat.pdf`.

[60] A. Airapetian *et al.*, "The HERMES recoil detector," *Journal of Instrumentation*, vol. 8, pp. P05012–P05012, may 2013.

[61] M. A. Ross *et al.*, "Performance of a polarized hydrogen storage cell target," *Nucl. Instrum. Meth.*, vol. A344, pp. 307–314, 1994.

[62] C. Baumgarten *et al.*, "An atomic beam polarimeter to measure the nuclear polarization in the HERMES gaseous polarized hydrogen and deuterium target," *Nucl. Instrum. Meth.*, vol. A482, pp. 606–618, 2002.

[63] C. Baumgarten *et al.*, "A gas analyzer for the internal polarized target of the HERMES experiment," *Nucl. Instrum. Meth.*, vol. A508, pp. 268–275, 2003.

[64] Lauda GmbH & Co. KG, "LAUDA Heating and Cooling Systems." `https://www.lauda.de/en/individual-temperature-control-systems/industrial-heating-and-cooling-systems.html`.

[65] Lauda GmbH & Co. KG, "Product data sheet Integral T 1200." `https://www.lauda.de/pimimport/assets/context/pdmarticle/85/8585/8585/attachments/Export.8585.2018-10-24-15-53-07.964202ab.pdf`.

[66] SAES Getters. `https://www.jlab.org/accel/inj_group/vacuum/Cartridge-heater-manual.pdf`, 2002.

[67] Pfeiffer Vacuum GmbH. `https://static.pfeiffer-vacuum.com/productPdfs/PMP05205.en.pdf`.

[68] SAES Getters, "Non evaporable getters activatable at low temperatures." https://psec.uchicago.edu/getters/St%20707%20Brochure.pdf.

[69] A. Mussgiller, *Identification and Tracking of low Energy Spectator Protons*. PhD thesis, Universität zu Köln, 2007.

[70] Epoxy Technology, Inc. https://www.epotek.com/site/files/brochures/pdfs/low_outgassing_brochure.pdf, 2013.

[71] Integrated Detector Electronics AS – IDEAS, "Va32ta2 datasheet." https//www.ideas.no, 2003.

[72] W. Erven, A. Ackens, P. Wüstner, and G. Kemmerling, "VERTEX-Module for MATE3 and VA32. Zentrallabor für Elektronik, Forschungszentrum Jülich. Berichte zum Datenerfassungssystem für physikalische Experimente.," 2010.

[73] W-IE-NE-R Power Electronics, GmbH, "Mpod crate." http://www.wiener-d.com/sc/power-supplies/mpod--lvhv/.

[74] iseg Spezialelektronik GmbH, "iseq module." https://iseg-hv.com/en/home.

[75] Pfeiffer GmbH. https://www.pfeiffer-vacuum.com/.

[76] S. Agostinelli *et al.*, "GEANT4: A Simulation toolkit," *Nucl. Instrum. Meth.*, vol. A506, pp. 250–303, 2003.

[77] G. G. Ohlsen and P. W. Keaton, "Techniques for measurement of spin-1/2 and spin-1 polarization analyzing tensors," *Nucl. Instrum. Meth.*, vol. 109, pp. 41–59, 1973.

Acknowledgements

I'd like to thank my research supervisor Prof. Paolo Lenisa for the opportunity to perform such work in a state of the art laboratory, my Russian colleagues Dr. Sergey Trusov, Dr. Sergey Mikirtytchiants and Dr. Sergey Merzliakov, Dr. Sergey Dymov who worked at this project before and continue now for the experience of work with electronics, programming, my German colleague Thomas Krings, who shared his experience of work with sensitive silicon sensors. I'd like to thank my friends, who support me, and of course my parents, who miss me in my home country.

Conformity declaration

I assure you that I have independently written the dissertation I have submitted, that I have given full details of the sources and aids used and that I have indicated in each individual case as borrowed the parts of the work - including tables, maps and illustrations - taken from other works in their wording or in their meaning; that this dissertation has not yet been submitted to any other faculty or university for examination; that it has not yet been published - apart from the partial publications listed below - and that I will not make such a publication before completion of the doctoral procedure. I am aware of the provisions of the doctoral regulations. The dissertation I submitted was supervised by Prof. Paolo Lenisa. Anton Kononov.